SPECTRAL ANALYSIS OF P-PHASES FROM MINING EXPLOSIONS RECORDED IN THE SOCORRO, NEW MEXICO AREA

by

Peter C. Guynn

Submitted in partial

fulfillment

of

the requirement

of

Geophysics 590

and the

Master's Degree Program

at

New Mexico Institute

of

Mining and Technology

March 1978

Geophysics Open-File Report No. 22
Geoscience Department
New Mexico Tech
Socorro, NM 87801

SPECTRAL ANALYSIS OF P-PHASES FROM MINING EXPLOSIONS RECORDED IN THE SOCORRO, NEW MEXICO AREA

by

Peter C. Guynn

Submitted in partial
fulfillment
of
the requirement
of
Geophysics 590
and the
Master's Degree Program
at
New Mexico Institute
of
Mining and Technology

March 1978

The research described in this paper was sponsored by the New Mexico Energy Institute - New Mexico State University (EI-176-032 and EI-177-083).

Abstract

Seismic energy from open-pit mining explosions was digitally recorded at three sites in the Socorro area. The data processed and interpreted in this paper were from explosions at the Morenci, Arizona copper mine to the southwest of Socorro and the Jackpile and St. Anthony uranium mines to the north. This study was undertaken to determine if crustal anomalies could be detected by attenuation of seismic waves from these explosions.

The basic parameter measured was the variation of relative amplitudes at discrete frequencies between pairs of stations. From this data, attenuation was either measured or compared between segments of the crust.

Source parameters were eliminated by using spectral amplitude ratios. Station effects were observed and eliminated in the interpretation. The method applied suggests a variation in upper crustal attenuation to the north of the three sites and higher attenuation to P-phase arrivals which must pass through a known deep extensive magma body.

Introduction

The primary objective of this study was detection of seismic attenuation anomalies caused by an extensive magma body which lies approximately at the 18.0 km level under the Rio Grande rift near Socorro.

A fast Fourier transform was applied to the Moho head-wave compressional phase (P_n) and the direct compressional phase (P_g) of three Morenci explosions recorded at stations SC and WT and of three Morenci explosions recorded at stations WT and DM. Analysis of a Conrad head-wave compressional phase (P*) was applied for the three Morenci explosions recorded at SC and WT. Spectral analysis was also applied to the P_g phase, the P-wave reflected from the Conrad (P*P) and the P-wave reflected from the Moho (P_mP) for Jackpile and St. Anthony explosions recorded at the same station pairs.

Spectral amplitude ratios of the various phases for each explosion recorded at each station pair were compared to test the reproducibility of the ratios in the frequency range 0-50 Hz. From the Morenci P_g amplitude ratios, the Q for the upper crust was estimated. Jackpile and St. Anthony data were analyzed to detect attenuation differences in propagation paths and to provide complementary information to the Morenci data regarding station effects on the amplitudes.

Attenuation Theory

The basic equation for amplitude loss of a planar wave is:

$$A_2 = A_1 e^{\frac{-\pi f r}{Qv}} , \qquad (1)$$

where f is frequency, r is the distance between station 1 and station 2, v is the velocity of the medium and Q is the measure of elasticity of the

medium. Q is found to be frequency-independent for friction losses in solids, while it is inversely proportional to frequency for viscous and friction losses in liquids (Knopoff, 1964). Because

$$Q = \frac{\pi f r}{v\left[\log_e \frac{A_1}{A_2}\right]} \quad \text{or} \quad \log_e \frac{A_1}{A_2} = \frac{\pi f r}{vQ} \quad , \qquad (2)$$

the logarithmic ratio must increase directly with the frequency for a Q characteristic of a solid and must increase at a greater rate than frequency for a liquid or solid-liquid mixture. A determination of Q can be made if the values of the ratio A_1/A_2 are known over a range of frequency for a station pair which lies along a common raypath to the source.

The amplitude spectrum obtained at any particular station is determined by the source spectrum $S(\omega)$, a geometrical spreading function $G(r)$, attenuation along the propagation path $P(\omega)$, attenuation from the propagation path to the station $PS(\omega)$ and the station effects $Stat(\omega)$. Figure 1 shows the various paths which P_n energy must travel to reach a station

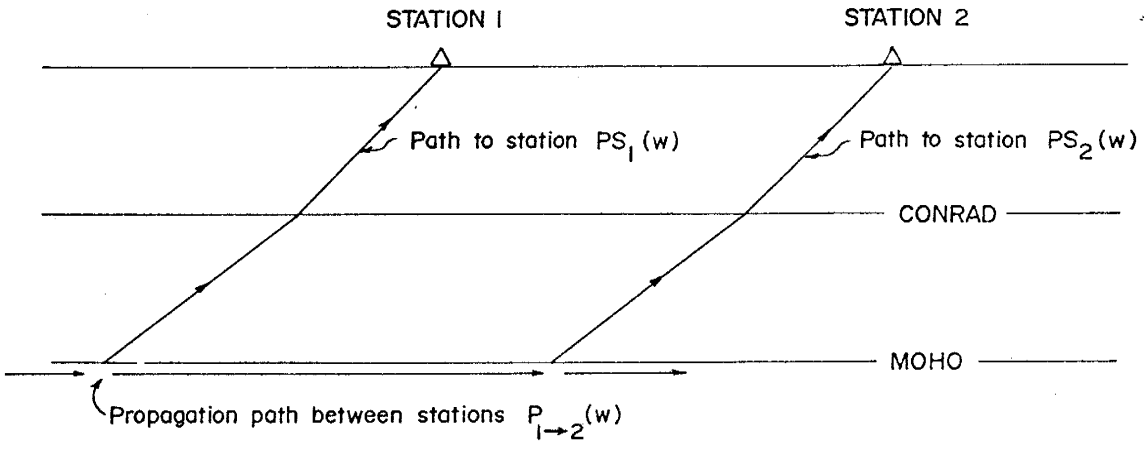

Figure 1. Paths of P_n to stations.

pair and the functions which affect the spectra due to attenuation along these raypaths. The resulting spectrum at a given station is:

$$A(\omega) = G(r) * S(\omega) * P(\omega) * PS(\omega) * Stat(\omega) \quad . \qquad (3)$$

If geometrical spreading is ignored the spectral amplitude ratio between stations 1 and 2 is

$$\frac{A_1(\omega)}{A_2(\omega)} = \frac{P_1(\omega) * PS_1(\omega) * Stat_1(\omega)}{P_2(\omega) * PS_2(\omega) * Stat_2(\omega)} \quad . \qquad (4)$$

The attenuation of the propagation path between the stations is

$$P_{1-2}(\omega) = \frac{P_2(\omega)}{P_1(\omega)} \quad , \qquad (5)$$

so that the spectral amplitude ratio is

$$\frac{A_1(\omega)}{A_2(\omega)} = \frac{PS_1(\omega) * Stat_1(\omega)}{P_{1-2}(\omega) * PS_2(\omega) * Stat_2(\omega)} \quad . \qquad (6)$$

The ratio is not affected by the source spectrum, so that differences in source character are eliminated by taking ratios. If a correction for relative station effects between the two stations can be found or if it is negligible, then

$$\frac{A_1(\omega)}{A_2(\omega)} = \frac{PS_1(\omega)}{P_{1-2}(\omega) * PS_2(\omega)} \quad , \qquad (7)$$

and only the attenuation functions remain. For waves which propagate in the upper crust such as the P_g, $PS_1(\omega)/PS_2(\omega)$ can be ignored so that

$$\frac{A_1(\omega)}{A_2(\omega)} = \frac{1}{P_{1-2}(\omega)} = e^{\frac{-\pi f \Delta r}{vQ}} \tag{8}$$

and a Q may be determined for the propagation path. For head waves such as P_n, $PS_1(\omega)/PS_2(\omega)$ cannot be ignored and the amplitude ratio due to attenuation will be given by equation (7) such that the location of an attenuation anomaly is uncertain. If $1/P_{1-2}(\omega)$ can be ignored, then

$$\frac{A_1(\omega)}{A_2(\omega)} = \frac{PS_1(\omega)}{PS_2(\omega)} \tag{9}$$

and the amplitude ratio due to attenuation would reflect the difference in attenuation from the propagation paths to the stations.

Any analysis applied to detect attenuation from the spectral amplitude ratios is critically dependent upon the elimination of the relative station effects $Stat_1(\omega)/Stat_2(\omega)$. Relative station effects can be caused by three mechanisms, all of which are frequency-dependent. Differences in velocity and density of rocks beneath the two station sites will cause an amplitude difference for the same quantity of seismic energy. Because energy of a wave can be expressed as

$$E = 2\pi^2 \rho f^2 \bar{v} A^2 \tag{10}$$

where ρ is density, a change of ρ or $\bar{v}$ requires that the amplitude A be adjusted to conserve the energy. Amplitude differences caused by differences

in the thickness of low density and low velocity overburden at a station pair is frequency dependent (Gutenberg, 1956). The amplitudes of wave-motion with wavelengths long in comparison to the thicknesses of the overburden at the two stations are not affected, whereas higher frequencies are. The station effect is probably constant for high frequencies. If station effects are only the result of this mechanism and the crust is solid then a plot of $\log_e A_1/A_2$ versus frequency leads to a non-zero intercept as frequency approaches zero if there were no geometrical spreading. If there were no station effect, then

$$A_1(\omega) = G(r_1)S(\omega)e^{\frac{-\pi f r}{Qv}} , \qquad (11)$$

and $$A_2(\omega) = G(r_2)S(\omega)e^{\frac{-\pi f r}{Qv}}$$

so that

$$\log_e\left(\frac{A_1 G(r_2)}{A_2 G(r_1)}\right) = \frac{\pi f \Delta r}{Qv} \qquad (12)$$

and Q will be frequency independent only if the correction for geometrical spreading is applied.

If there is a station effect caused by the mechanism discussed above, then

$$\log_e\left(\frac{A_1 G(r_2)\,Stat_2(\omega)}{A_2 G(r_1)\,Stat_1(\omega)}\right) = \frac{\pi f \Delta r}{Qv} \qquad (13)$$

and Q will be frequency independent only if the correction for geometrical spreading and station effects is applied such that the intercept of the logarithmic amplitude ratios would approach zero as frequency goes to zero. For example, if these effects result in an observed $\log_e A_1/A_2$ ratio which is greater than the effects of attenuation, then the Q values plotted against frequency would appear as is shown in Figure 2 (assuming

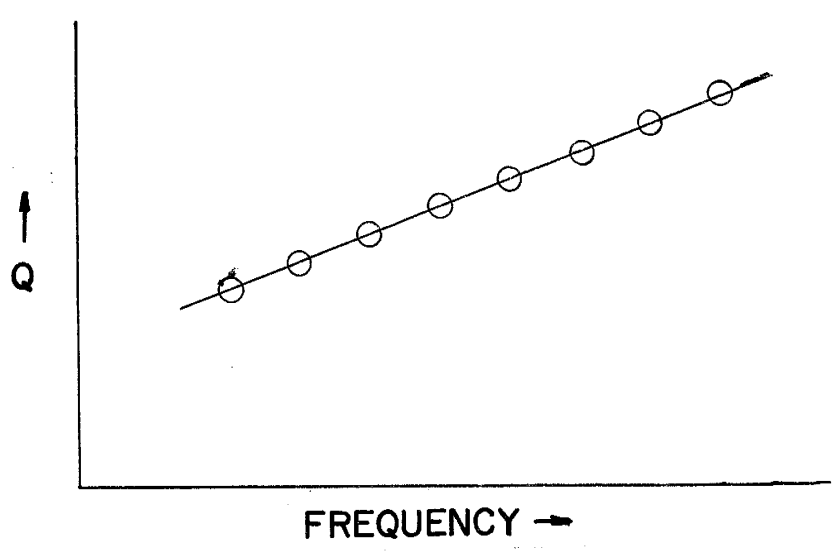

Figure 2. Q versus frequency when corrections for station effects and geometrical spreading are not applied.

frequency-independent station effects). If a solid crust can be assumed, then a correction applied to $\log_e A_1/A_2$ such that Q be constant over the frequency range of interest can be made. The constant Q would then be the actual Q of the crust.

Reflection from the free surface results in an amplitude doubling for a station at the surface. A difference in depth of station seismometers below the surface will cause a station effect. Amplitudes at a station beneath the surface will be reduced to 0.5 their value in comparison to a station at the free-surface for frequencies the wavelength of which are

comparable to the depth of the station.

Constructive and destructive interference caused by layering of rock beneath the stations will cause a frequency-dependent station effect. Constructive and destructive interference will occur also at a station beneath the surface as a result of reflections from the free-surface.

Explosions radiate energy symmetrically about the source, so that a comparison of attenuation along raypaths to stations at the same distance from the source may be made. If the distances are equivalent, then

$$A_1(\omega) = G(r)S(\omega)e^{\frac{-\pi fr}{Q_1 v}}$$

$$A_2(\omega) = G(r)S(\omega)e^{\frac{-\pi fr}{Q_2 v}} \qquad (14)$$

and

$$\frac{A_1(\omega)}{A_2(\omega)} = e^{\frac{-\pi fr}{v}\left(\frac{1}{Q_1} - \frac{1}{Q_2}\right)} = \frac{P_1(\omega) * PS_1(\omega)}{P_2(\omega) * PS_2(\omega)} \qquad (15)$$

which is valid only if the relative station effects are negligible. The difference between the two raypaths can be expressed in terms of a new parameter P which is given by

$$\frac{1}{P} = \frac{1}{Q_1} - \frac{1}{Q_2} \quad \text{or} \quad P = \frac{Q_1 Q_2}{Q_2 - Q_1} \quad . \qquad (16)$$

If either Q_1 or Q_2 shows a liquid behavior, then P will be highly frequency-dependent.

Instrumentation

Two Sprengnether DR-100 digital event recorders were available for this study. Sampling rate was 100/sec. Gains were set at 6 db intervals in the range 78-96 db. Filters were set at Low-out and Hi-out throughout the data acquisition period.

Seismometers used were the Mark-Products L4-C vertical geophone (1.0 Hz natural frequency).

The playback system consisted of a Sprengnether DP-100 tape playback unit and a Beckman Dynograph strip-chart recorder.

The digitizing equipment consisted of a Hewlet-Packard mini-computer and digitizer.

Data Used in the Experiment

Three Morenci explosions and two Jackpile explosions were simultaneously recorded at SC and WT. Three Morenci explosions, three Jackpile explosions and one St. Anthony explosion were simultaneously recorded at WT and DM. Table 1 lists all of the events and other pertinent information.

Events were checked for location of the source by the P_n-P_g or P_g-S_g time differences and station time delays. Morenci events have a P_n-P_g interval of approximately 3.0 sec. and a P_g-S_g interval of 33 sec. Station time delays are 1.75 sec. between SC and WT and 1.65 sec. between WT and DM. For Jackpile and St. Anthony events the source was checked by the near equivalence of arrival times at the stations and a P_g-S_g difference

of 15 sec.

Table 1. Explosion Data used for the Study

Event	Stations	day	time	phases & number of samples digitized
Morenci	SC, WT	270	22:31	P_n, 180 ; P*, 100 ; P_g, 550
Morenci	SC, WT	271	22:31	P_n, 180 ; P*, 100 ; P_g, 550
Morenci	SC, WT	272	22:31	" " " " " "
Morenci	WT, DM	251	22:31	P_n, 180 ; P_g, 550
Morenci	WT, DM	254	22:37	P_n, 180 ; P_g, 550
Morenci	WT, DM	255	22:30	" " " "
Jackpile	SC, WT	270	18:07	P_g and P*P, 193 ; P_mP, 200
Jackpile	SC, WT	273	00:14	P_g and P*P, 193 ; P_mP, 200
Jackpile	WT, DM	190	19:30	P_g, 100
Jackpile	WT, DM	208	22:29	P_g, 100
Jackpile	WT, DM	237	19:57	P_g, 100 ; P_mP, 200
St. Anthony	WT, DM	202	21:59	P_g, 100 ; P_mP, 200

The first arrival from Morenci explosions is the P_n phase. The P_n phase is weak in comparison to the P_g phase so that spectral analysis can only be applied if it is the first arriving phase. The P_g from Morenci has a long time window. The reflective arrivals, P*P and P_mP should arrive shortly after the P_g, however the Morenci seismograms show no discernible burst of energy after the P_g arrival.

Stations SC, WT and DM lie along a common raypath from Morenci so that a determination of Q can be made for the P_g phase (upper crust).

An extensive magma body at the 18 km level has been mapped by using S_xS reflection points from microearthquakes (Sanford, Alptekin and

Toppozada, 1973; Rinehart, 1976; Sanford et al., 1977). The raypath of a Morenci P_n phase at station DM should pass through the southern margin of the extensive body while the raypaths to SC and WT should not. Therefore a comparison between spectra for station pairs SC-WT and WT-DM should indicate the effect of the extensive magma body. Figure 3 shows the P_n raypaths to SC, WT and DM with respect to a crustal profile. The great

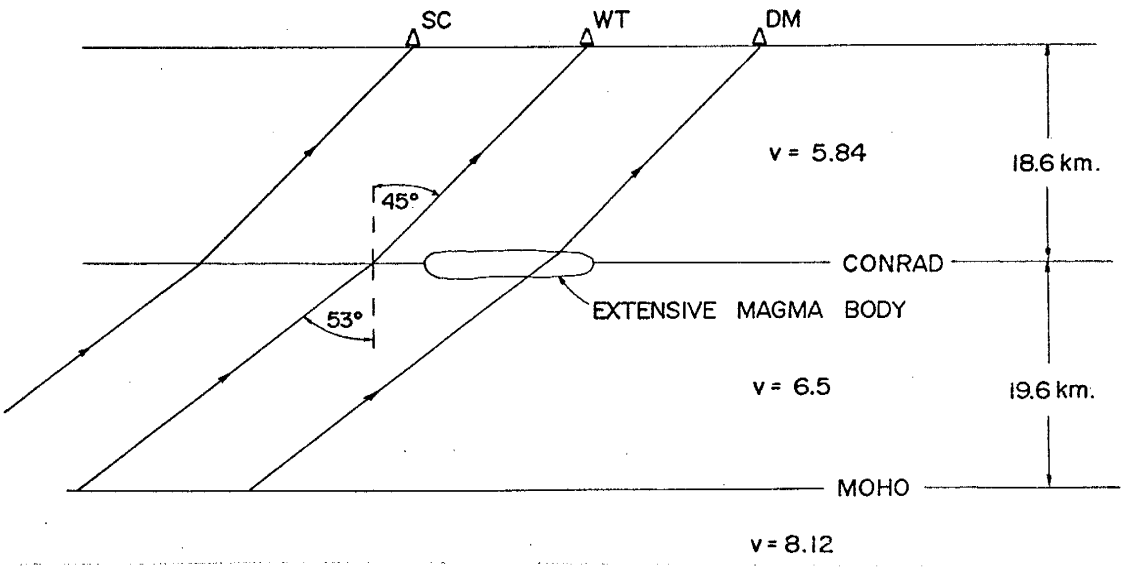

Figure 3. Various raypaths to the stations SC, WT and DM. Crustal thicknesses and velocities are from Toppozada and Sanford (1976).

distance (~59 km) of the raypaths to the stations in comparison to the station separation (~15 km) suggests that differences in the spectral content of P_n at each station pair due to attenuation should be dominantly a result of $PS_1(\omega)/PS_2(\omega)$ which will include the effects of the extensive magma body.

Along the station line, the raypaths from Morenci and those from the uranium mines to the north cross at near right angles. Table 2 lists the

distances to the mines from the stations. Because the distances from

Table 2. Distances from the Mines to the Stations (in km).

	Morenci	Jackpile	St. Anthony
SC	233.24	126.72	128.23
WT	248.16	123.48	124.16
DM	261.31	124.48	124.37

Jackpile (or St. Anthony) to the stations are approximately the same, differences in amplitudes at these stations due to distance and geometrical spreading are eliminated. This allowed an estimation of relative attenuations effects along three raypaths from the north. Also for these northern explosions the Moho reflection is a strong arrival; the raypath of which must pass through the extensive magma body to WT and DM but not to SC.

Figure 4 shows the locations of the stations and the raypaths to the explosions. The outline of the extensive magma body is shown and the positions of the points at which the Morenci P_n raypaths and the Jackpile and St. Anthony P_mP raypaths must pass through the 18 km level in the crust. Figure 5 shows the P_mP raypath to the stations from Jackpile explosions and the lateral distance from the stations to the points where the raypaths cross through the 18 km level in the crust.

Data Processing

A direct interface of the cassette tapes with a computer was not available so that conversion of the tapes into useful form was a detailed

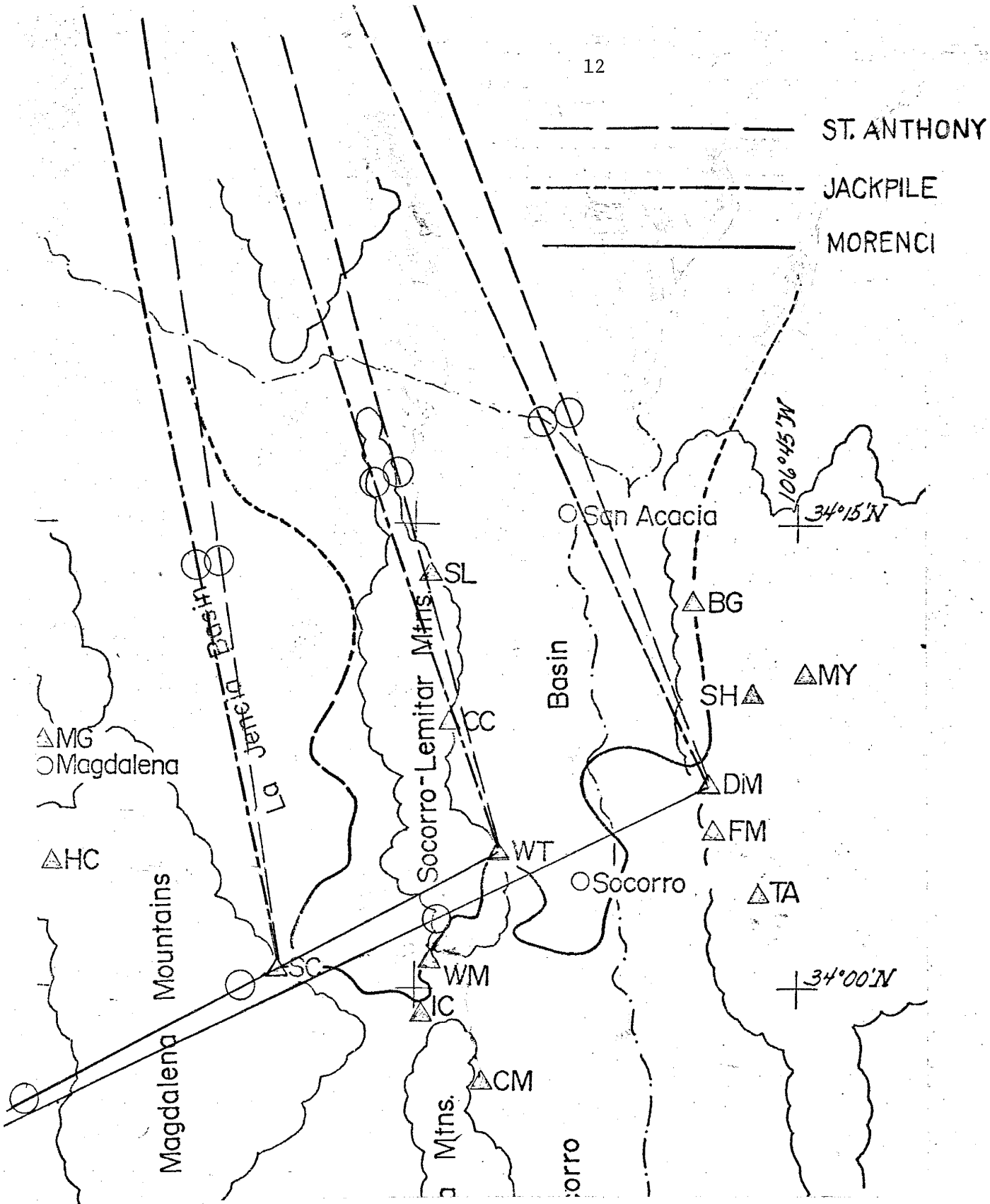

Figure 4. Map of the Socorro area showing station locations, raypaths to explosions and outline of the extensive magma body.

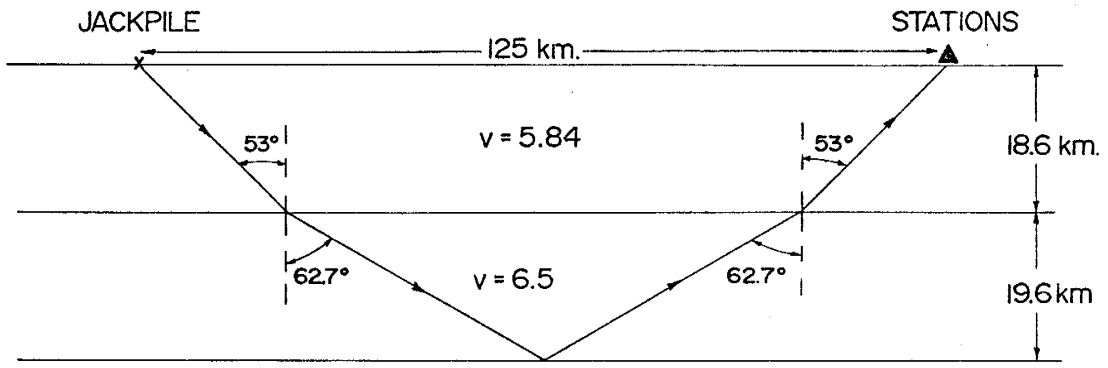

Figure 5. P_mP raypath from Jackpile to the stations.

and laborious process. Nevertheless the method employed did preserve the original sampling.

Fast paper output and hi-frequency response of the Dynograph produced a record that revealed the .01 sec. sampling interval. Figure 6 shows a typical example of a playback.

Figure 6. Playback of a Morenci P_n phase recorded at station WT.

Amplitudes were measured in terms of the deflection angle of the Dynograph pen. A relative voltage check of the Dynograph recorder showed the angle to be linear with voltage. During the digitizing corrections were automatically made for paper tilt, pen curvature and tape speeds by the mini-computer. A tolerance was set for each record (due to different

tape speeds) such that samples could only be taken in the length interval corresponding to .01 sec. Sampling was taken on the rise or drop of each step.

The resolution of the digitizing table was 0.25 mm. The Dynograph sensitivity was set such that the playback record showed the highest amplitudes possible. The amplitudes calculated were carried to three significant figures.

The amplitude data were then punched on IBM cards and submitted to the computer for CalComp plots which were used to check for digitizing errors. All amplitudes were normalized to 1.0 v/cm for the Dynograph and 90 db for the field recording units. No correction for instrument response was necessary because the filter settings in the field were always the same.

All digitizing was accomplished in this manner except for two Jackpile explosions which were hand-digitized due to the loss of the original magnetic tape data.

The various digitized phases were converted to the frequency domain by the Cooley-Tukey Fast Fourier Transform after the D.C. average was removed from the interval which was to be transformed. The Nyquiest frequency, 50 Hz, was well above any frequency components of the seismograms and thus aliasing was not a problem.

The arrival of P_n from Morenci was considered uncontaminated for the first 1.8 sec. Figure 7 shows a seismogram of the first 3.0 sec. of a Morenci event recorded at SC. The arrival at 1.8 sec. after the P_n arrival was interpreted to be a P* phase, a head wave generated along the Conrad discontinuity. The section of the seismogram from 2.0 to 3.0 sec. at stations SC and WT consists of this phase mixed with the P_n phase,

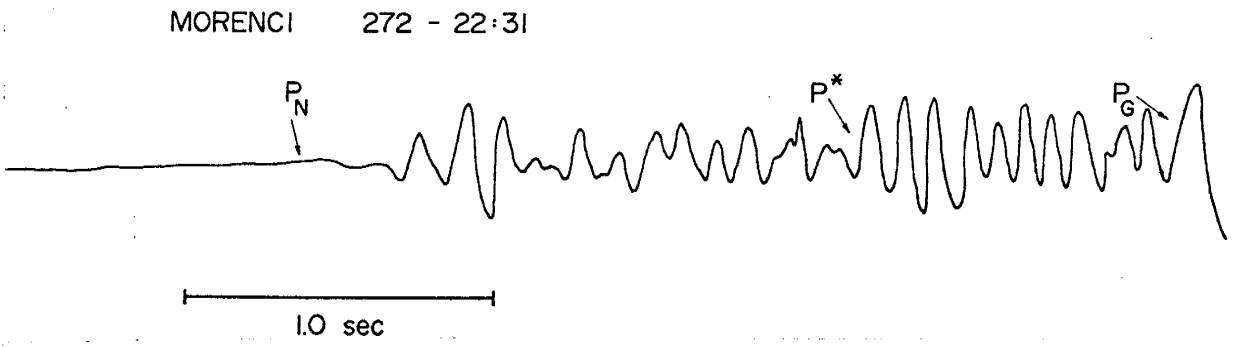

Figure 7. First 3 seconds of a Morenci explosion recorded at station SC.

neither of which is dominant. The Morenci P_g phase was digitized for 5.5 seconds from 3.0 to 8.5 sec. Figure 8 is the seismogram for a Morenci explosion recorded at WT showing the strength of the P_g phase relative to the other phases.

Figure 8. P phases for a Morenci explosion recorded at station WT.

Figures 9 and 10 display all of the unsmoothed spectra for the Morenci P_n and P_g phases. The dominant frequency of the P_g phase is generally less than 5.0 Hz while that for the P_n is greater than 5.0 Hz. Figure 11 shows the spectra for the Morenci P* (from 2.0 to 3.0 sec.) for the explosions recorded at SC and WT.

Figure 12 is a time-distance curve for Jackpile and St. Anthony

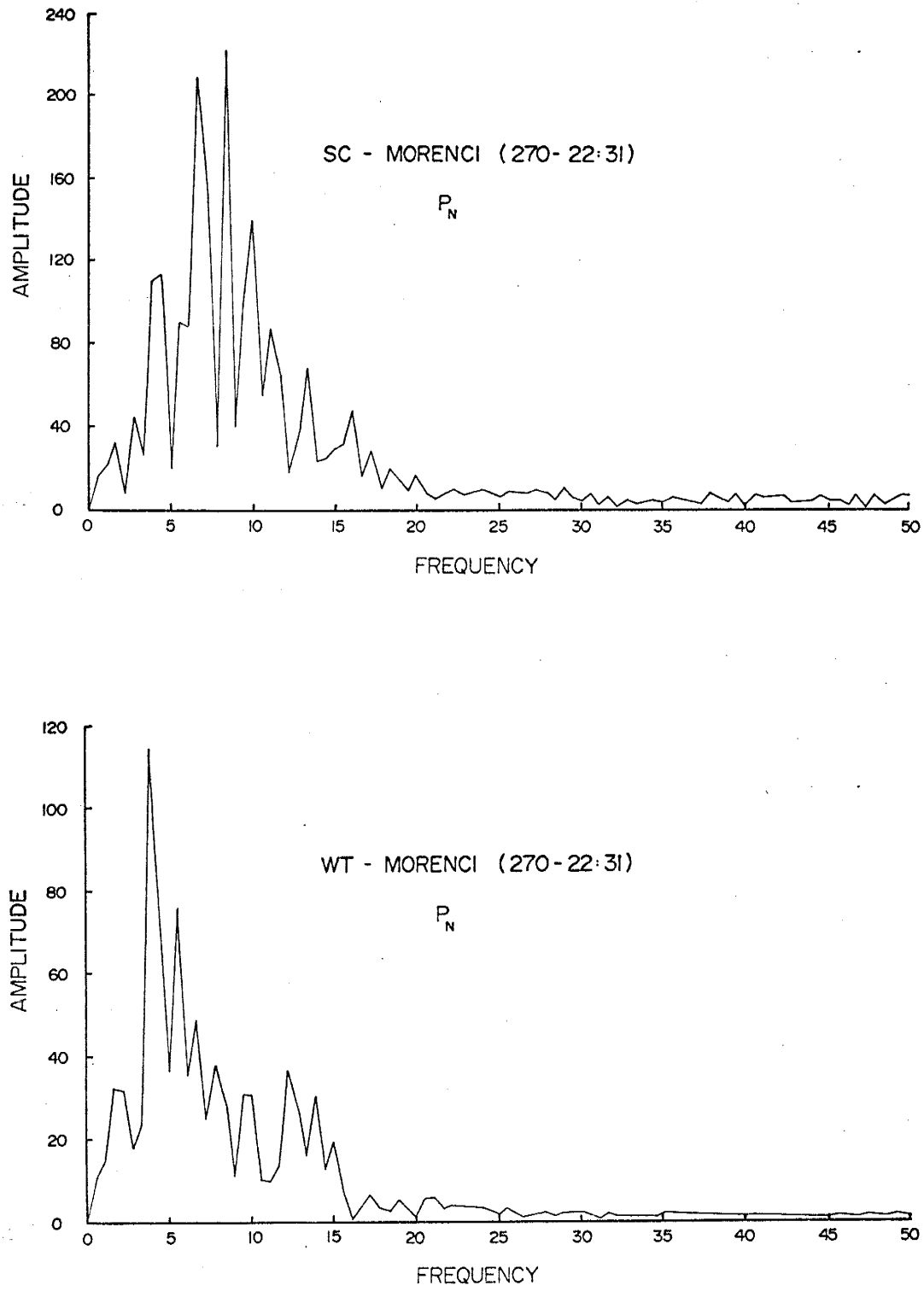

Figure 9. Spectra for the P_n phase from Morenci explosions.

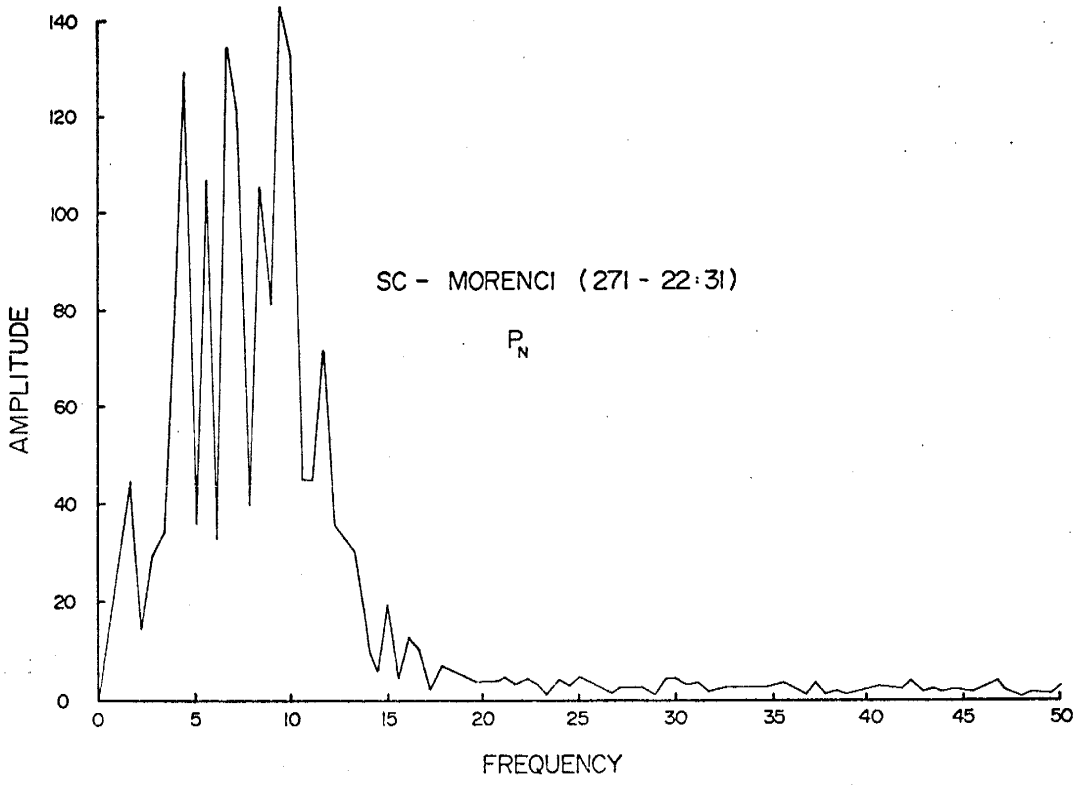

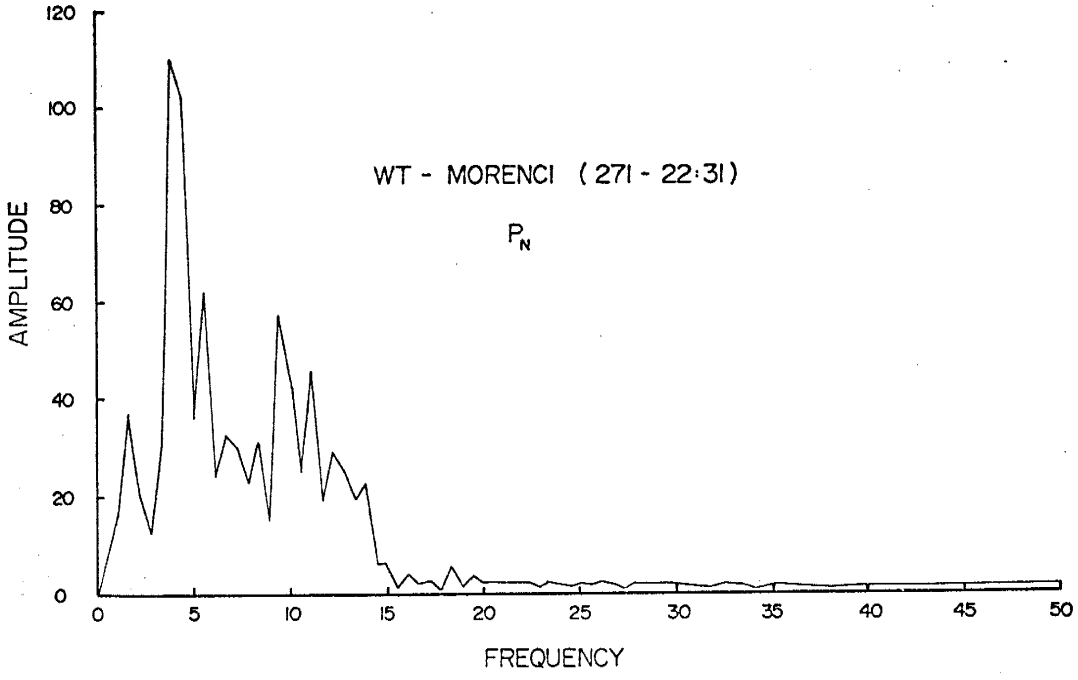

Figure 9. (Continued)

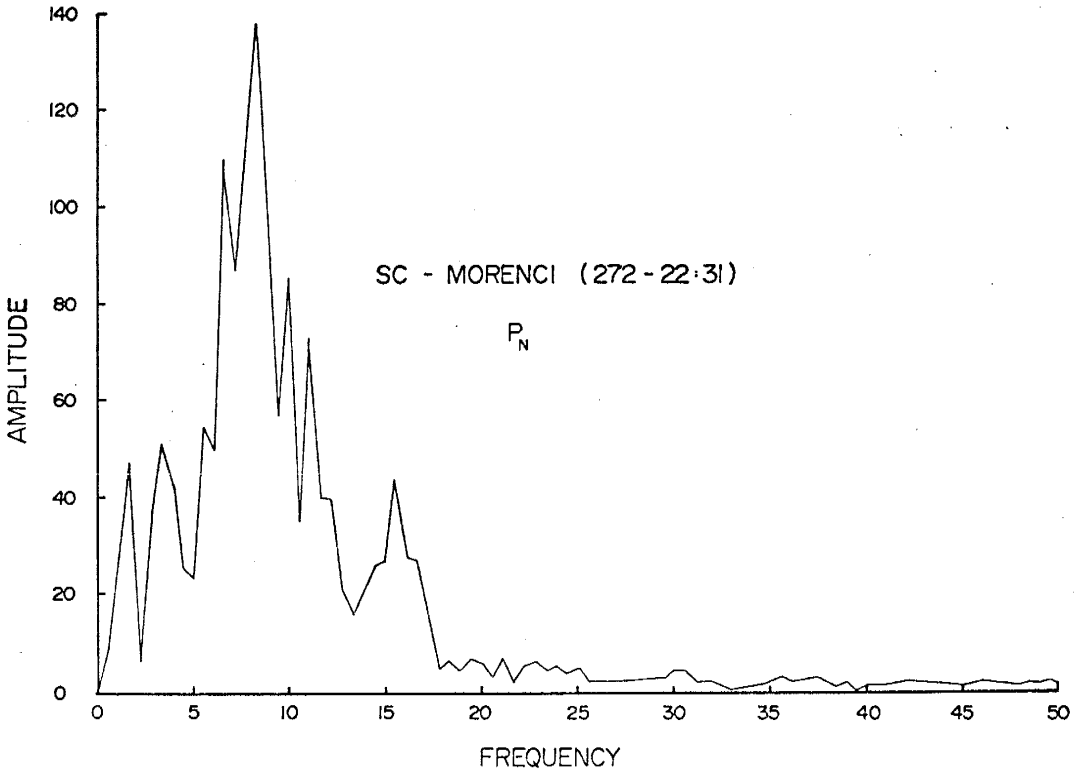

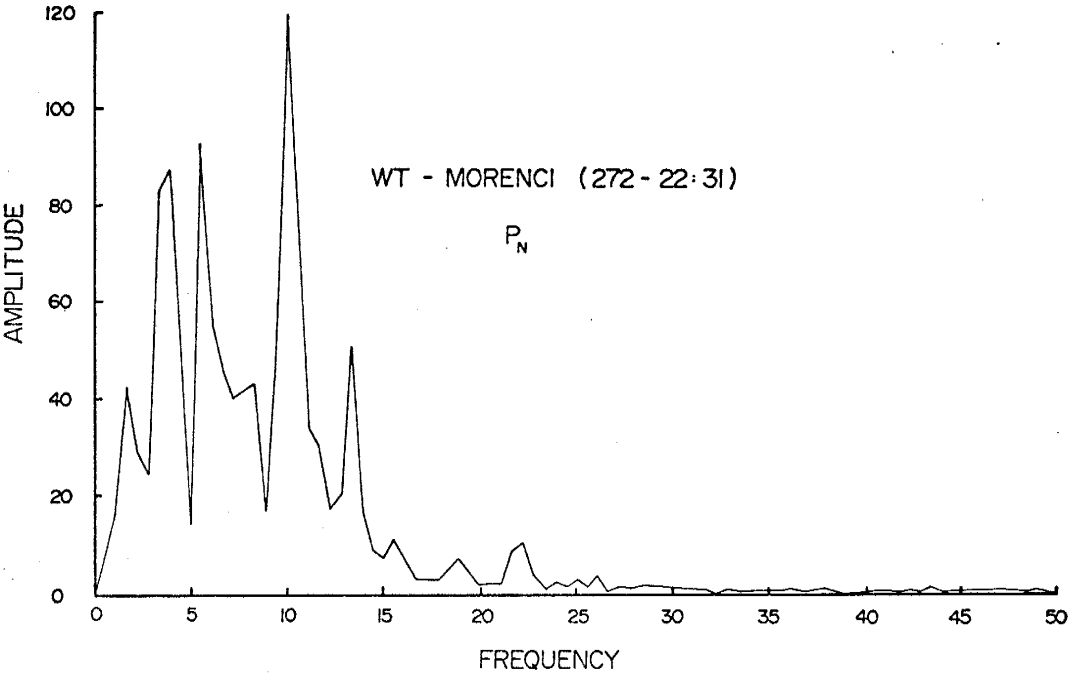

Figure 9. (Continued)

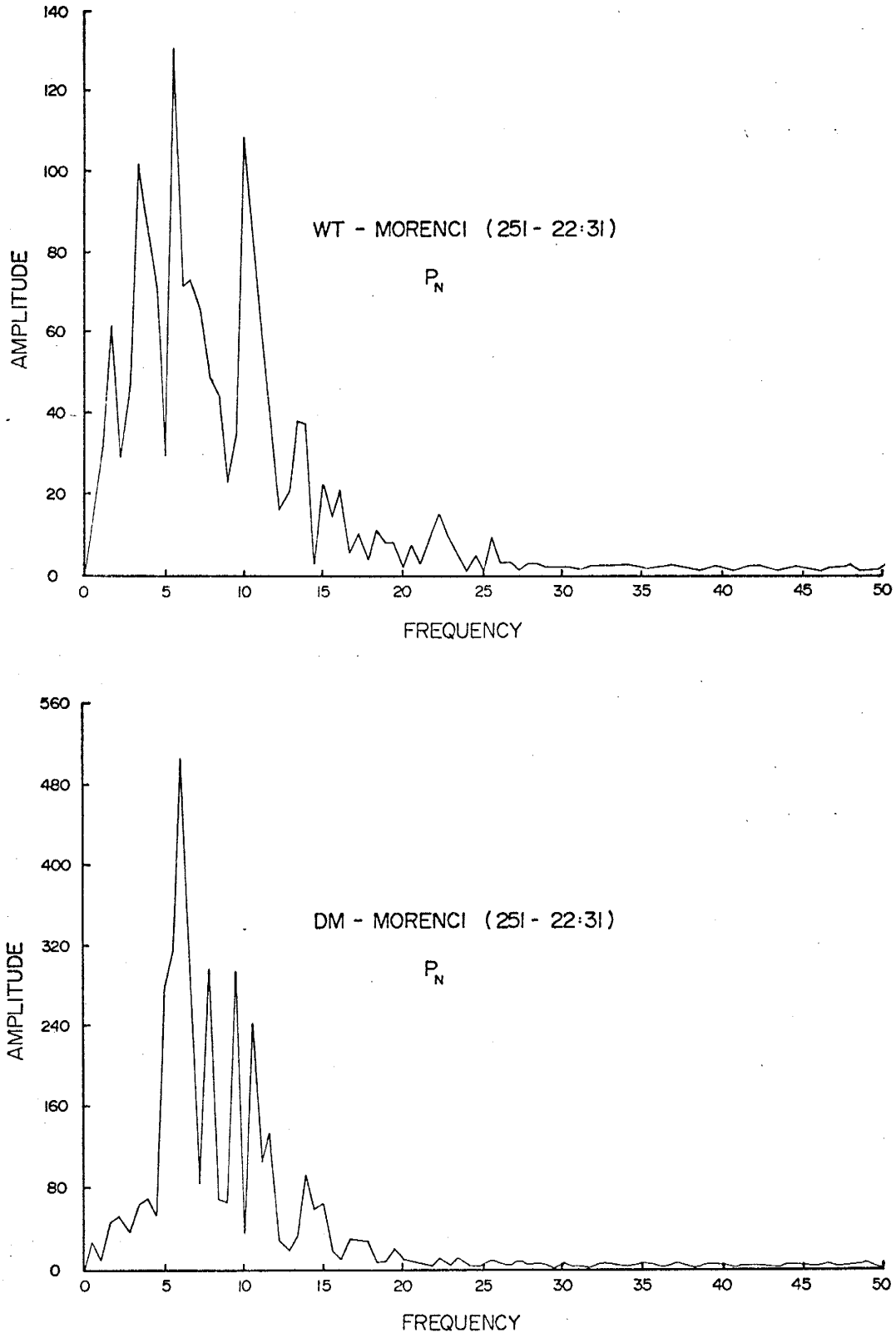

Figure 9. (Continued)

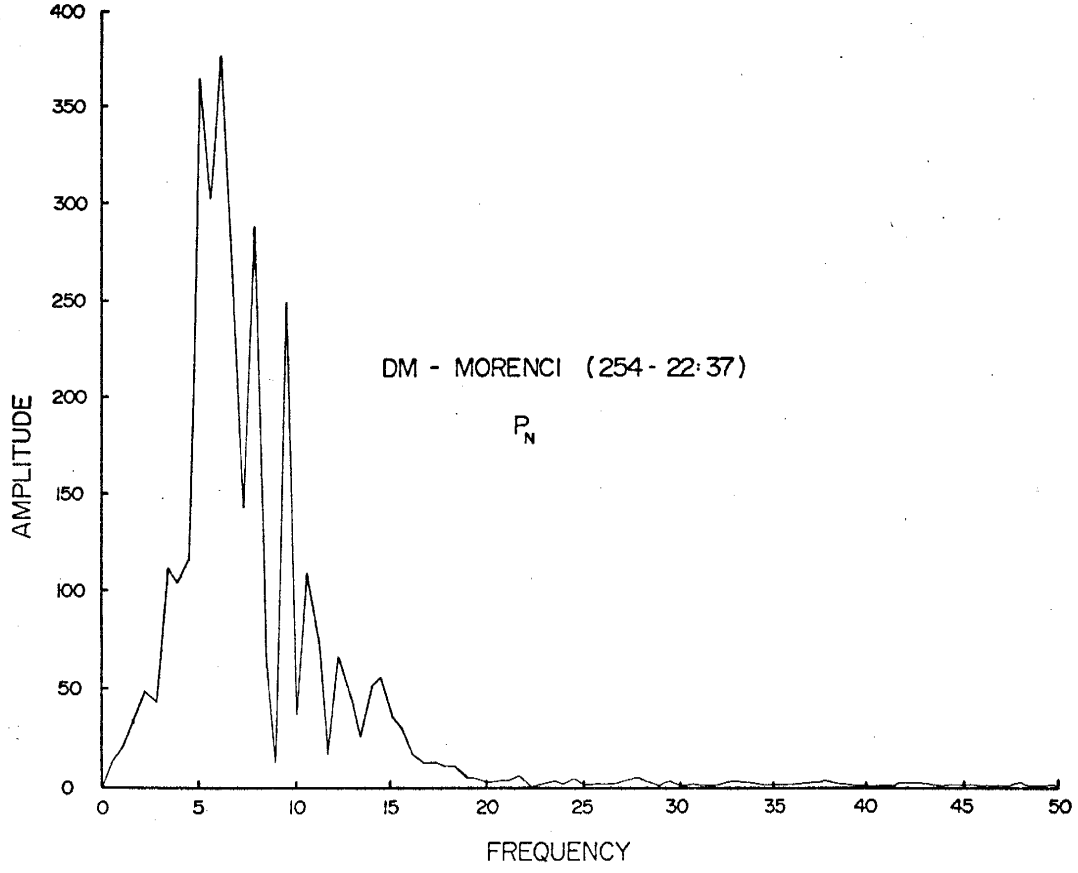

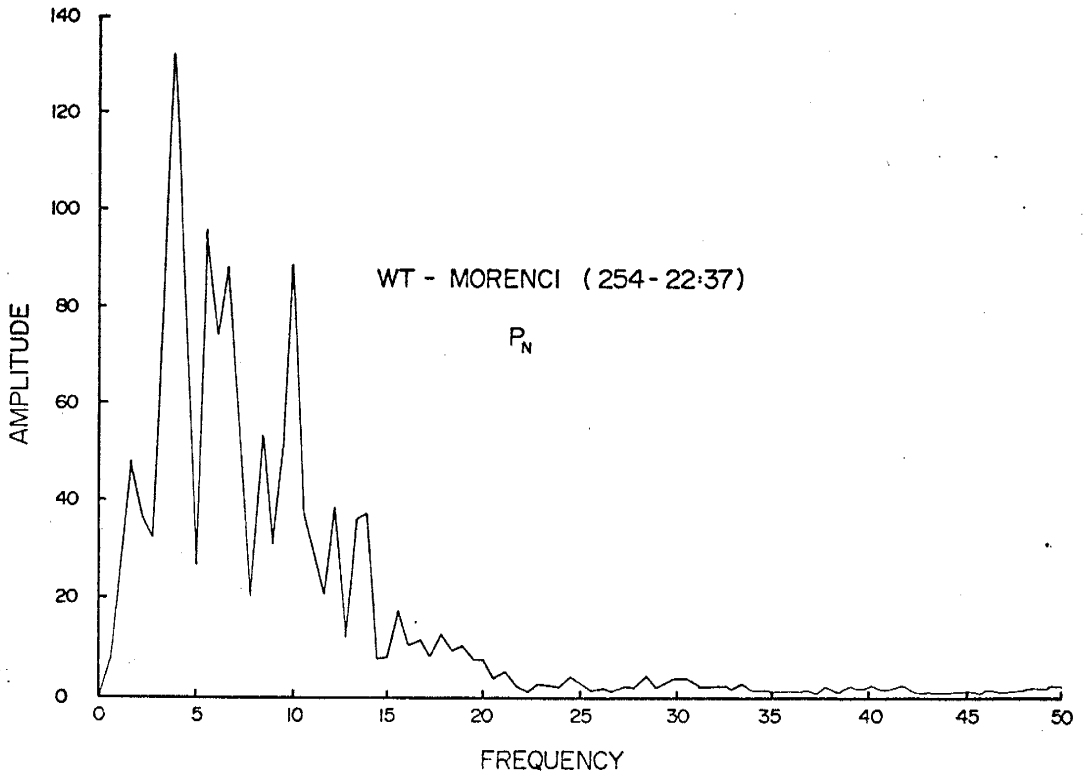

Figure 9. (Continued)

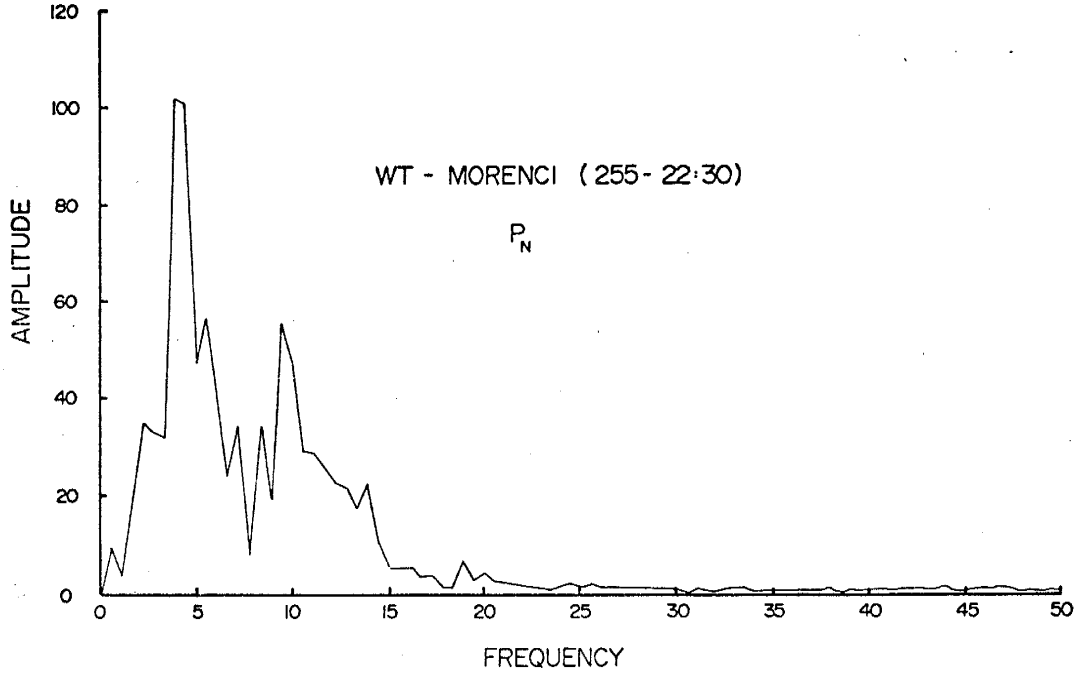

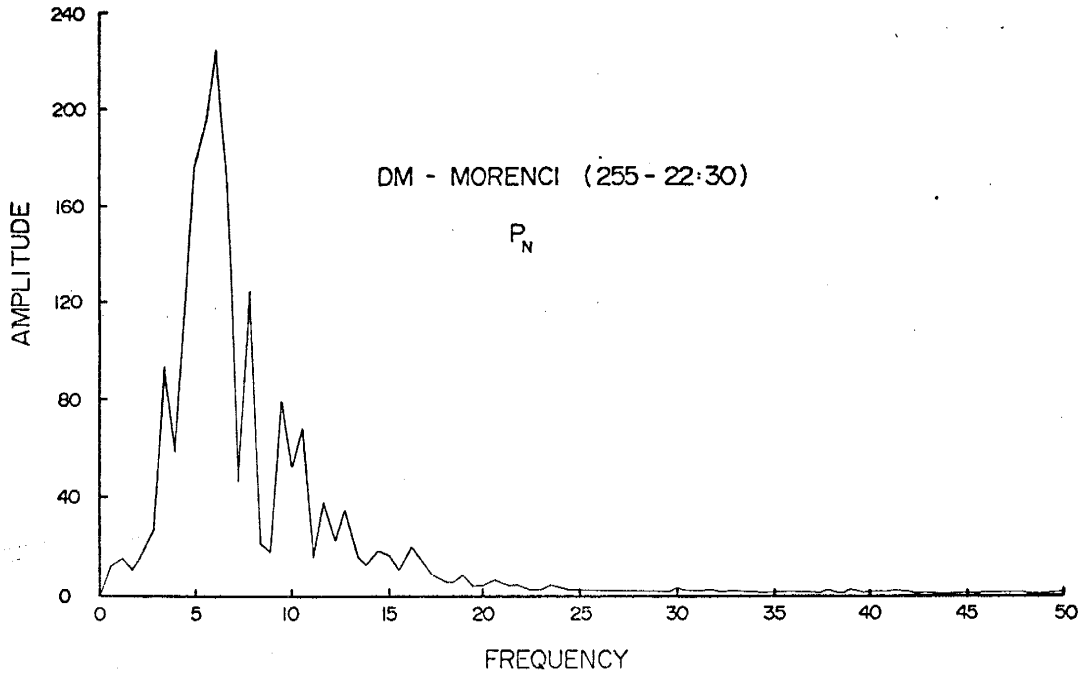

Figure 9. (Continued)

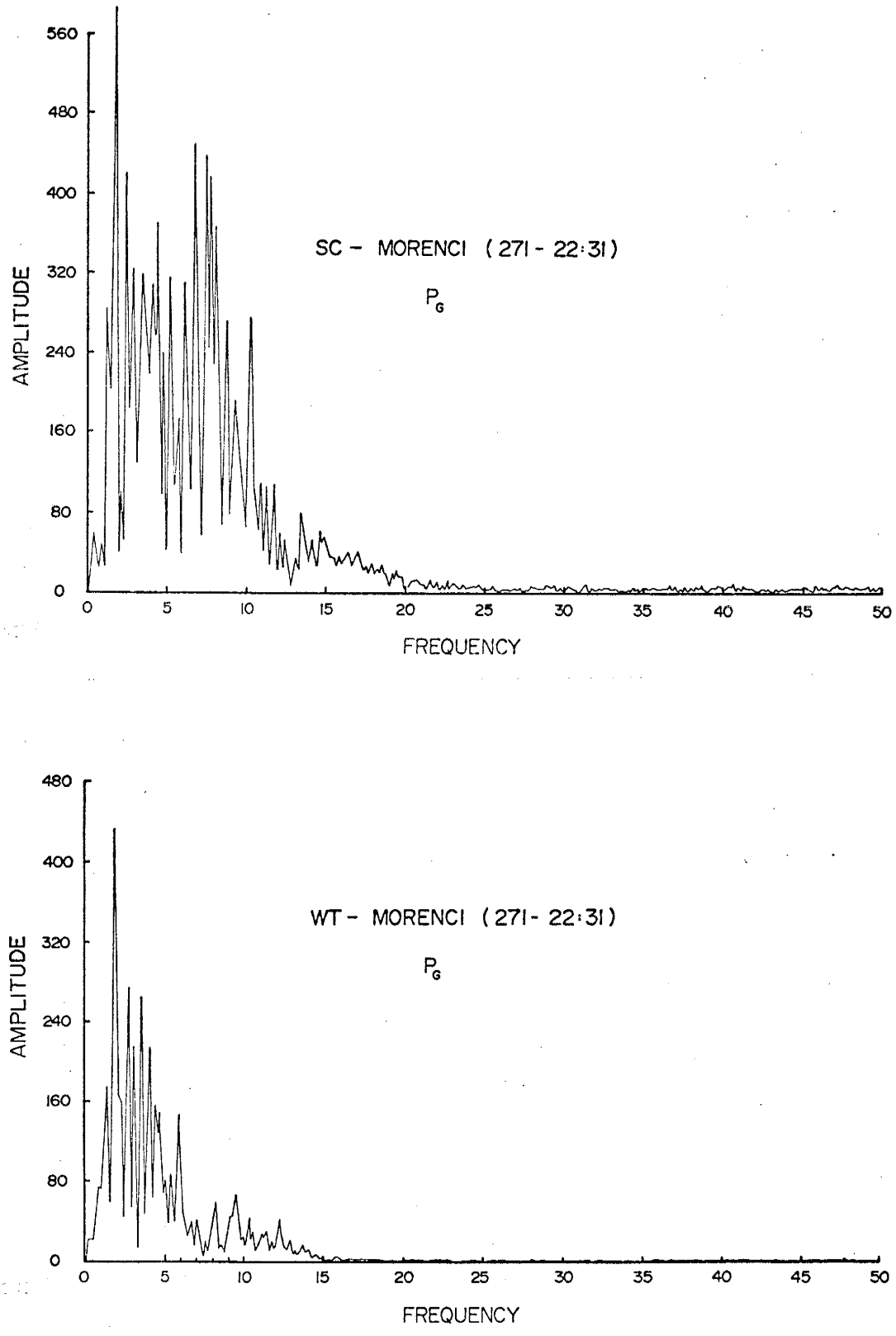

Figure 10. Spectra for the P_g phase from Morenci explosions.

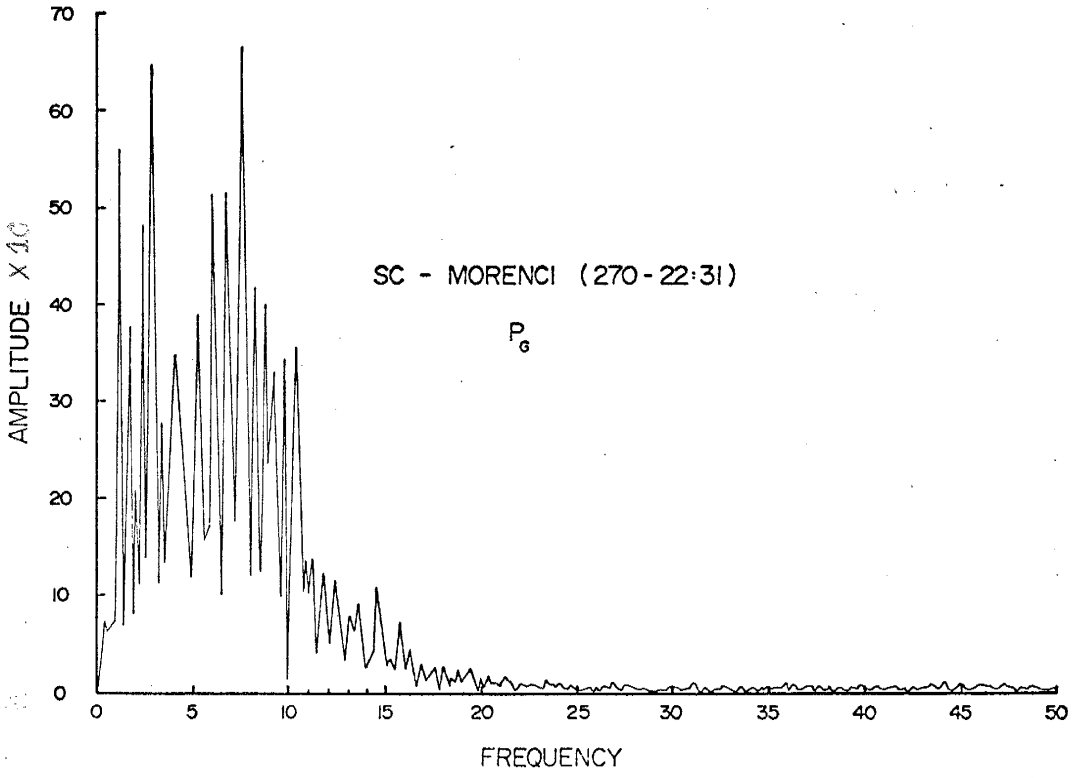

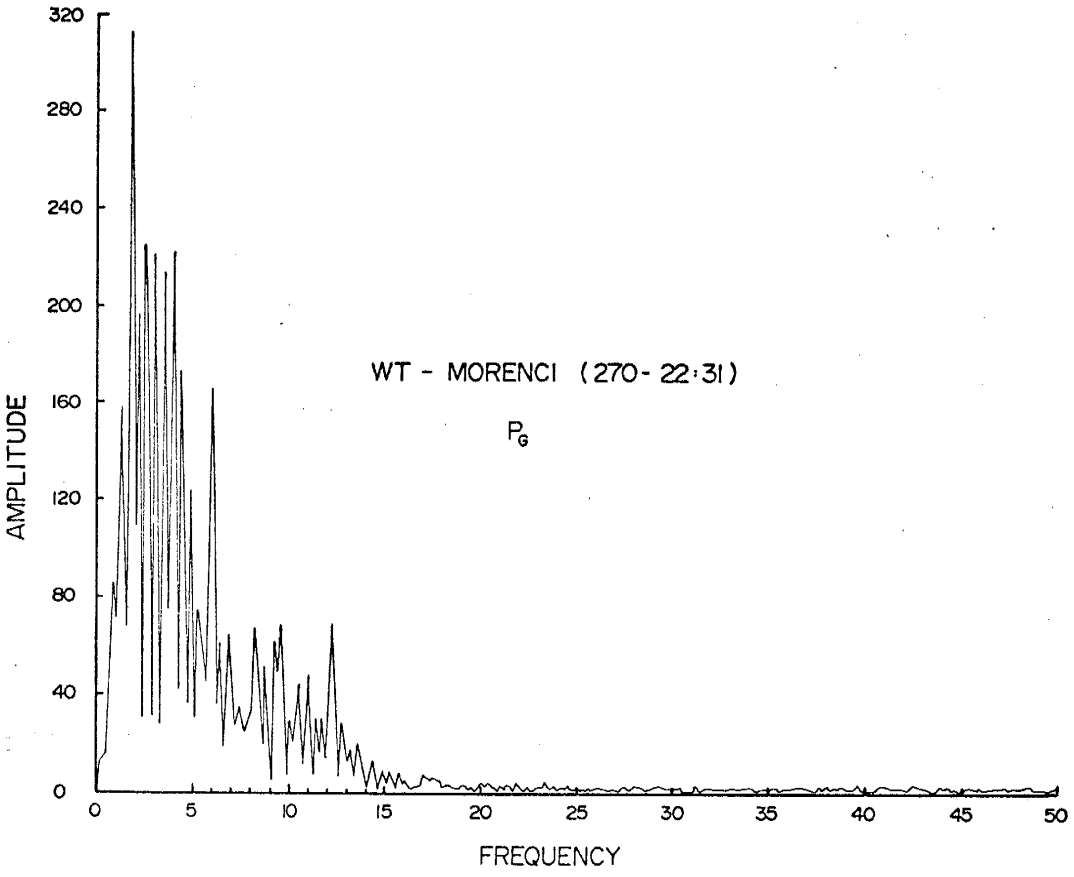

Figure 10. (Continued)

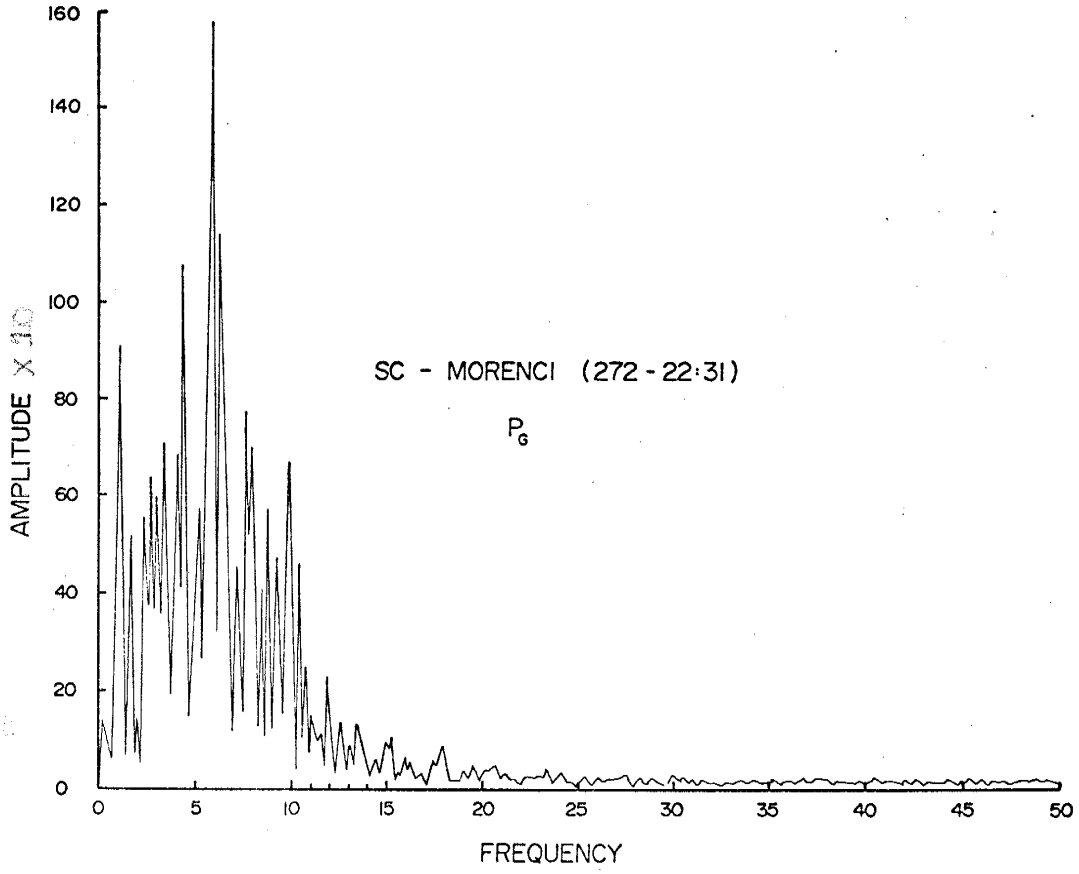

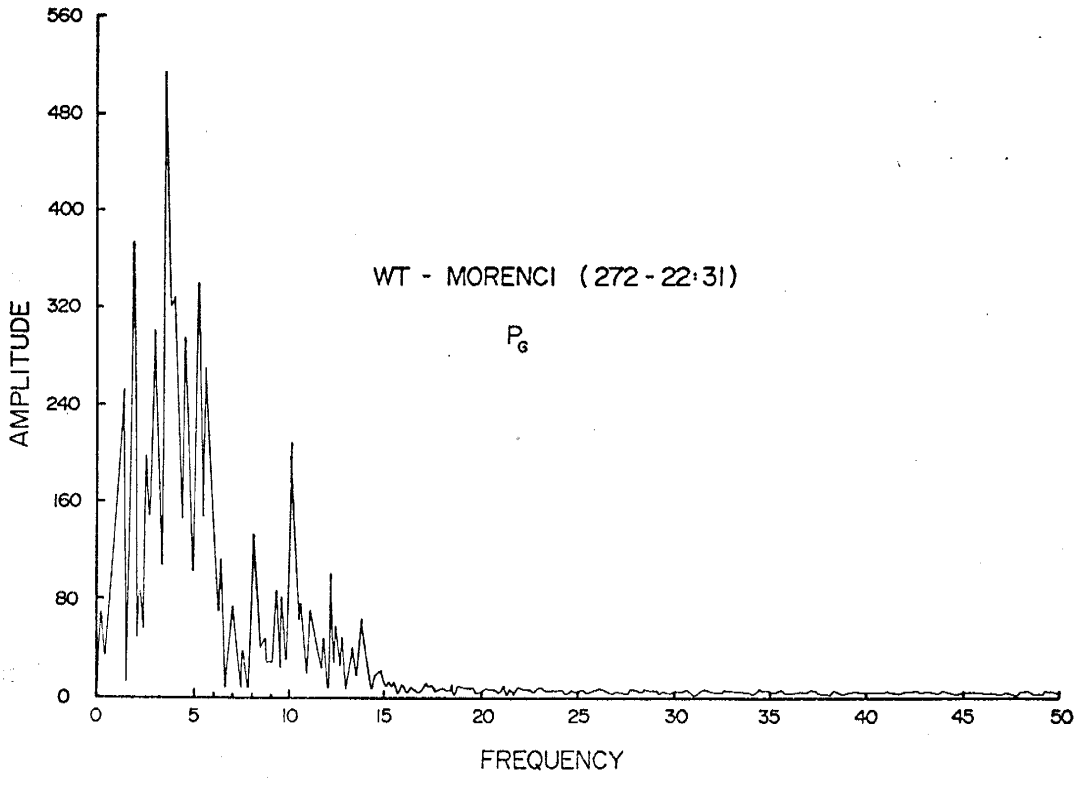

Figure 10. (Continued)

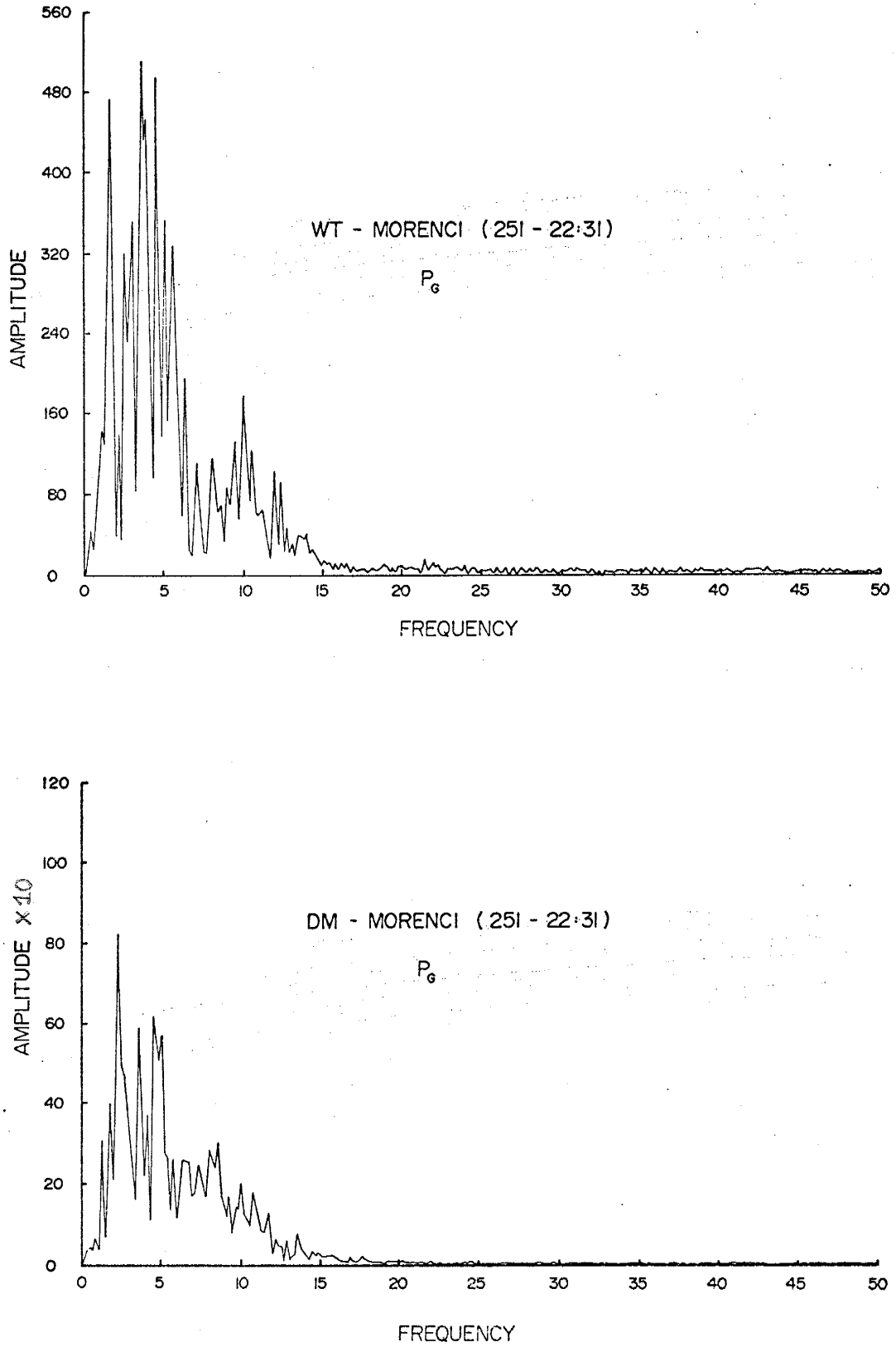

Figure 10. (Continued)

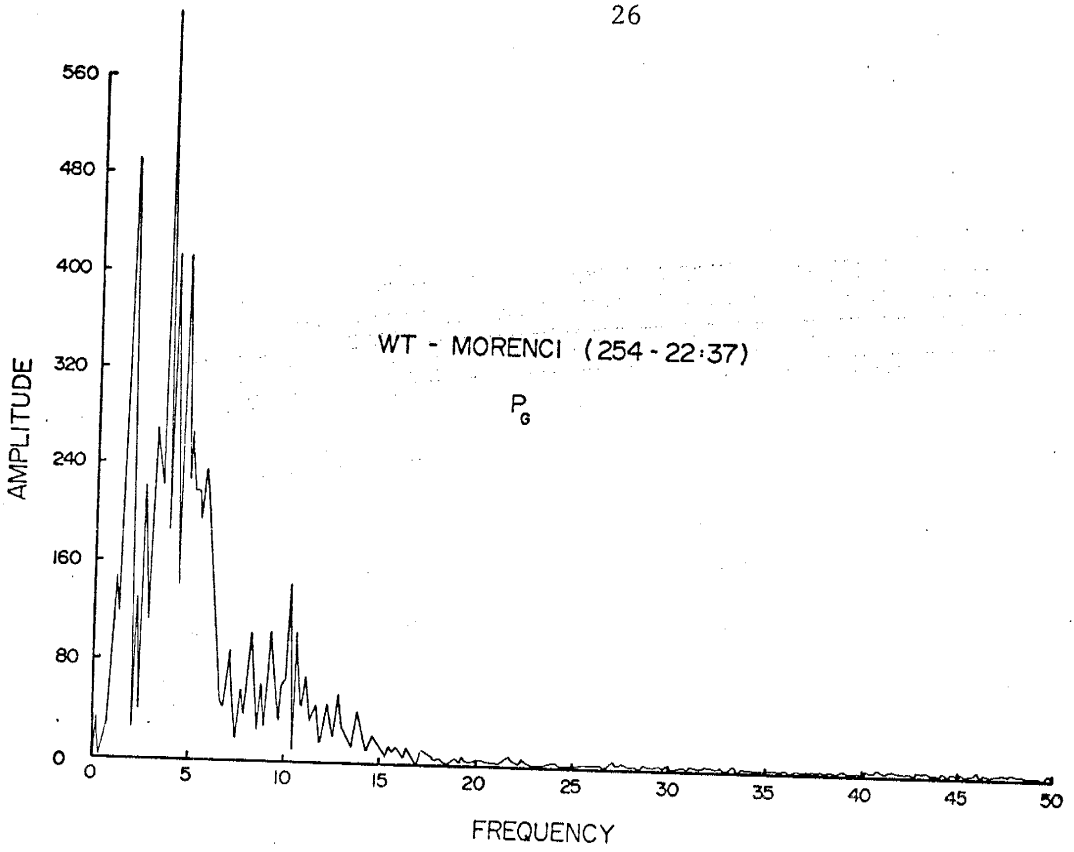

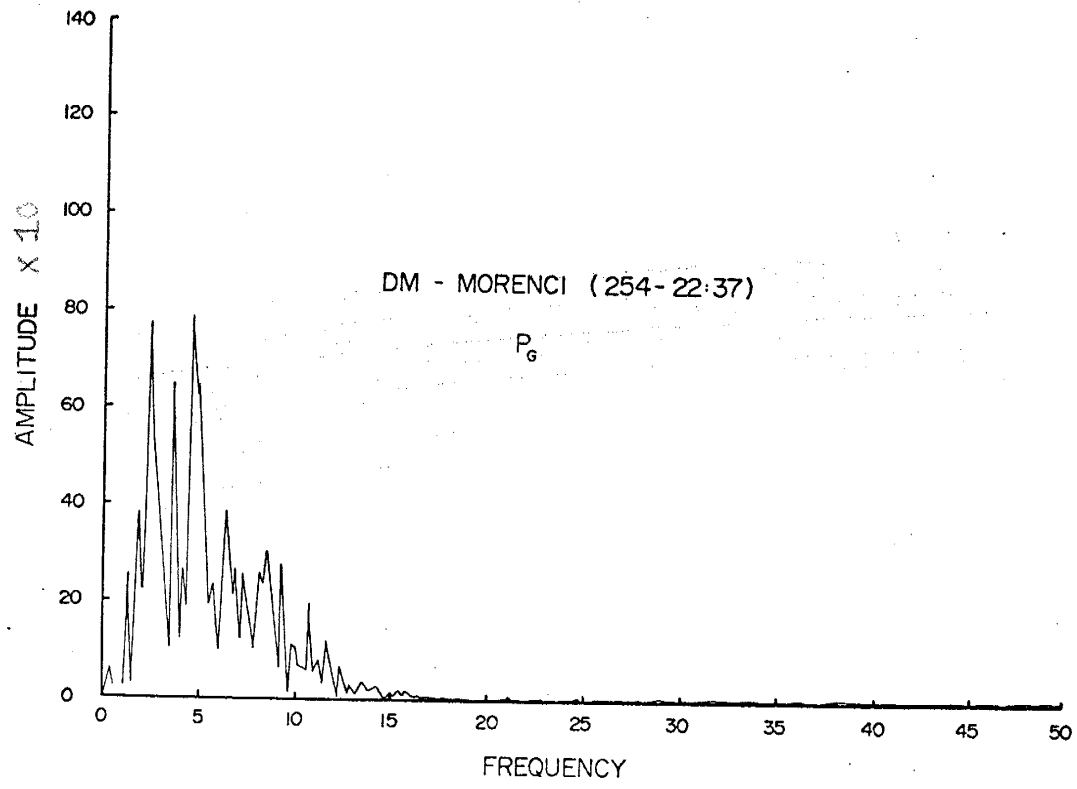

Figure 10. (Continued)

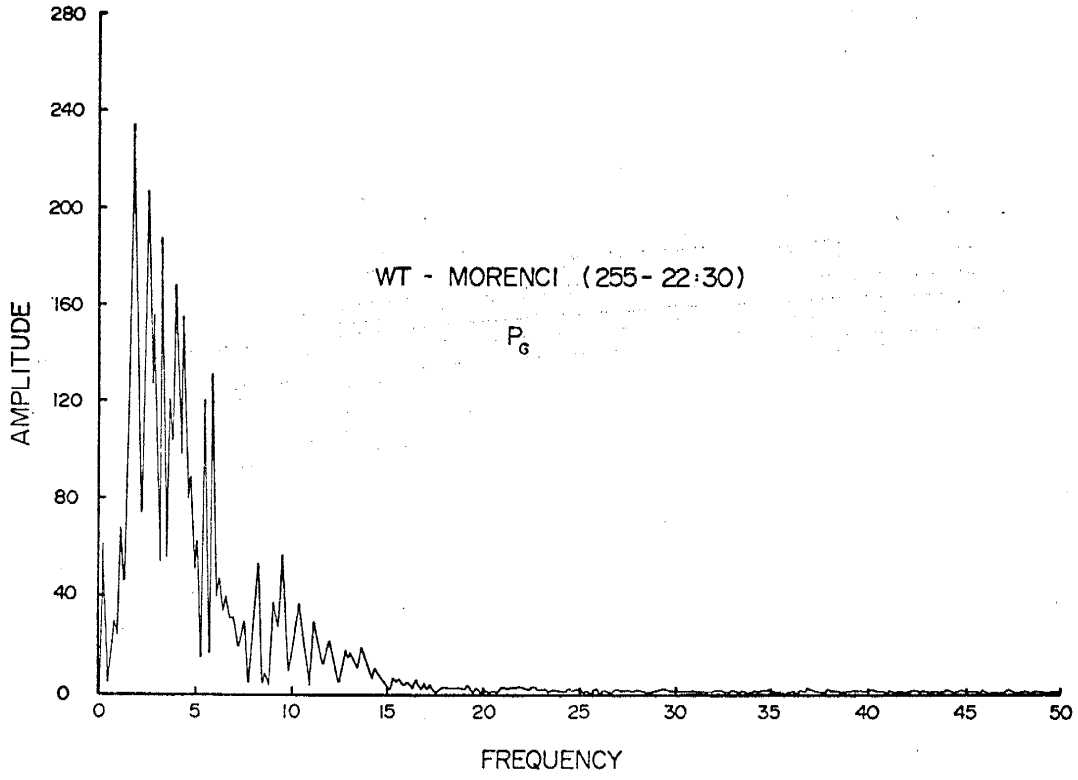

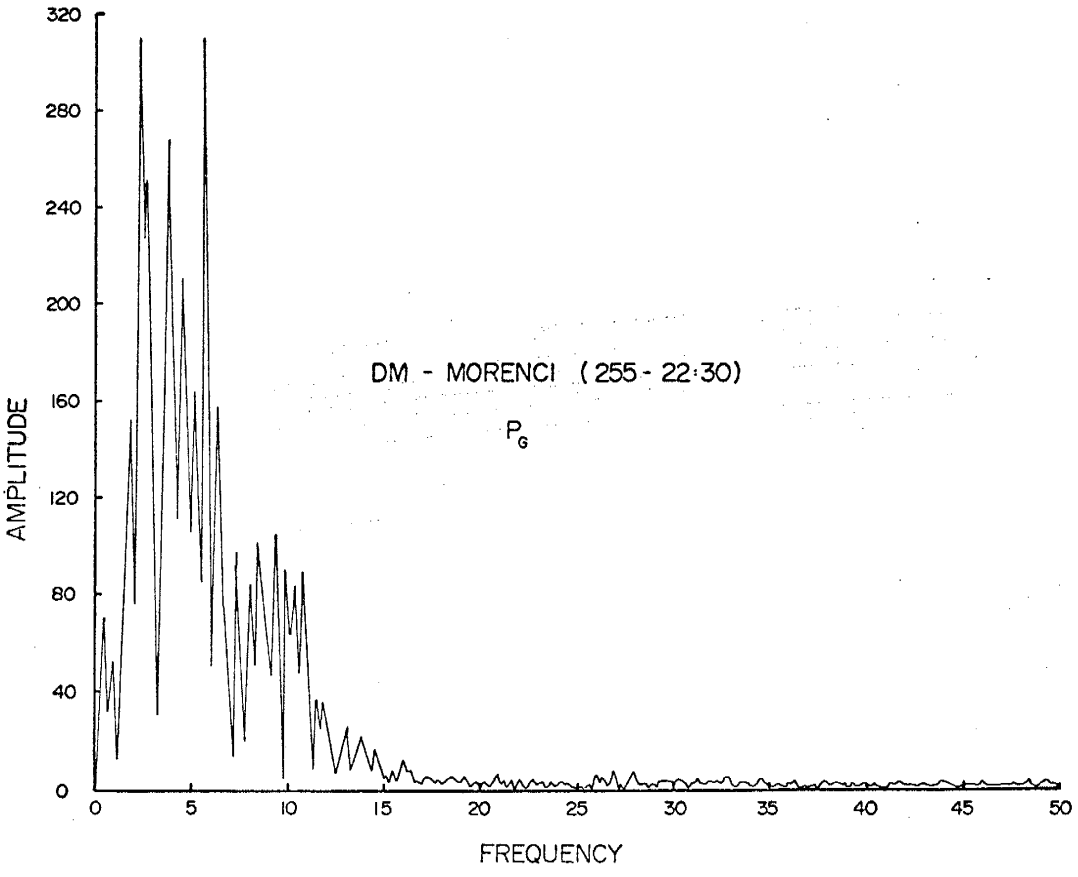

Figure 10. (Continued)

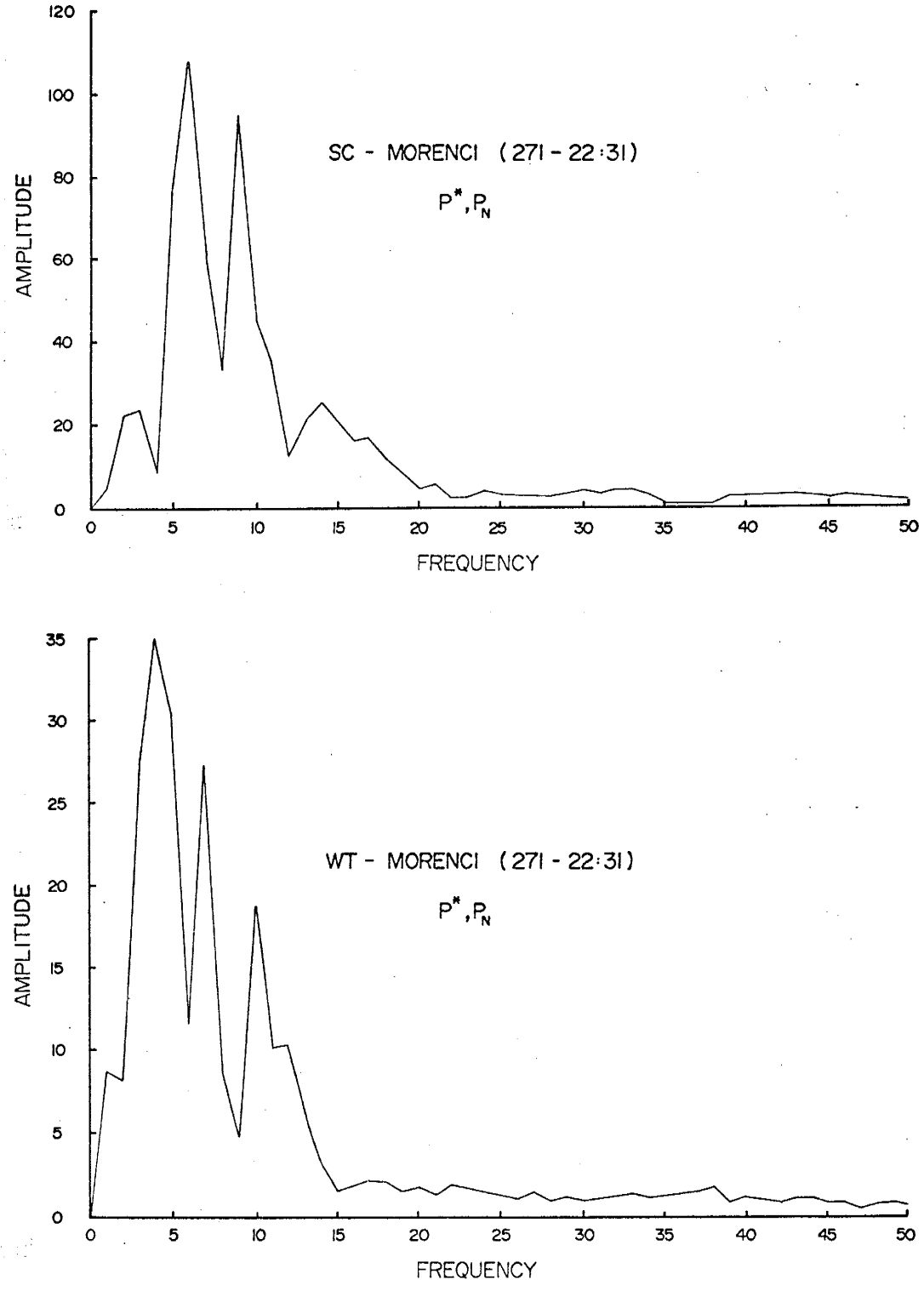

Figure 11. Spectra for the section of the Morenci seismograms containing the P* phase.

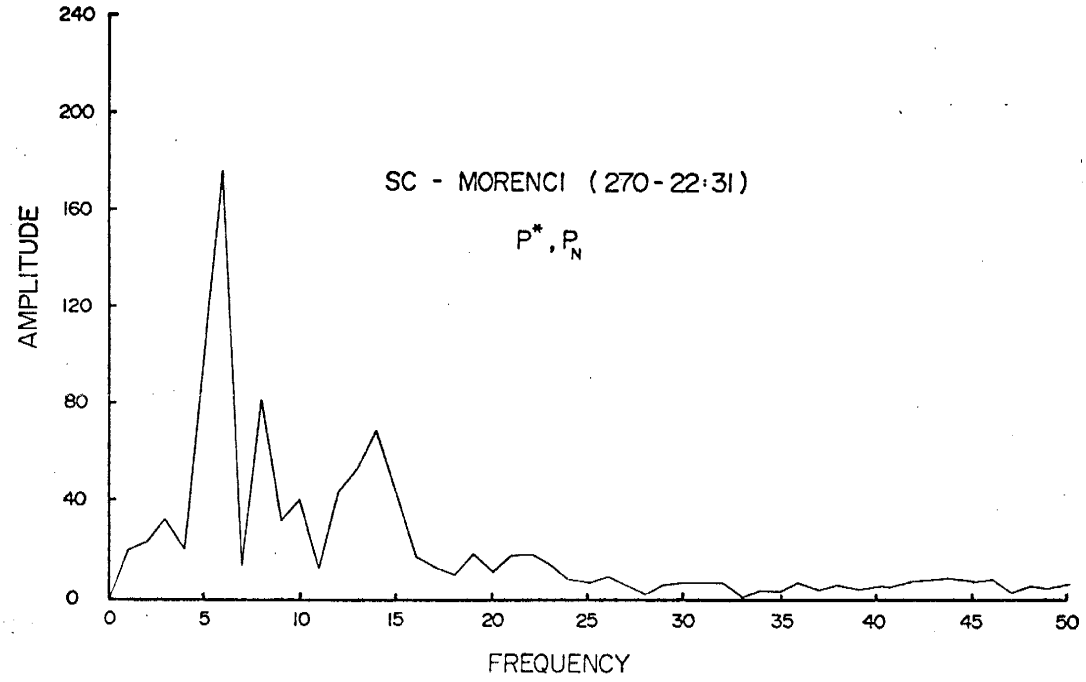

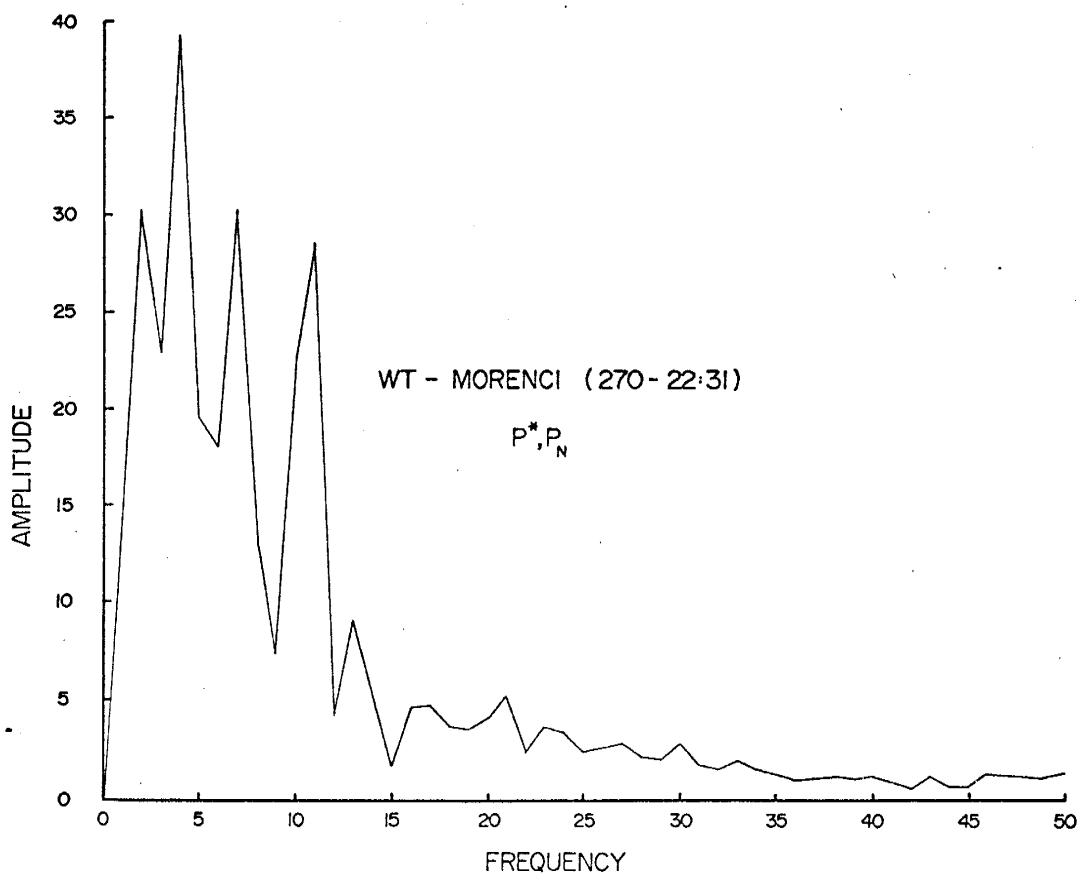

Figure 11. (Continued)

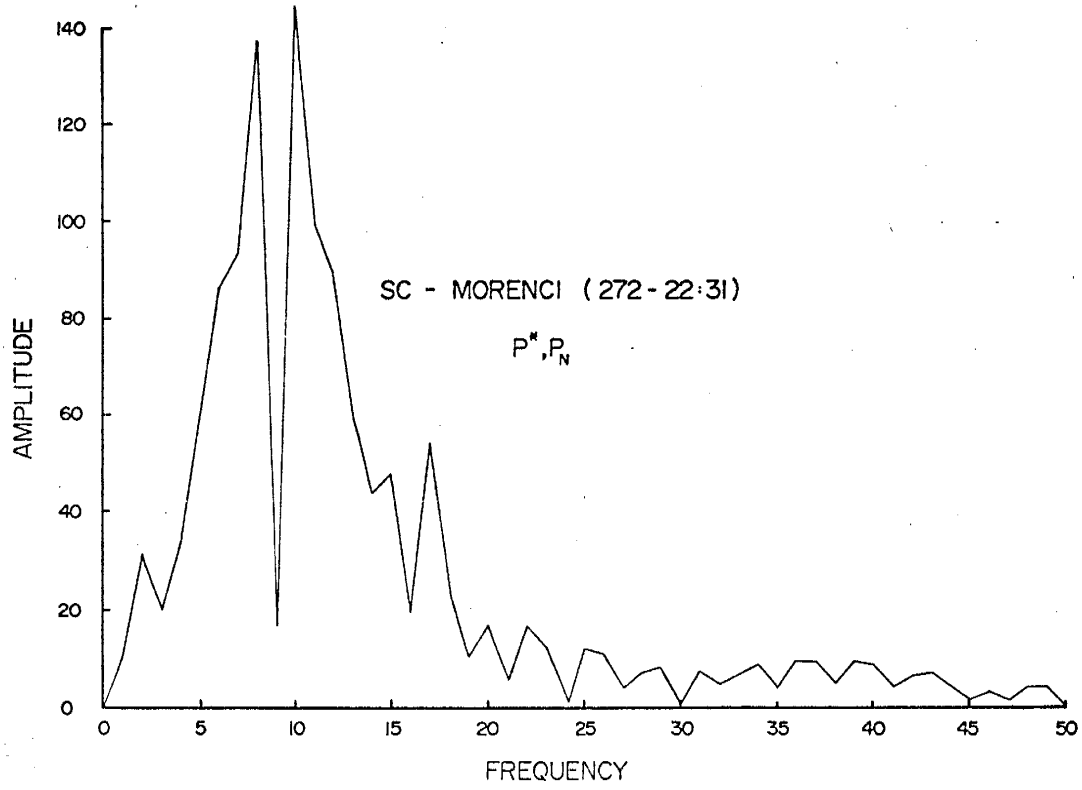

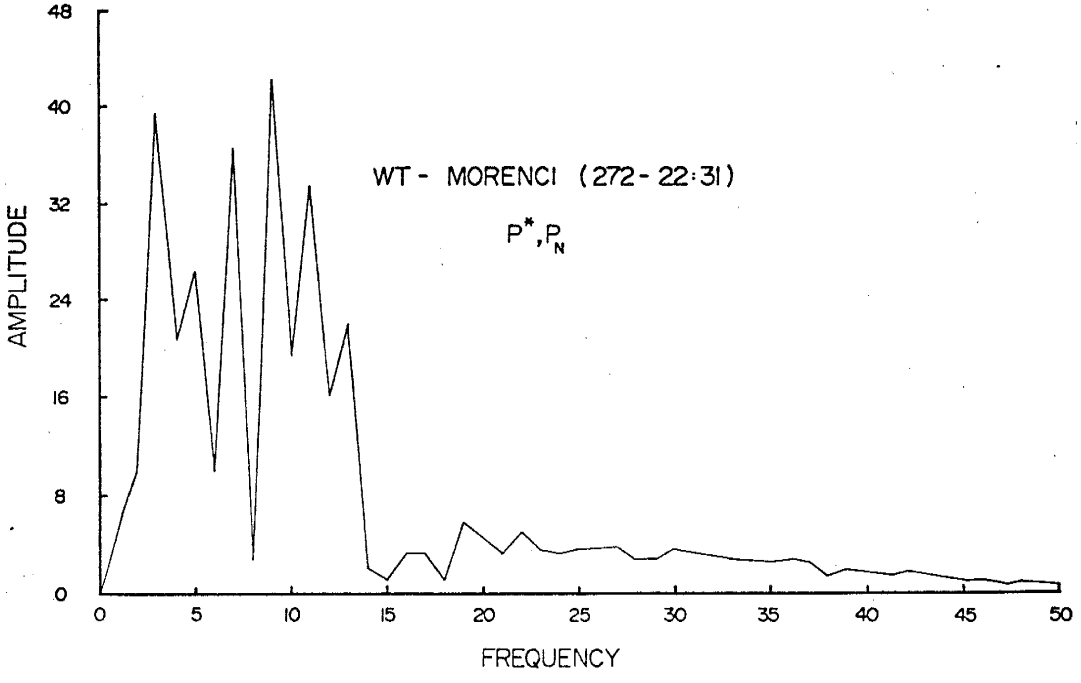

Figure 11. (Continued)

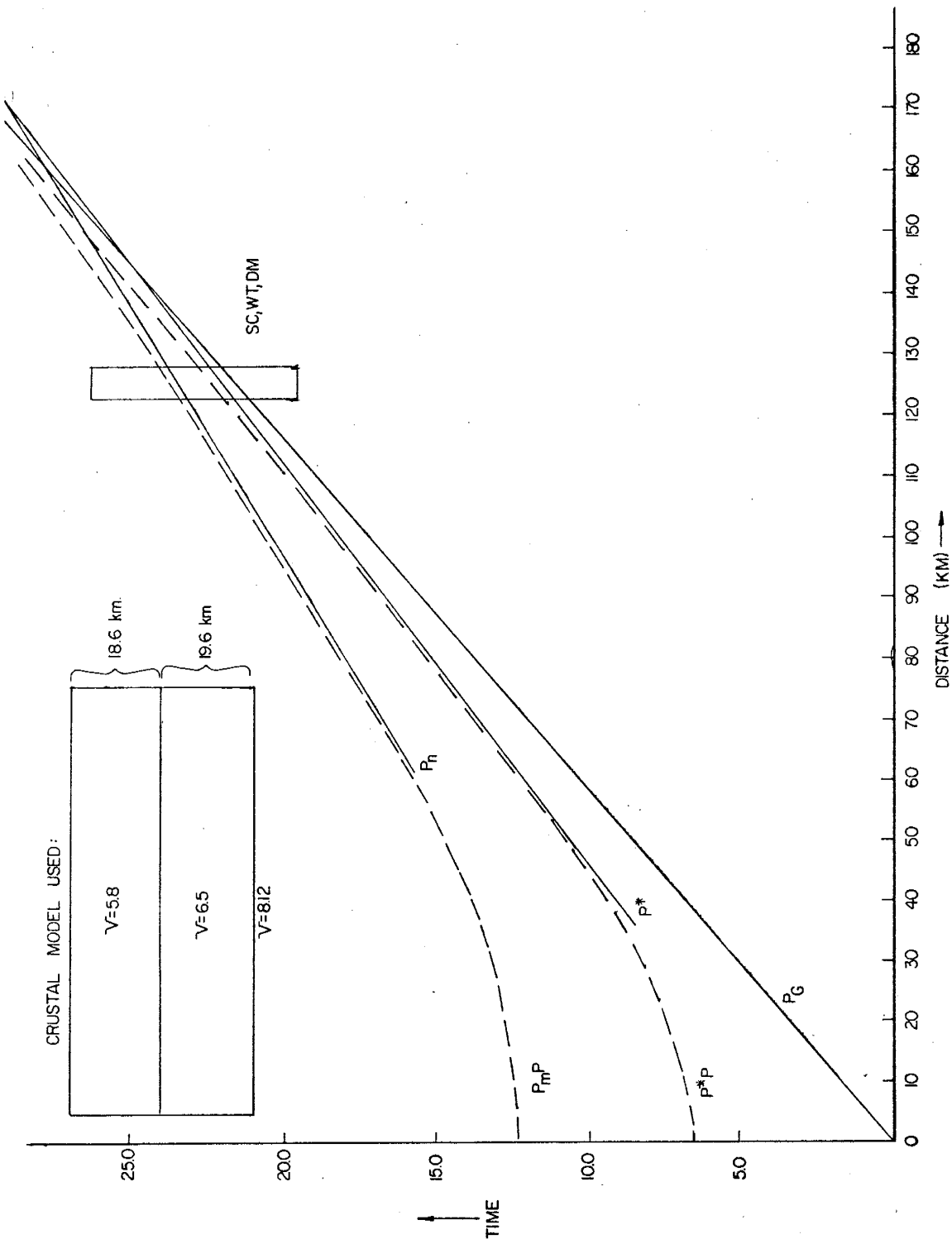

Figure 12. Time-distance curve for P-phases from Jackpile and St. Anthony explosions based on the crustal model given by Toppozada and Sanford (1976).

events computed from the crustal structure obtained from a Gasbuggy refraction profile (Toppozada and Sanford, 1976). Gasbuggy is an applicable crustal profile for Jackpile arrivals because it trends to the NNW of Socorro, only slightly to the east of the propagation paths to Jackpile. The curves in Figure 12 assume that raypaths from Jackpile lie entirely within the rift, such that the upper crust has a velocity of 5.8 km/sec. Figure 13 shows seismograms of Jackpile events recorded at SC, WT and DM with the expected arrivals based on the time-distance curve of Figure 12.

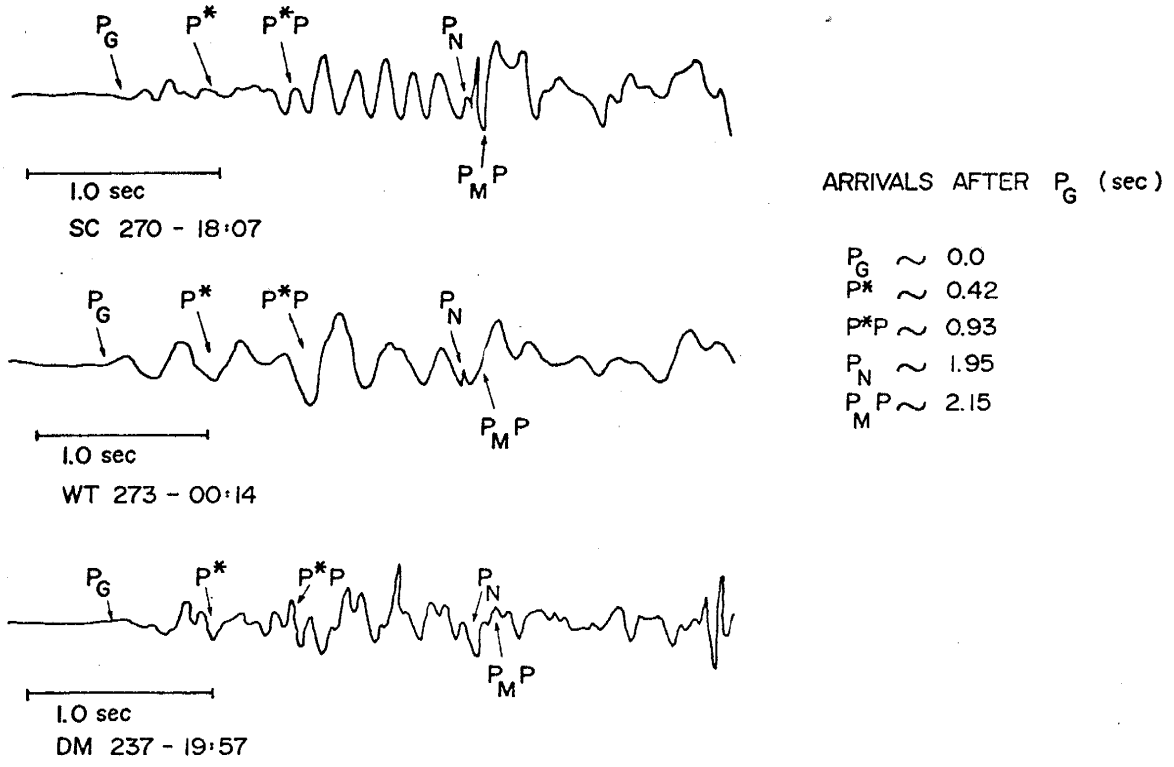

Figure 13. Seismograms for Jackpile events recorded at stations SC, Wt and DM.

It is evident that a strong arrival 2.0 sec. after P_g at station SC is the Moho reflection, since the P_n phase should be much weaker than any reflected phase. Another strong arrival is the Conrad reflection at 1.0 sec. after P_g. The intervals over which spectra were obtained were (1) 0.0 to 1.0 seconds for P_g (2) 0.0 to 1.93 seconds for P_g and P*P and (3) 2.0 to 4.0 seconds for P_mP. Figure 14 shows the spectra for the first 1.0 sec. for three Jackpile and one St. Anthony events recorded at WT and DM. Figure 15 shows the spectra for the first 1.93 sec. for two Jackpile events recorded at SC and WT. Figure 16 shows the spectra for the P_mP phase for the two Jackpile events recorded at SC-WT and Figure 17 shows the P_mP spectra for one St. Anthony and one Jackpile event recorded at WT and DM.

Spectra were smoothed by a moving average of amplitudes over a frequency span of 2.0 Hz. The number of amplitude samples per Hz for the spectra increases with record length and thus spectra for the long records are more detailed than the short records. For this reason, a 13 point moving average was applied to a record of 550 samples and a 5 point moving average for a record of 200 samples.

Amplitude ratios of the various phases for the station pairs were taken from the smoothed spectra at discrete frequencies. Shown in Figures 18 and 19 are the $\log_e$ SC/WT and $\log_e$ DM/WT ratio plots for Morenci P_n. The error bars are based on the assumption that the ratios are normally distributed. Figures 20 and 21 are the $\log_e$ SC/WT and $\log_e$ DM/WT ratio plots for the Morenci P_g phase. Figure 22 is the $\log_e$ SC/WT ratio plot for the Morenci P*. Figures 23 and 24 are the $\log_e$ SC/WT plots for the (1) P_g and P*P arrivals and (2) the P_mP arrival for two Jackpile events. Figures 25 and 26 are the $\log_e$ DM/WT plots for (1) P_g of three Jackpile events and one St. Anthony event and (2) the P_mP for one Jackpile and one St. Anthony event.

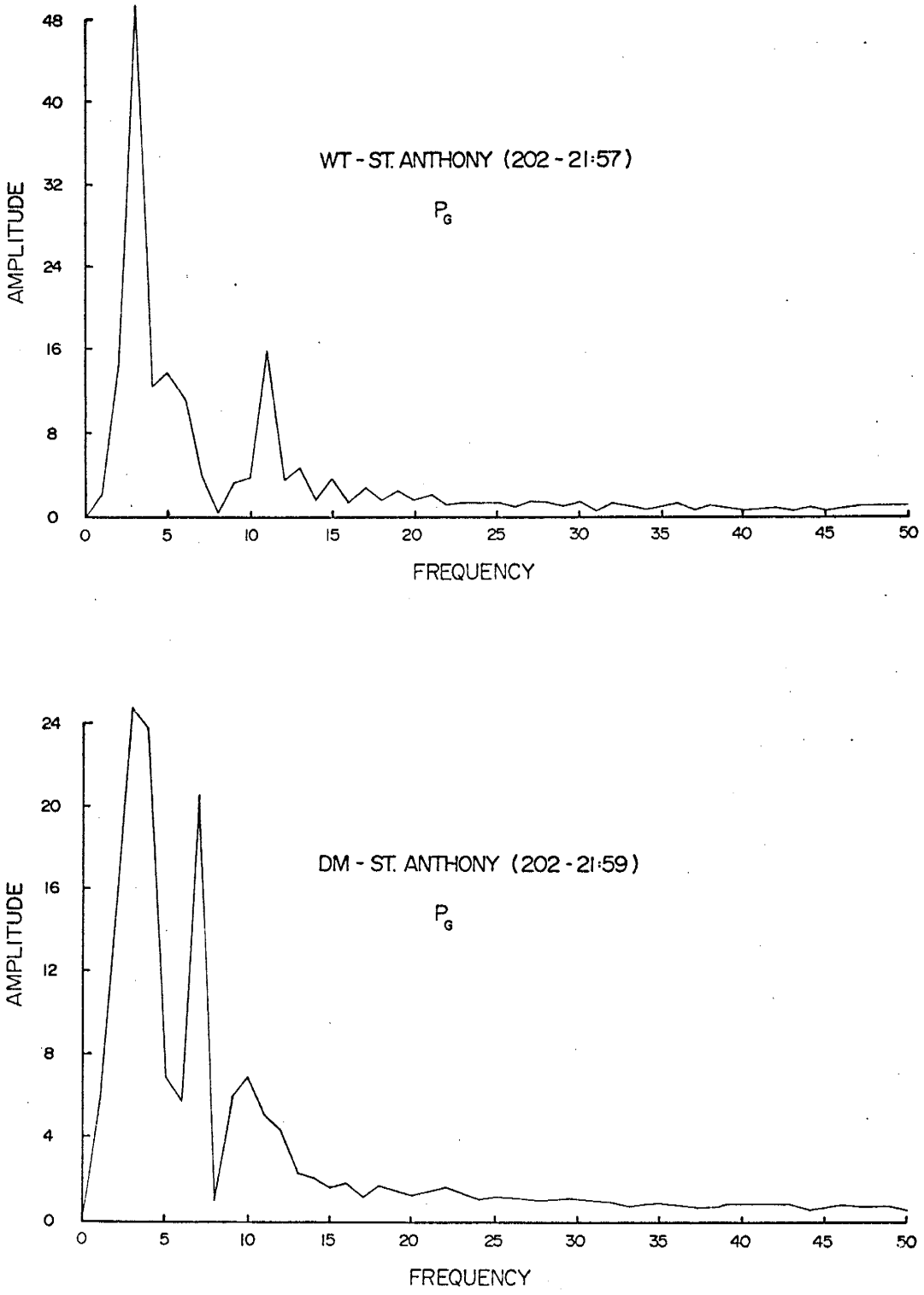

Figure 14. Spectra for the P_g phase from Jackpile and St. Anthony explosions.

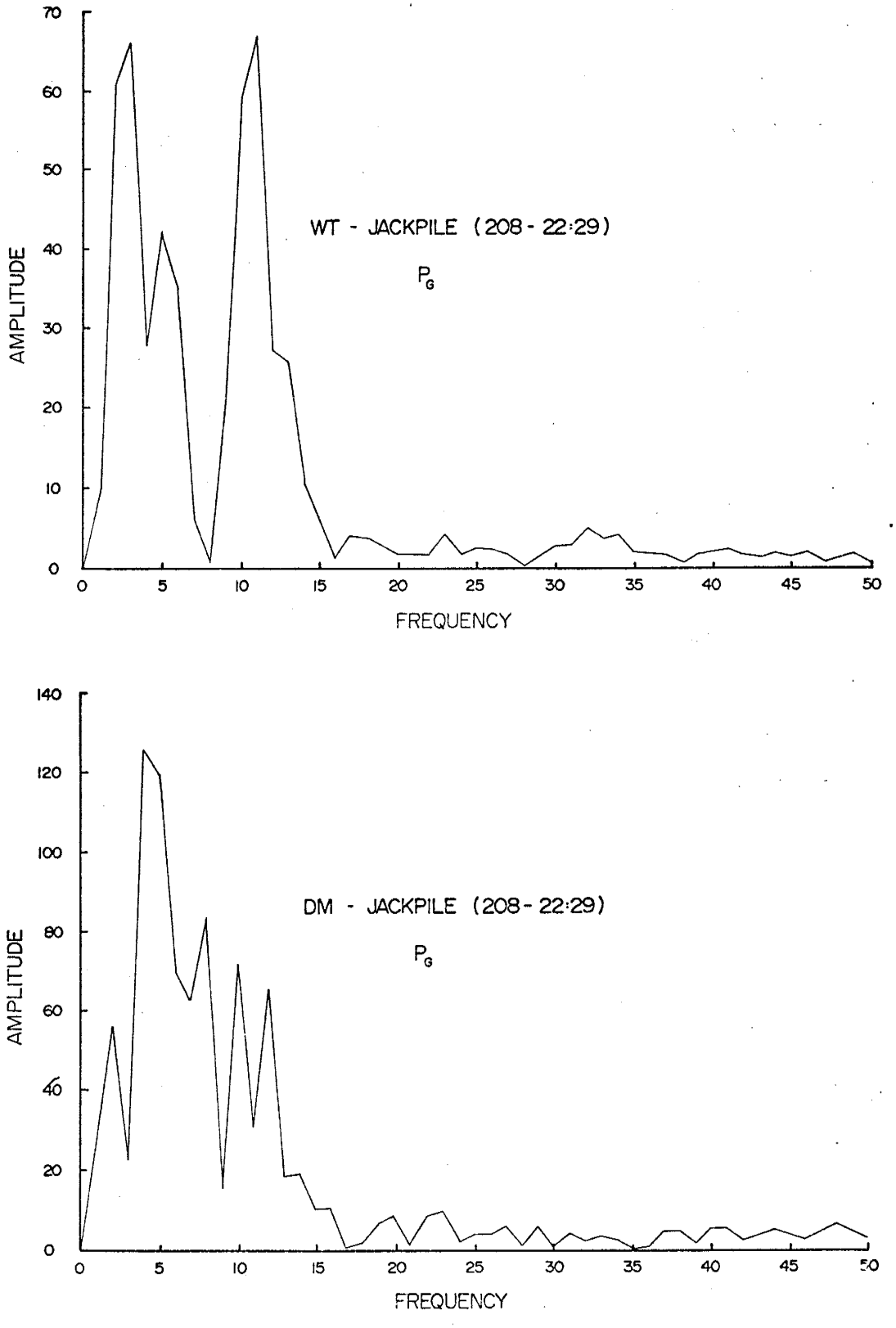

Figure 14. (Continued)

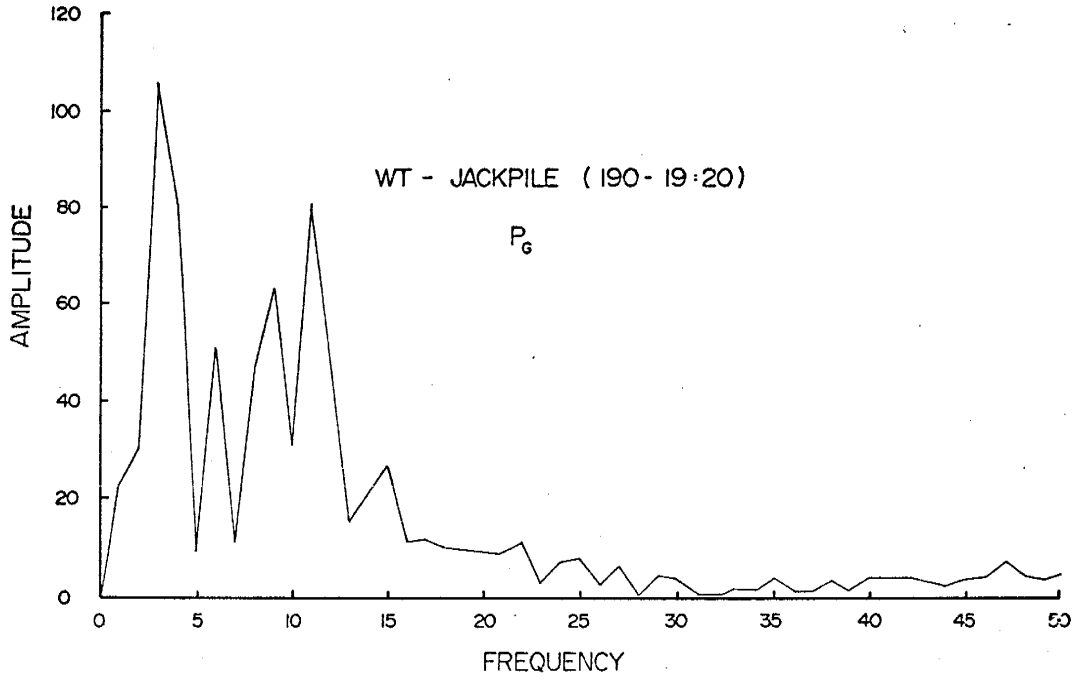

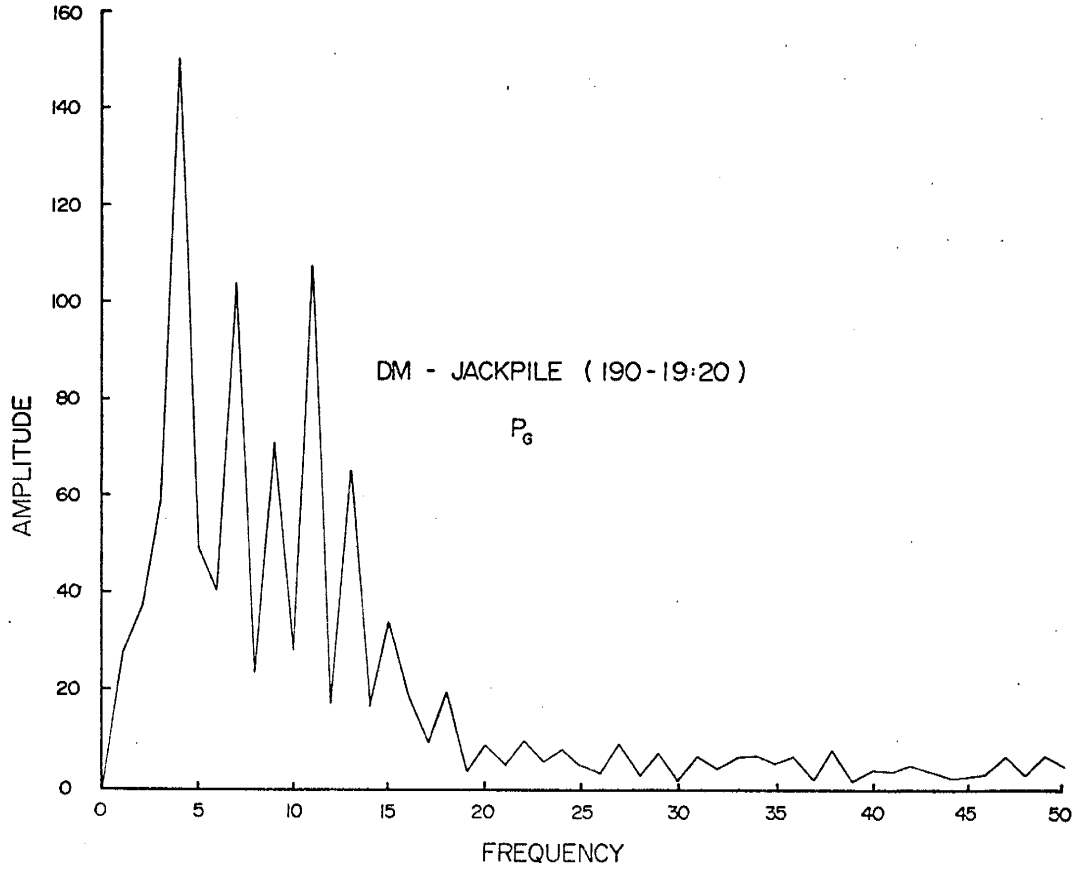

Figure 14. (Continued)

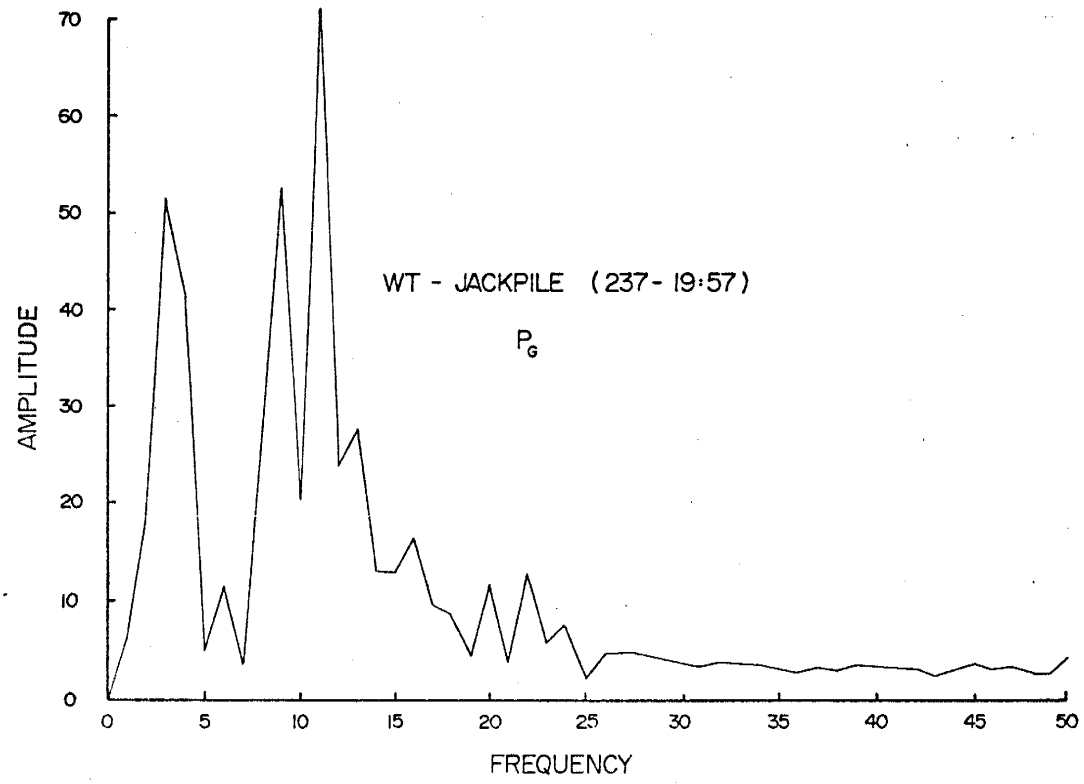

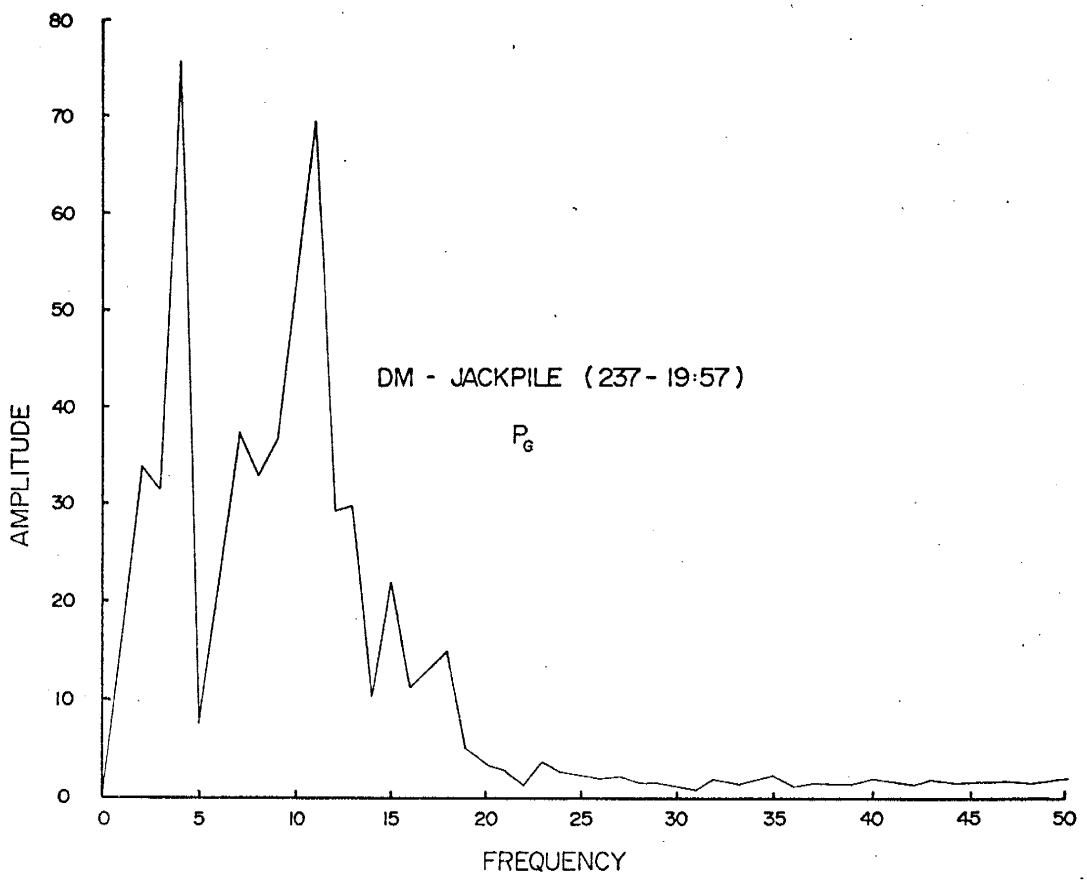

Figure 14. (Continued)

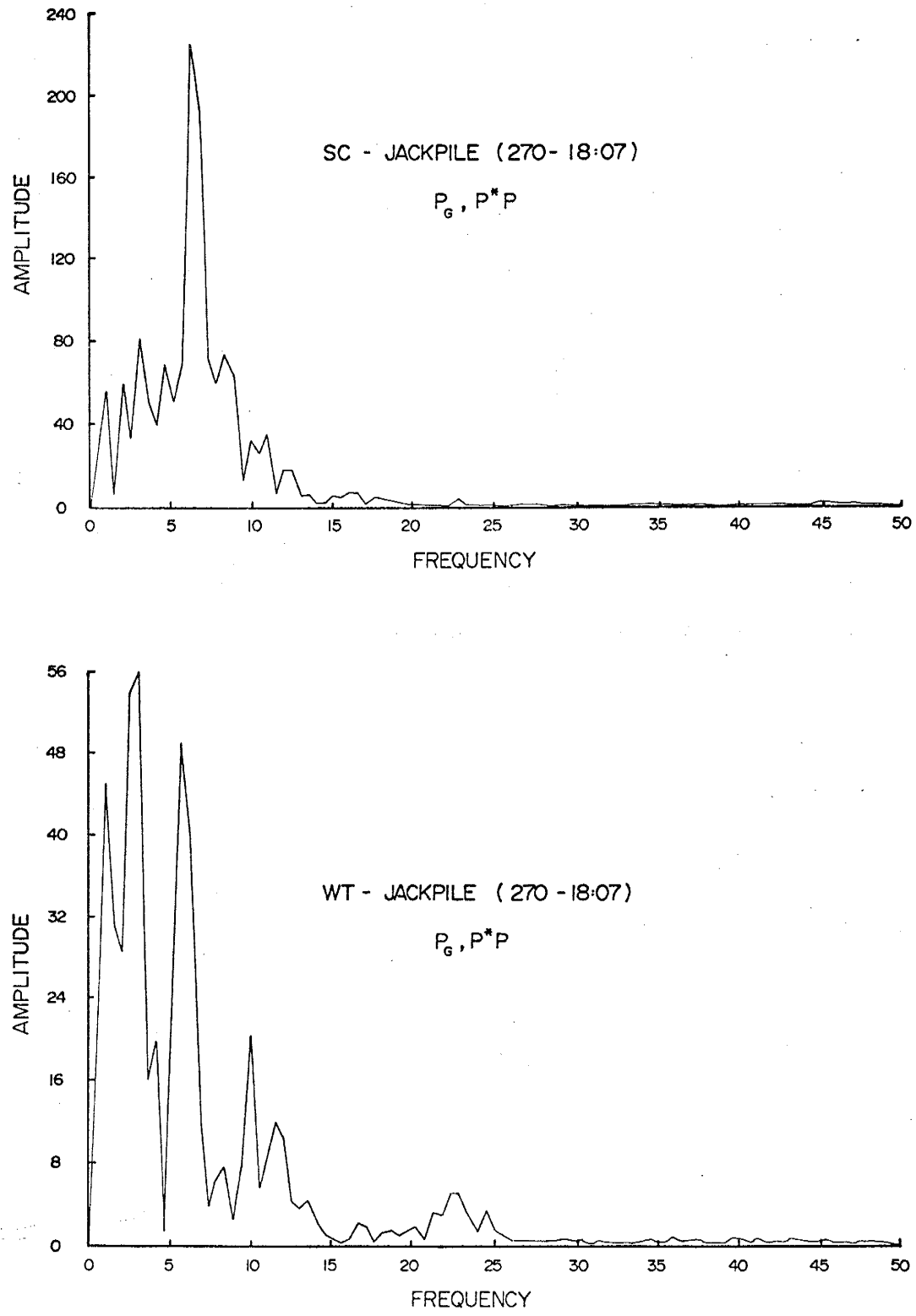

Figure 15. Spectra for the P_g and P*P phases from Jackpile explosions.

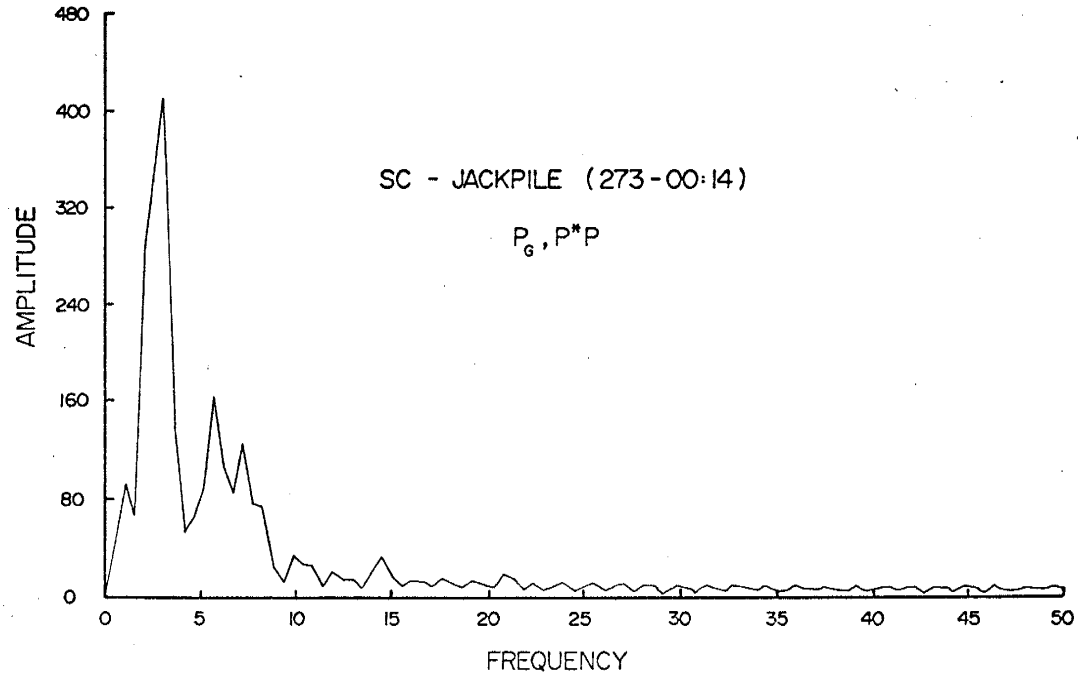

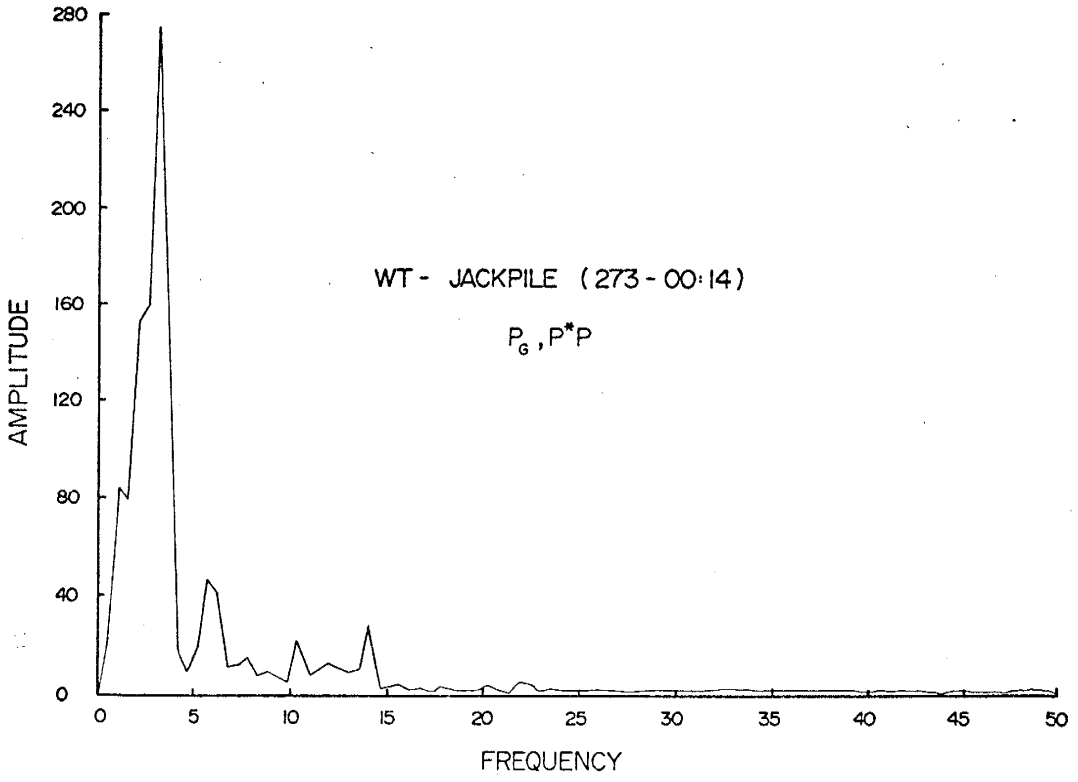

Figure 15. (Continued)

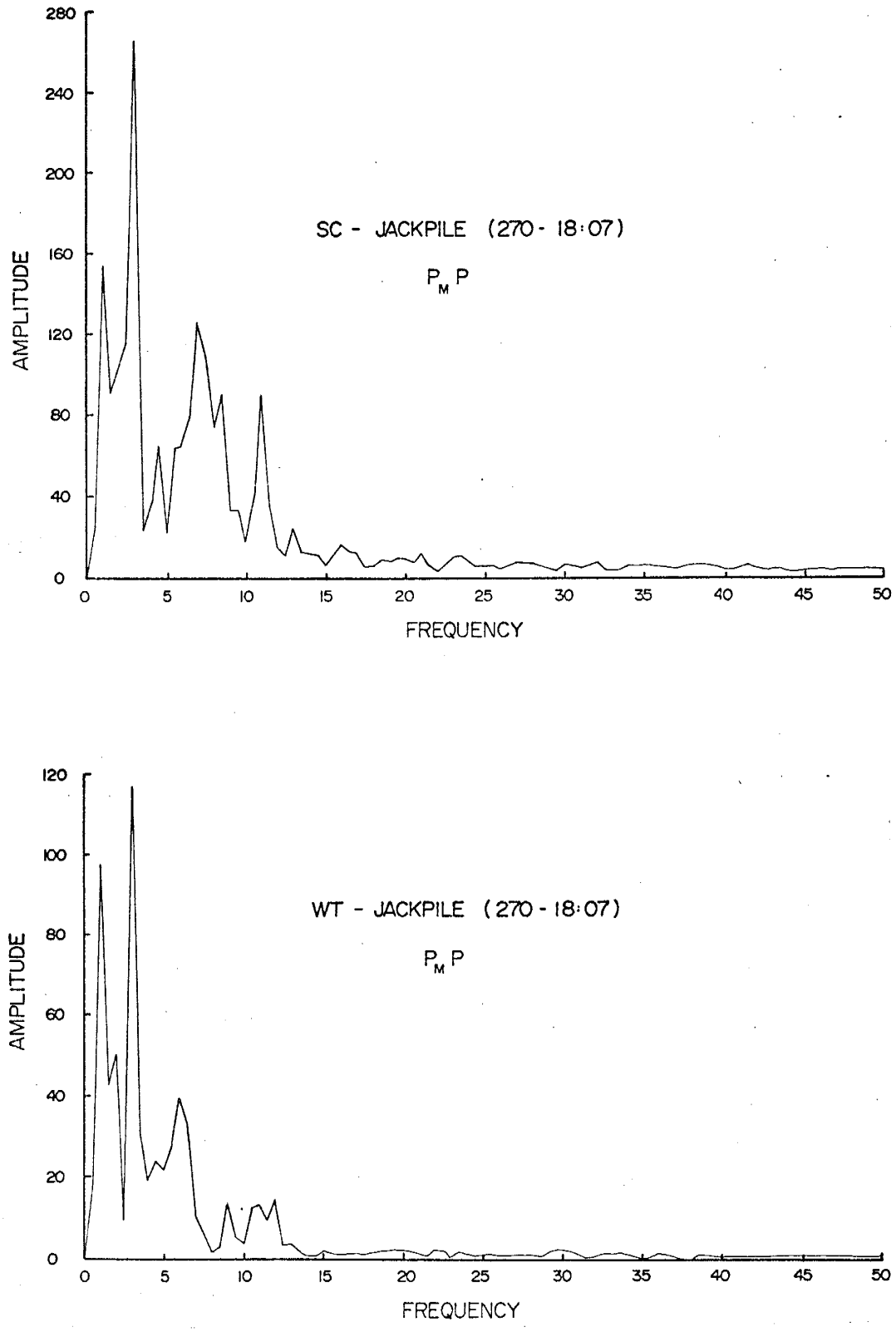

Figure 16. Spectra for the P_mP phase from Jackpile explosions.

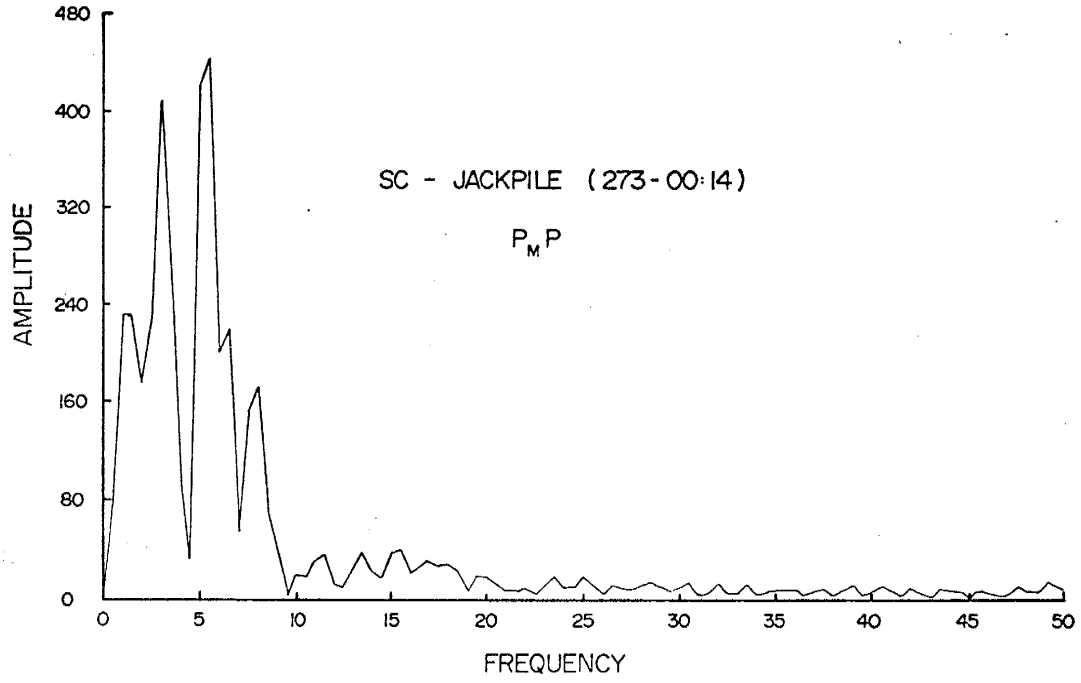

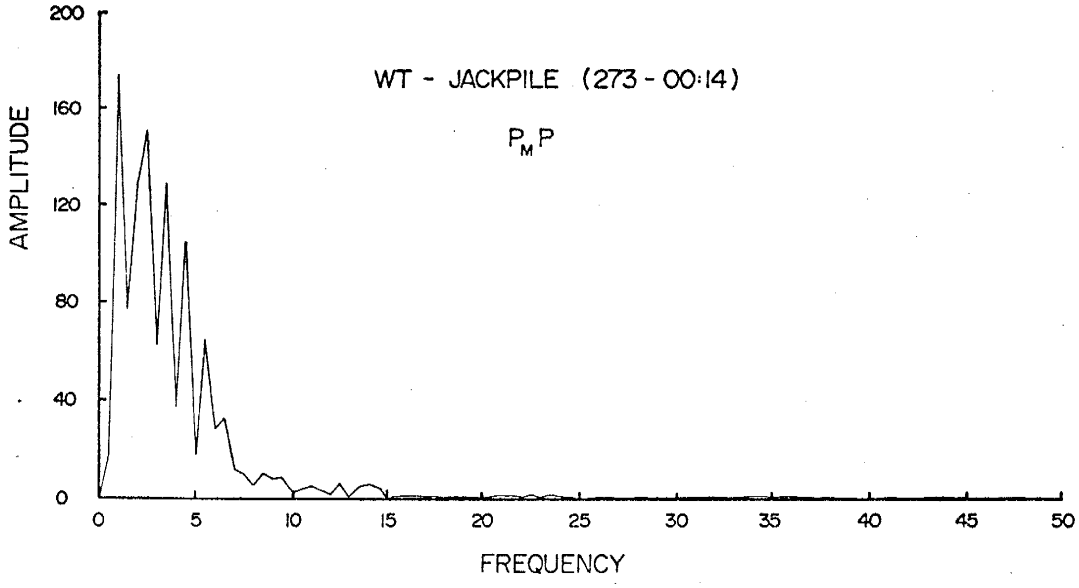

Figure 16. (Continued)

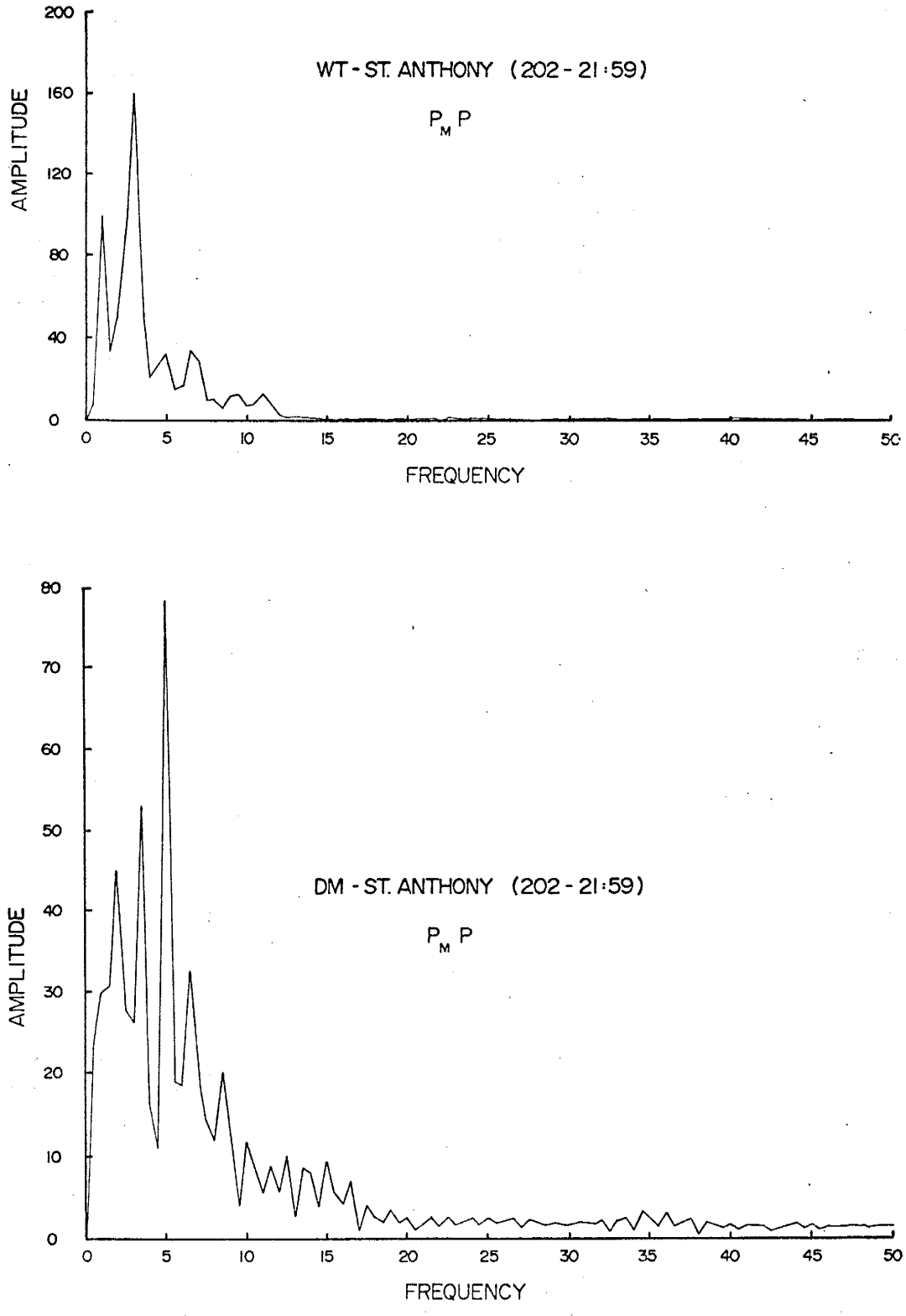

Figure 17. Spectra for the P_mP phase from Jackpile and St. Anthony explosions.

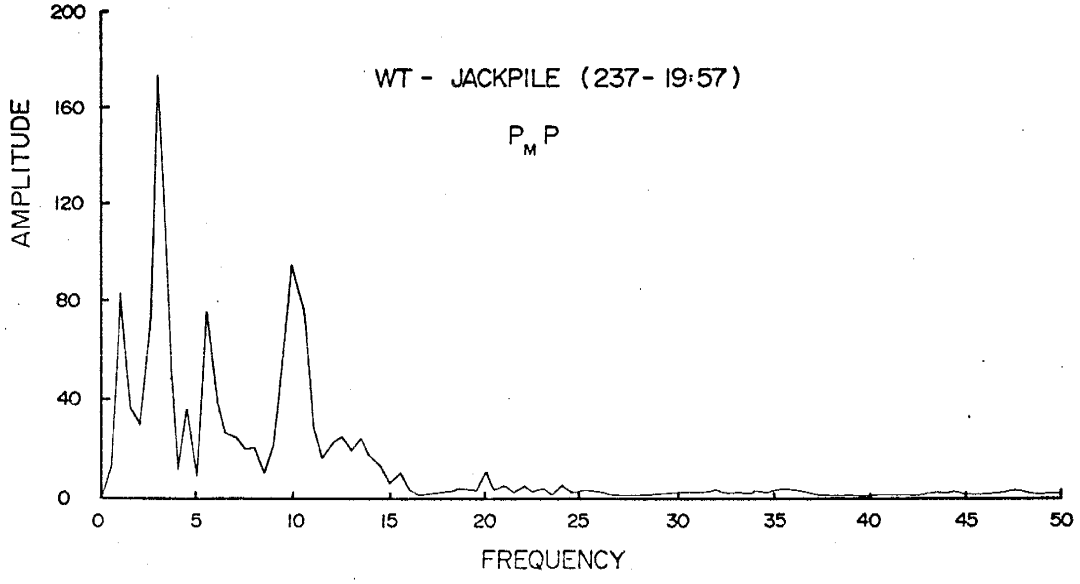

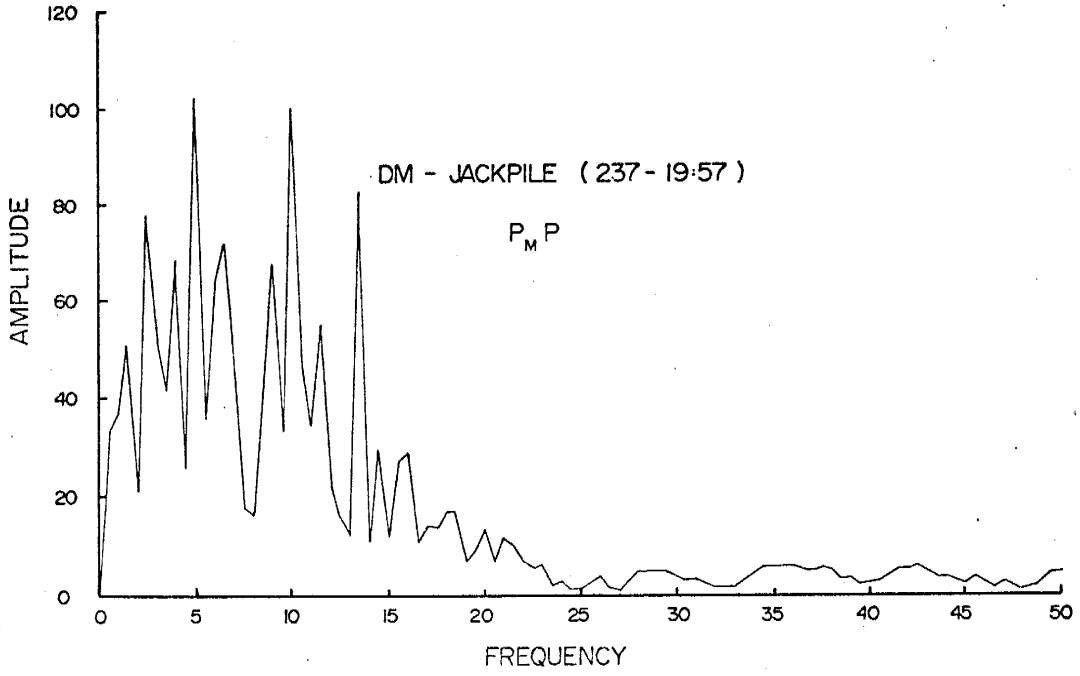

Figure 17. (Continued)

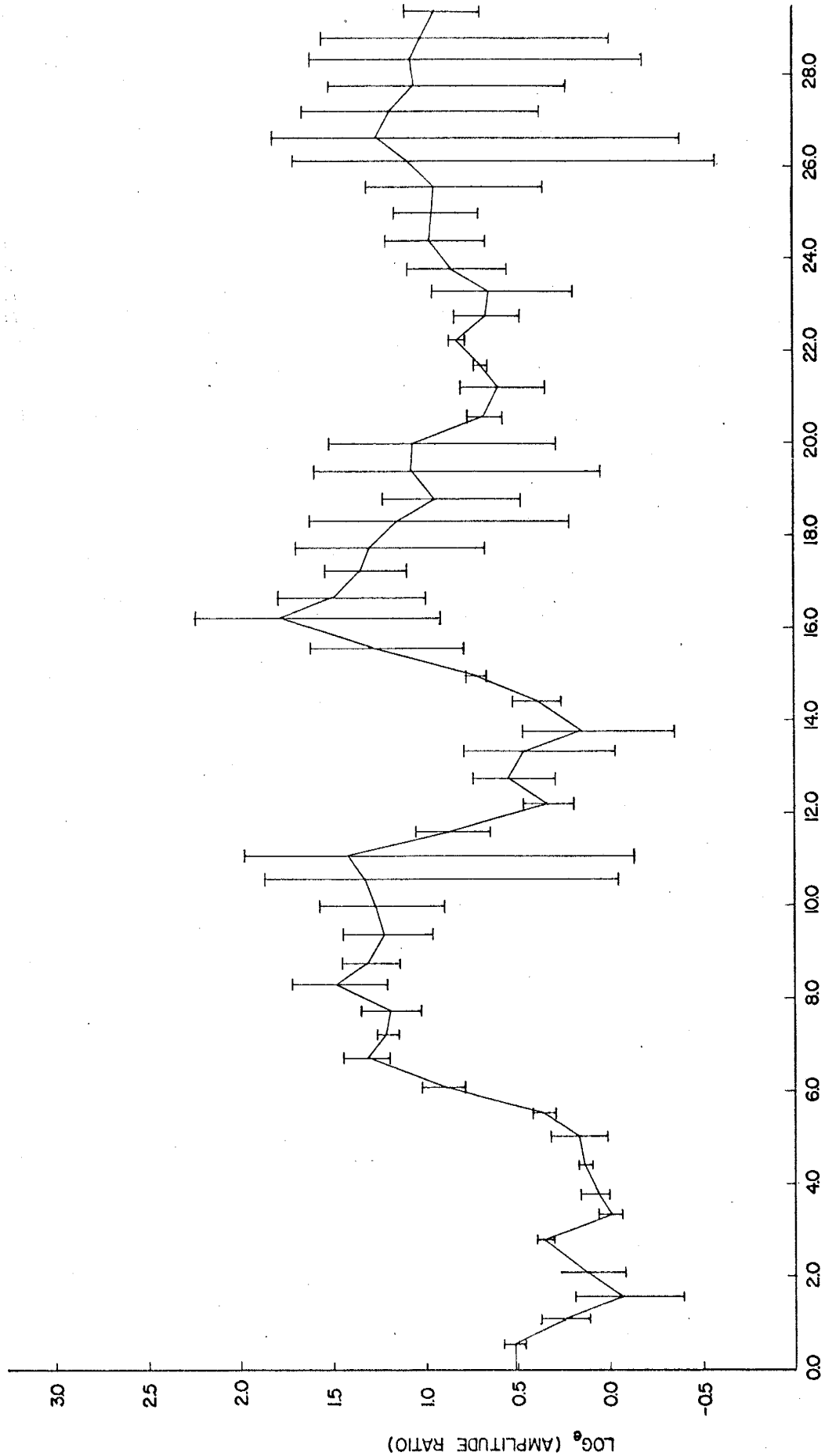

Figure 18. Values of $\log_e$ SC/WT versus frequency for the P_n phase from two Morenci explosions.

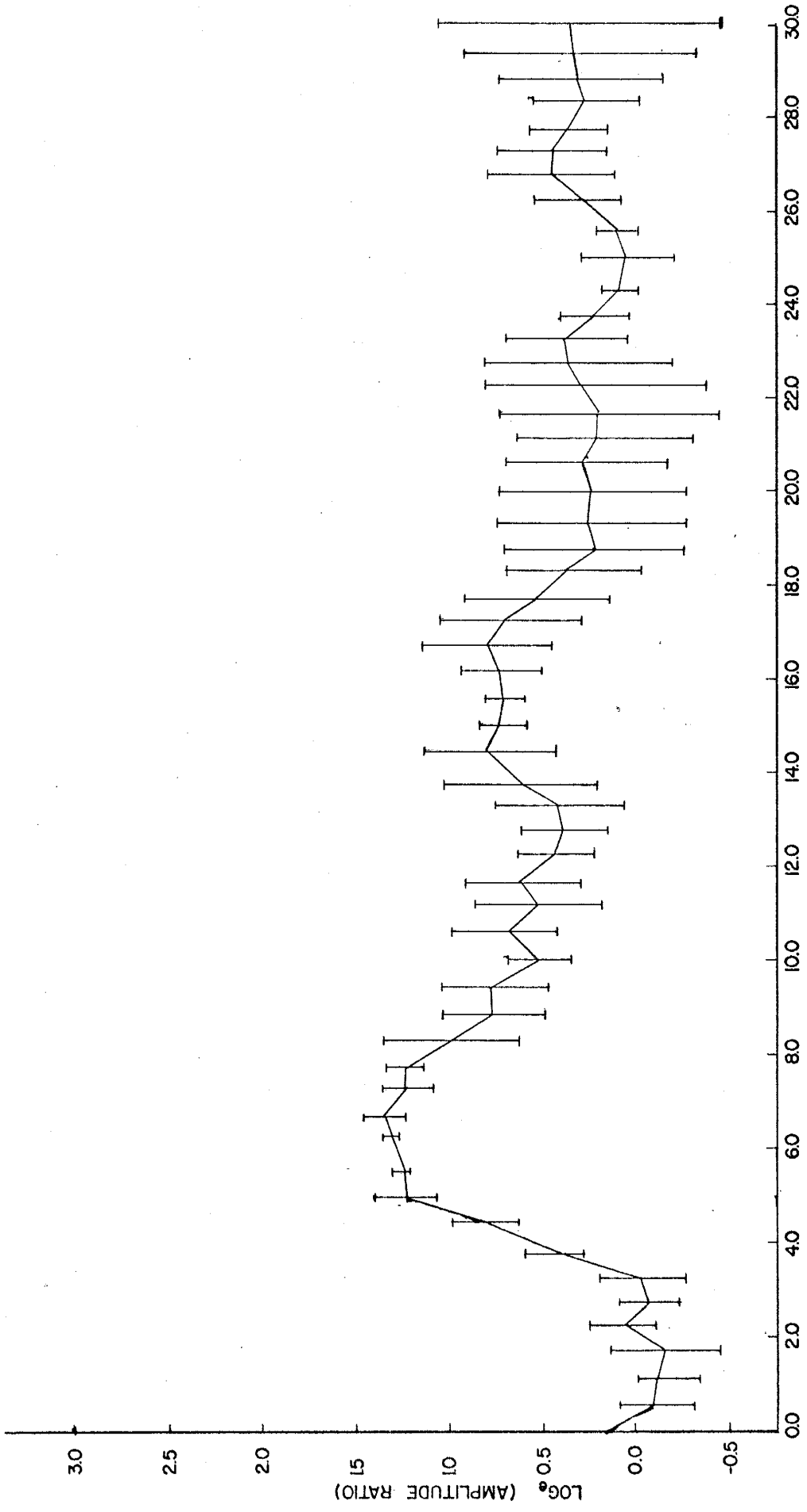

Figure 19. Values of $\log_e$ DM/WT versus frequency for the P_n phase from three Morenci explosions.

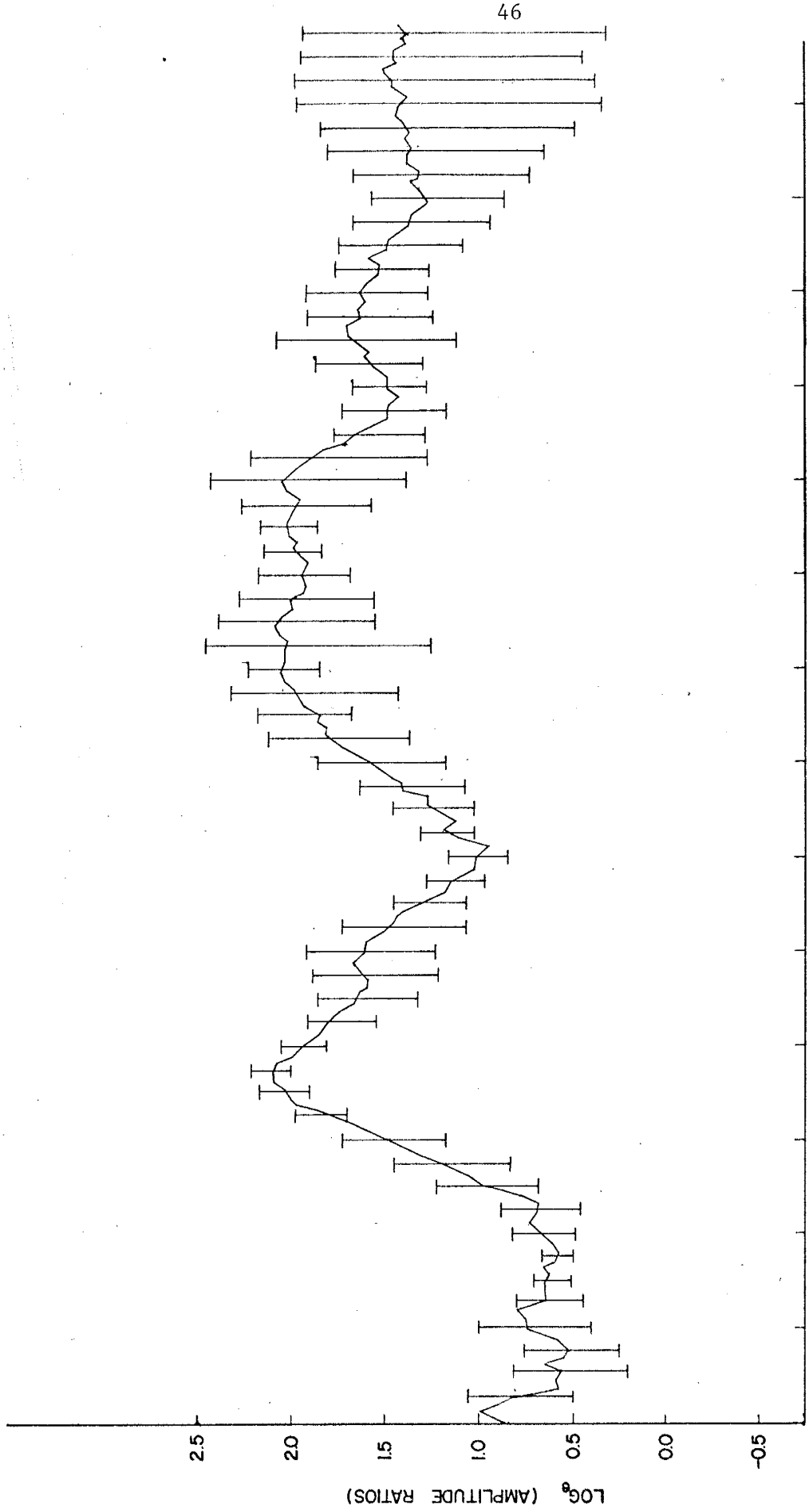

Figure 20. Values of $\log_e$ SC/WT versus frequency for the P_g phase from three Morenci explosions.

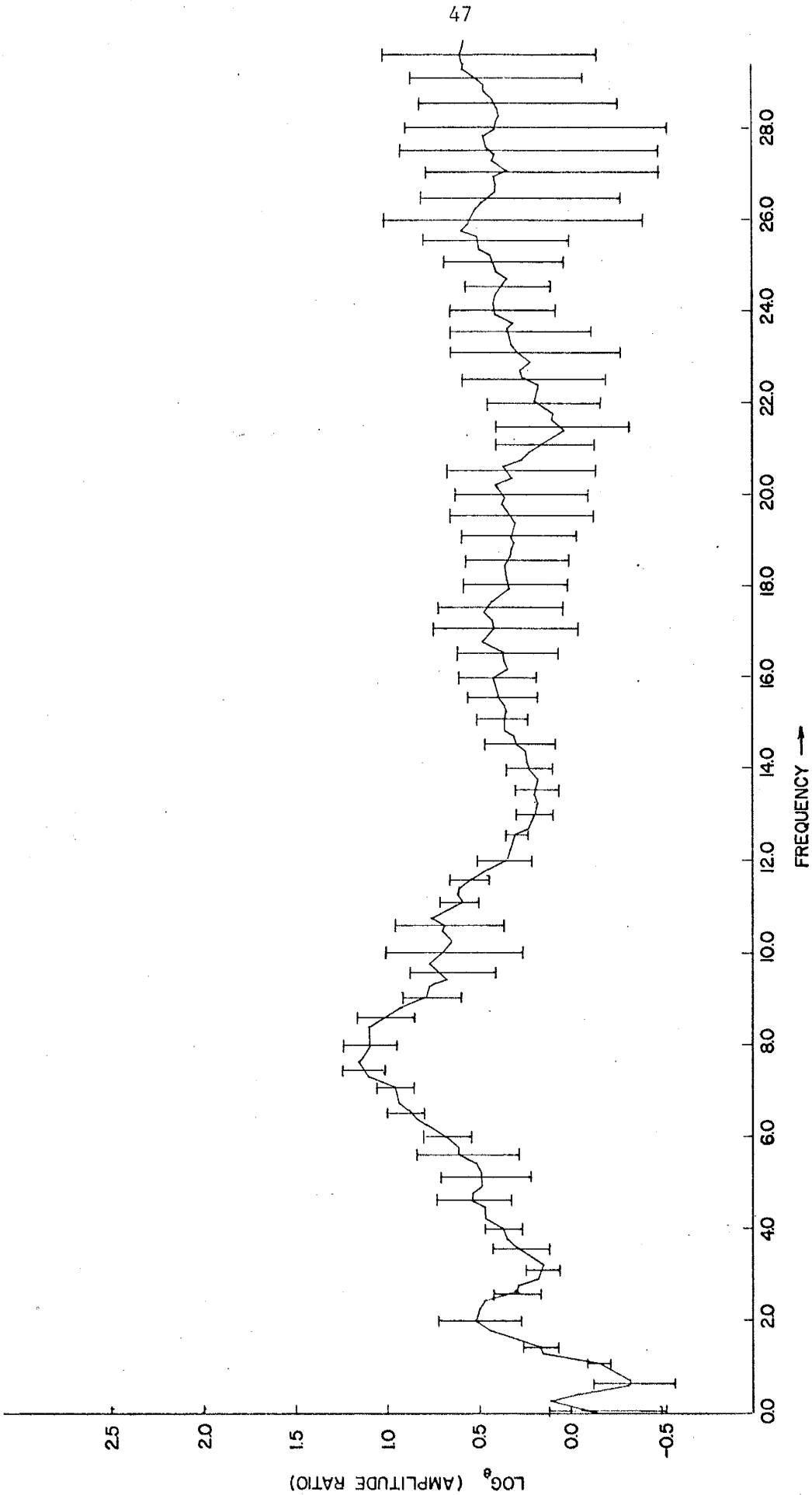

Figure 21. Values of $\log_e$ DM/WT versus frequency for the P_g phase from three Morenci explosions.

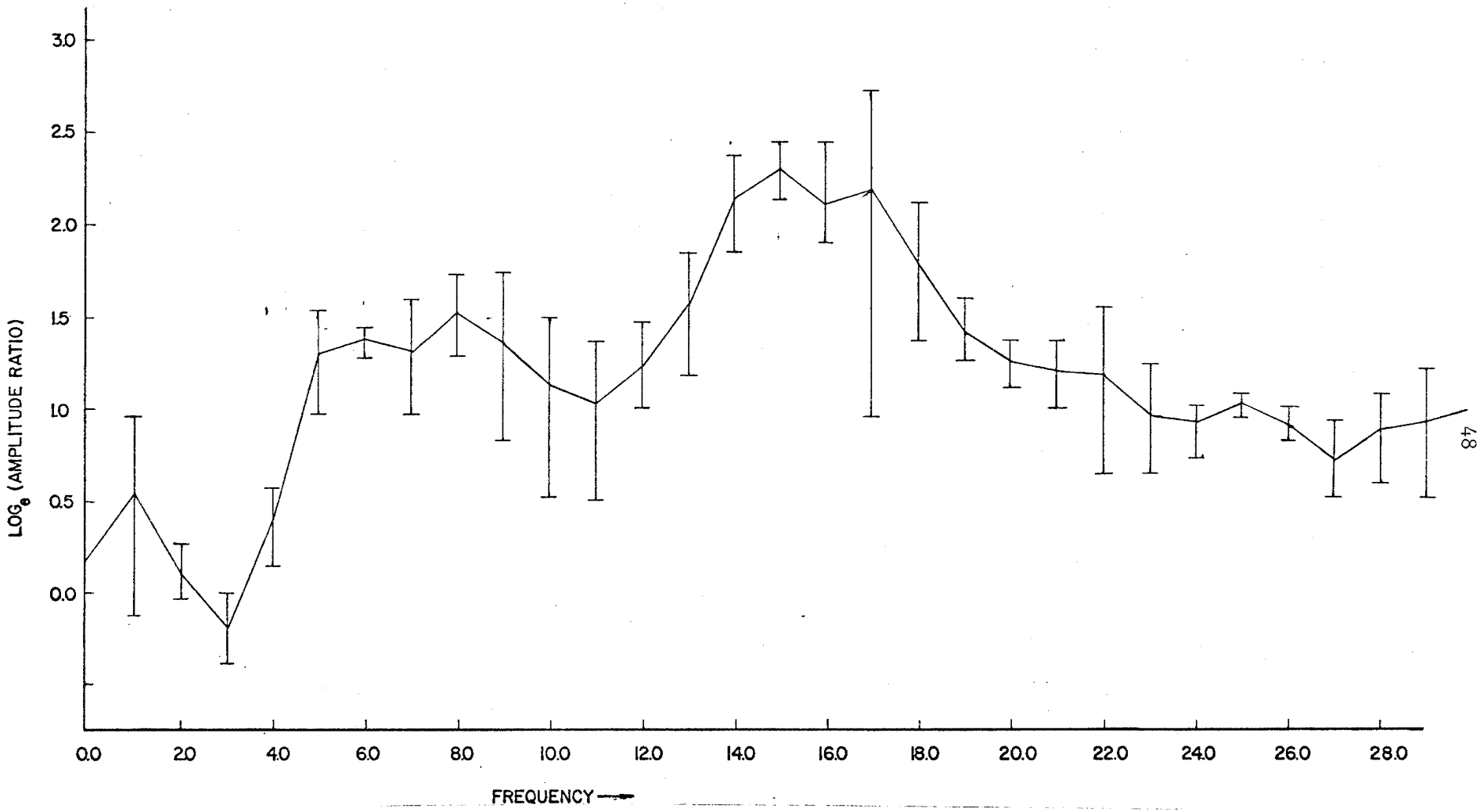

Figure 22. Values of $\log_e$ SC/WT versus frequency for the P* phase from three Morenci explosions.

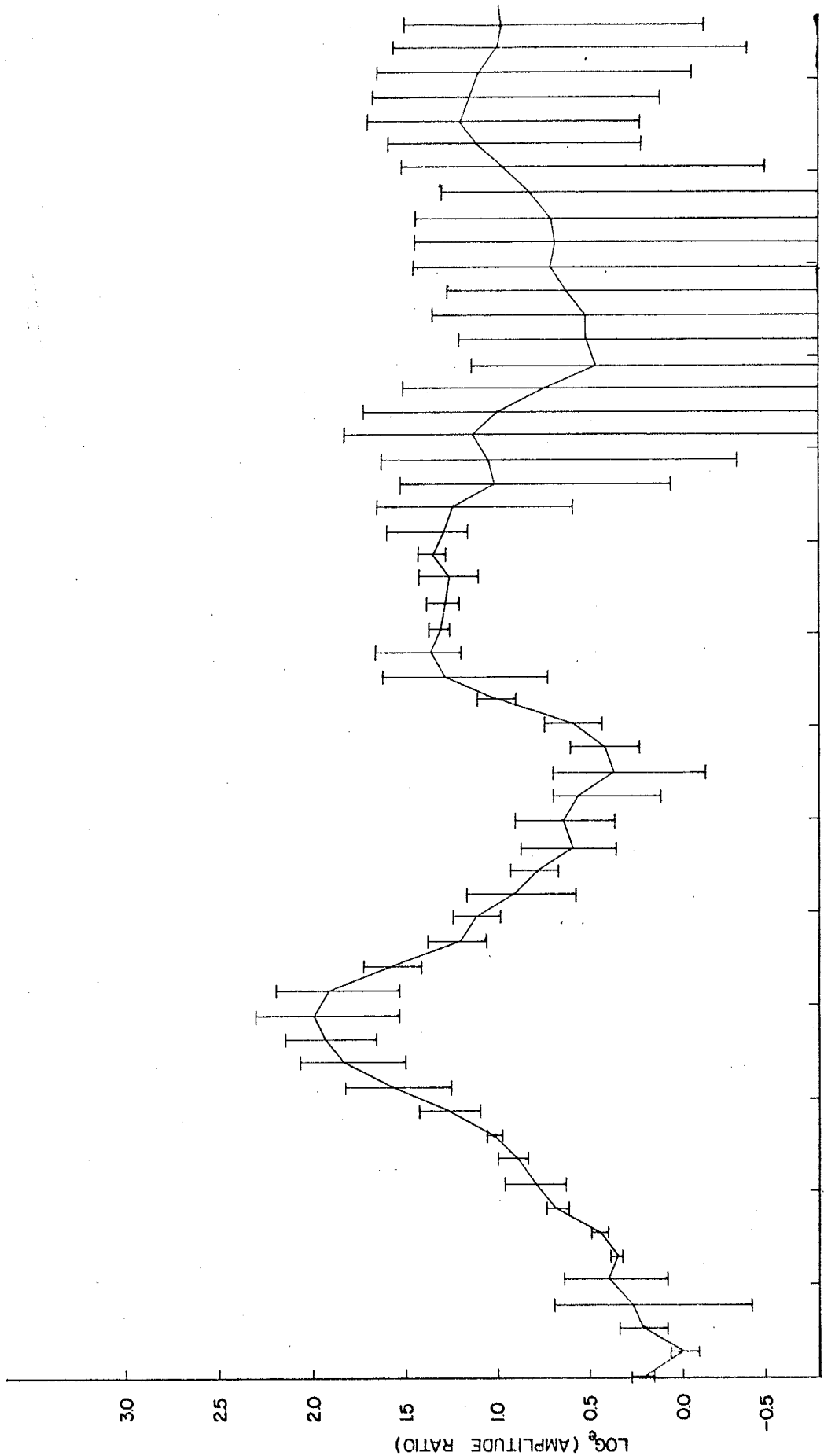

Figure 23. Values of $\log_e$ SC/WT versus frequency for the P_g and P*P phases from two Jackpile explosions.

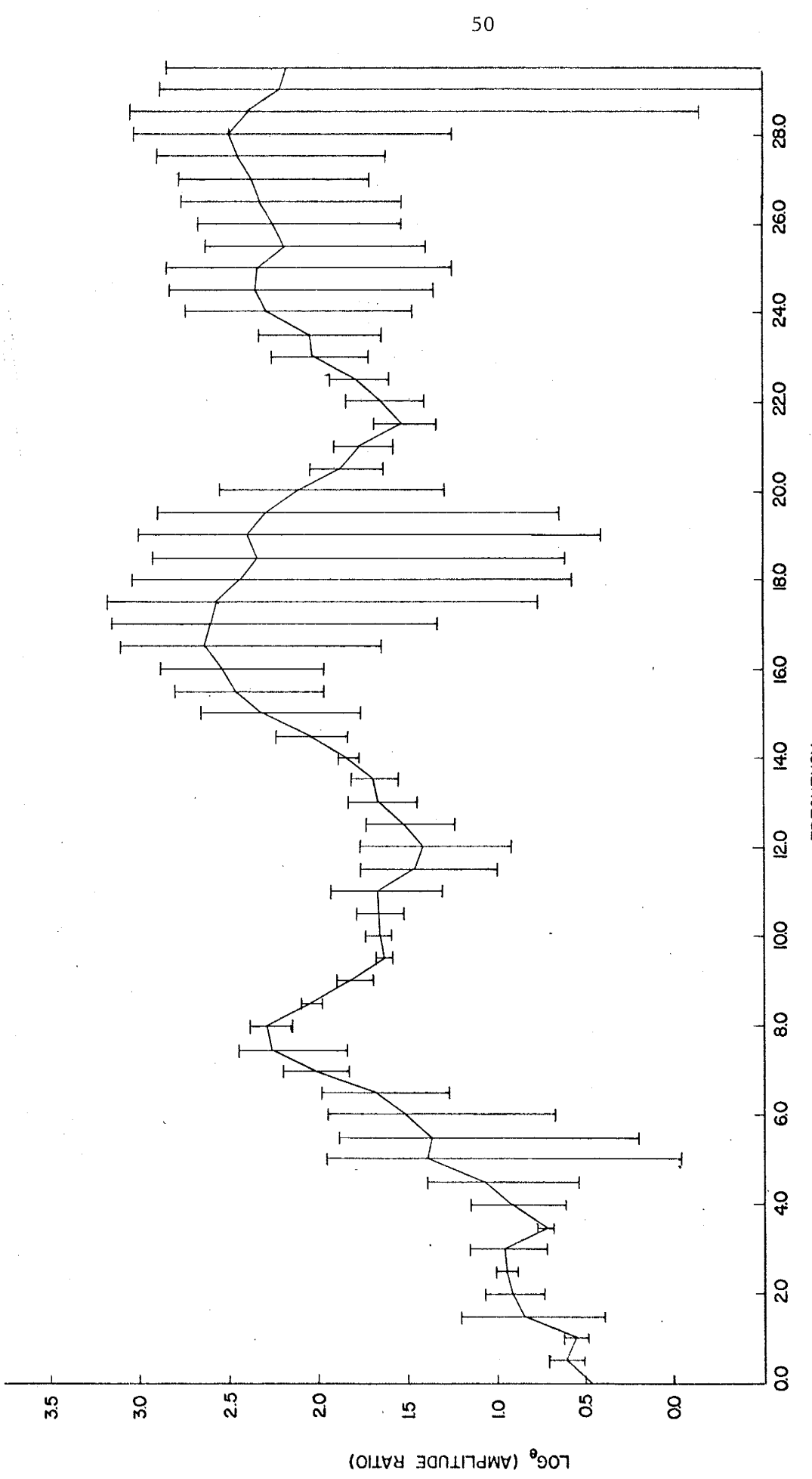

Figure 24. Values of $\log_e$ SC/WT versus frequency for the P_mP phase from two Jackpile explosions.

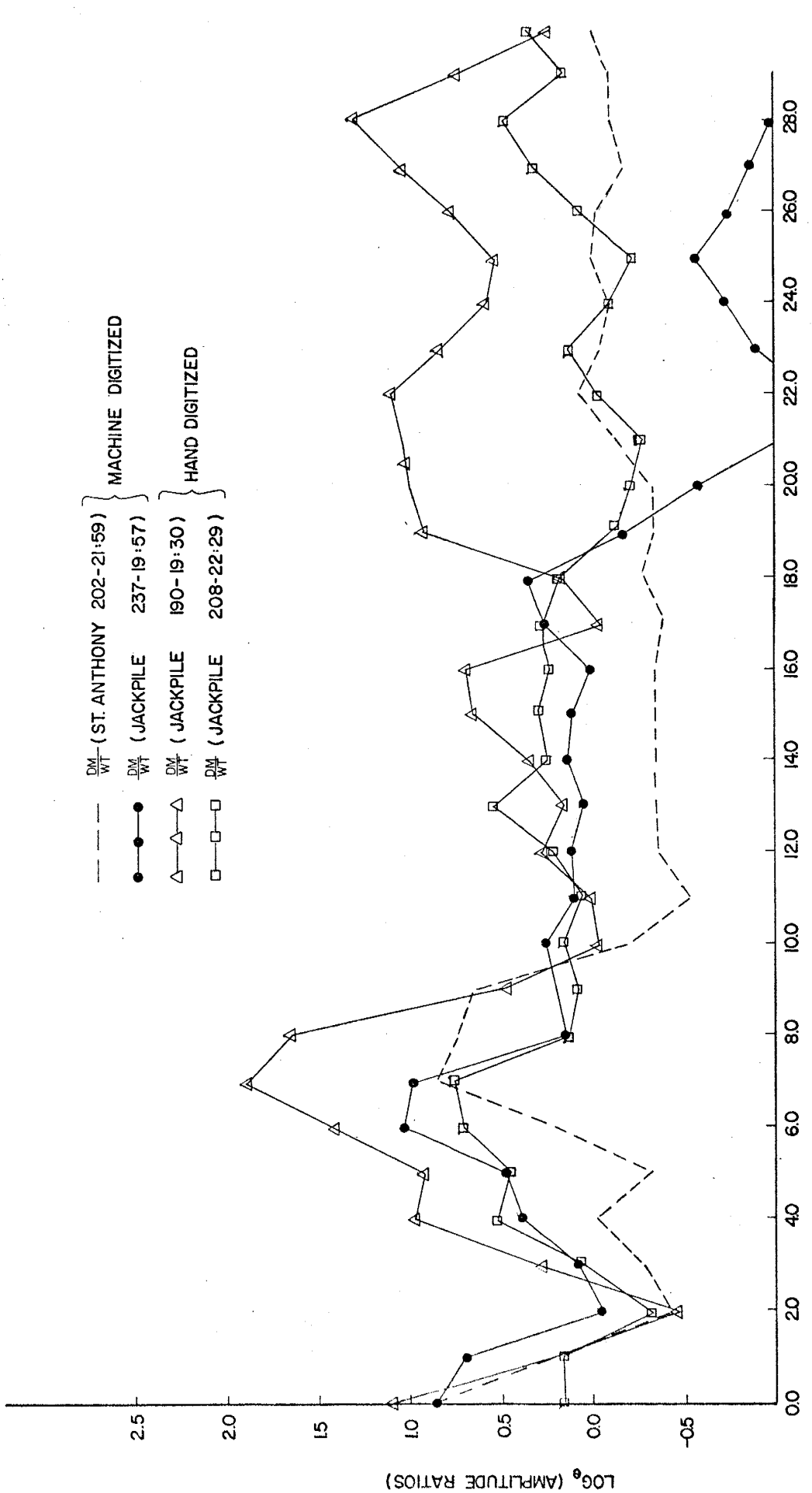

Figure 25. Values of $\log_e$ DM/WT versus frequency for the P_g phase from three Jackpile explosions and one St. Anthony explosion.

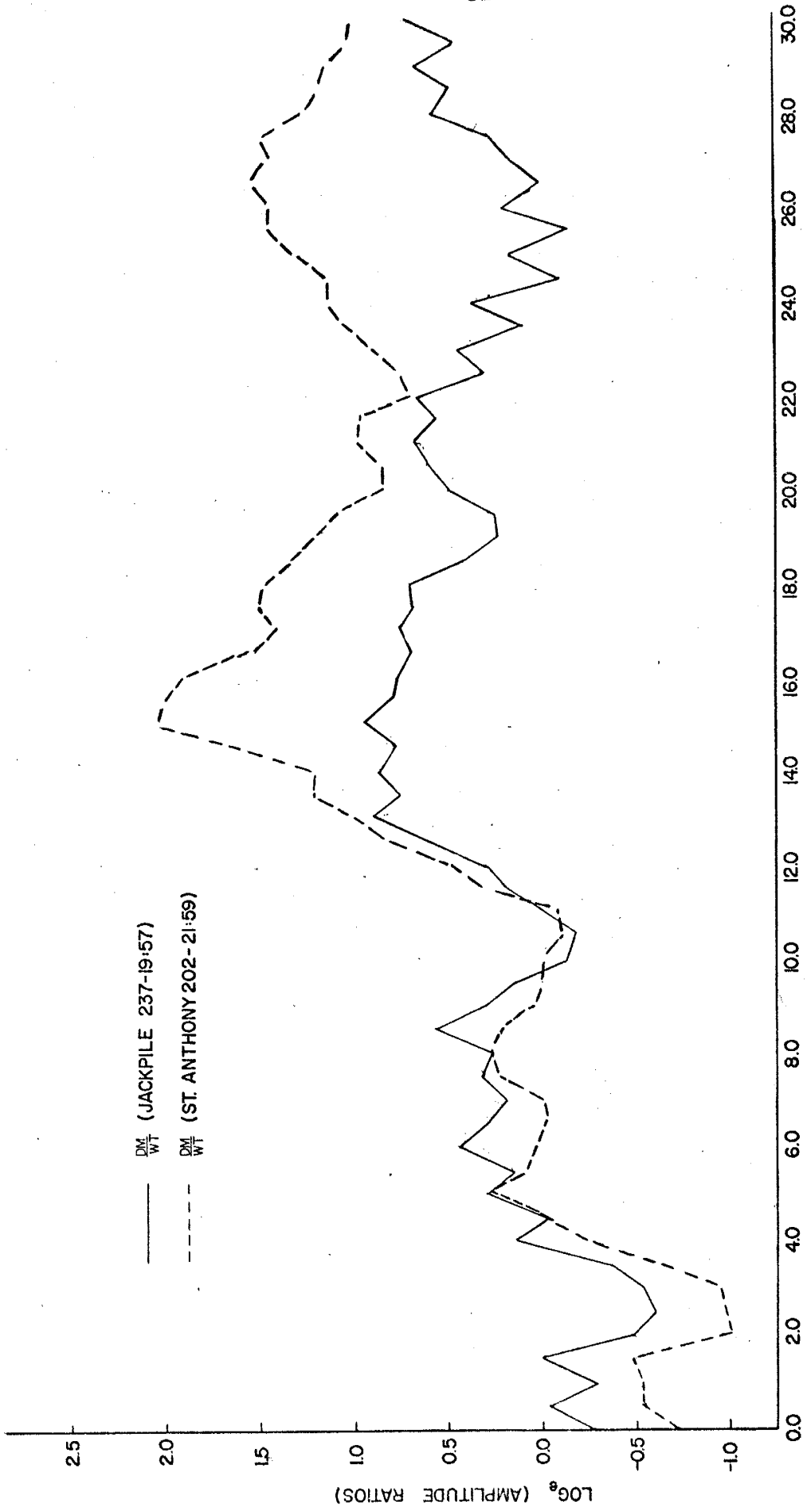

Figure 26. Values of $\log_e$ DM/WT versus frequency for the P_mP phase from one Jackpile explosion and one St. Anthony explosion.

Results and Interpretation

Elimination of Source Parameters

Figures 27 and 28 are graphs of $\log_e$ SC/SC versus frequency obtained from Morenci P_g smoothed spectra for different explosions. The uneven nature of the curves indicates that the source spectrum is different from one event to the next. However the graph of $\log_e$ SC/WT versus frequency in Figure 20 shows a reproducibility of the ratios from one explosion to the next. Thus source parameters can be eliminated by working with ratios of station pairs.

Range of Reliable Amplitude Ratios

The amplitude ratios for station pairs are reliable up to about 16 Hz. Most of the spectra show very little energy beyond 16 Hz. The $\log_e$ SC/WT for Morenci P_n (Figure 18) is the only data which do not appear reliable below 16 Hz. This is due entirely to one event (272-22:31), which may have been contaminated by noise during the P_n arrival. The ratios beyond 16 Hz up to 50 Hz are only believed to give a general idea of the true ratios in that frequency range. Noise becomes a contributing factor in the spectral amplitudes at the higher frequencies and thus spectral amplitude ratios are reduced at higher frequencies.

Station Effects

Prominent features of all log-ratio versus frequency curves involving station WT is (1) a high from 6.0 to 10.0 Hz, (2) a low from 10.0 to 14.0 Hz and (3) a rise at 14.0 Hz. Figure 29 is the plots of $\log_e$ SC/DM for the Morenci P_g phase from different explosions. For this station pair, the undulations do not exist. Thus the prominent peak and trough in curves involving station WT is due to geologic conditions at or beneath station WT.

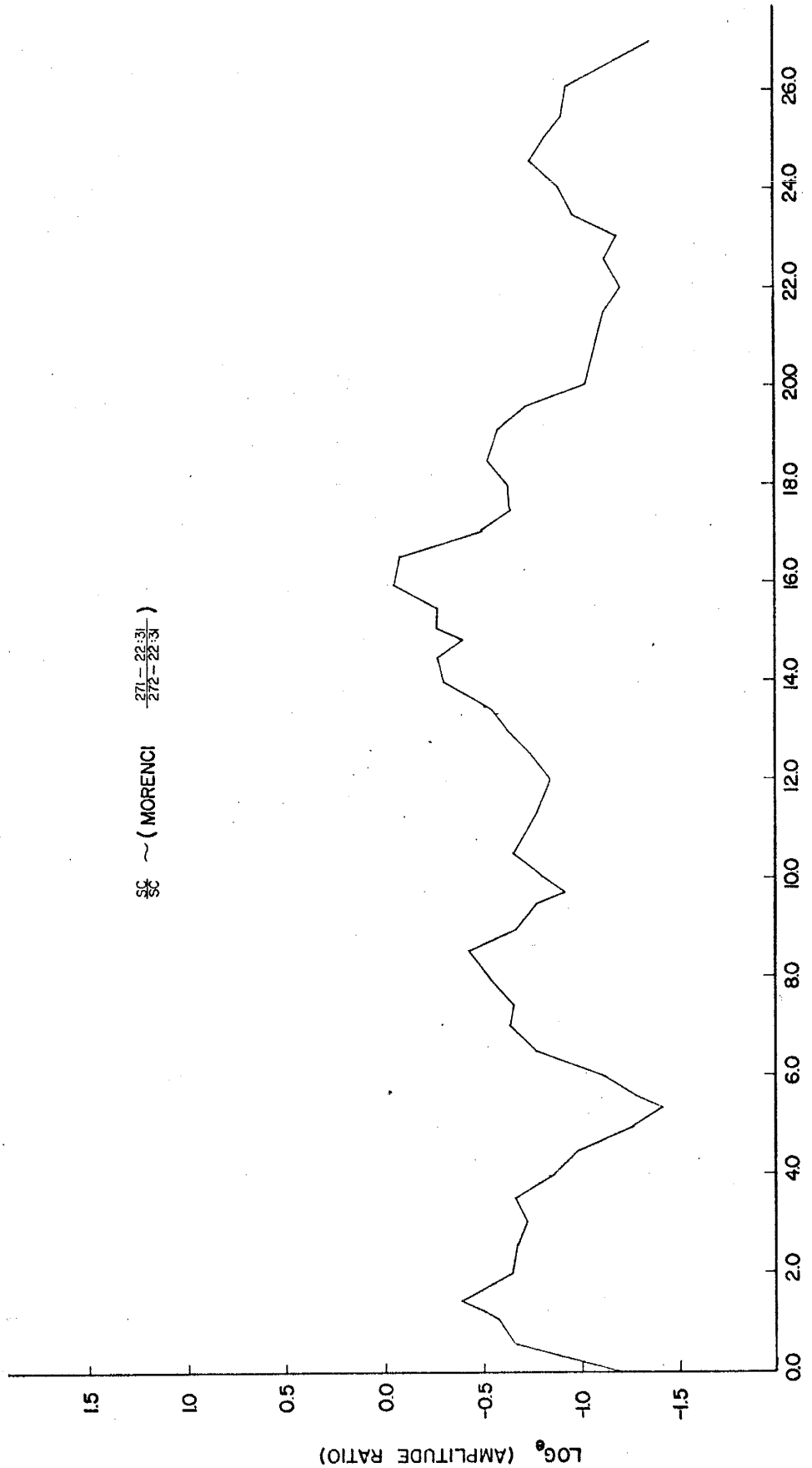

Figure 27. Values of $\log_e$ SC/SC versus frequency for the P_g phase from two different Morenci explosions.

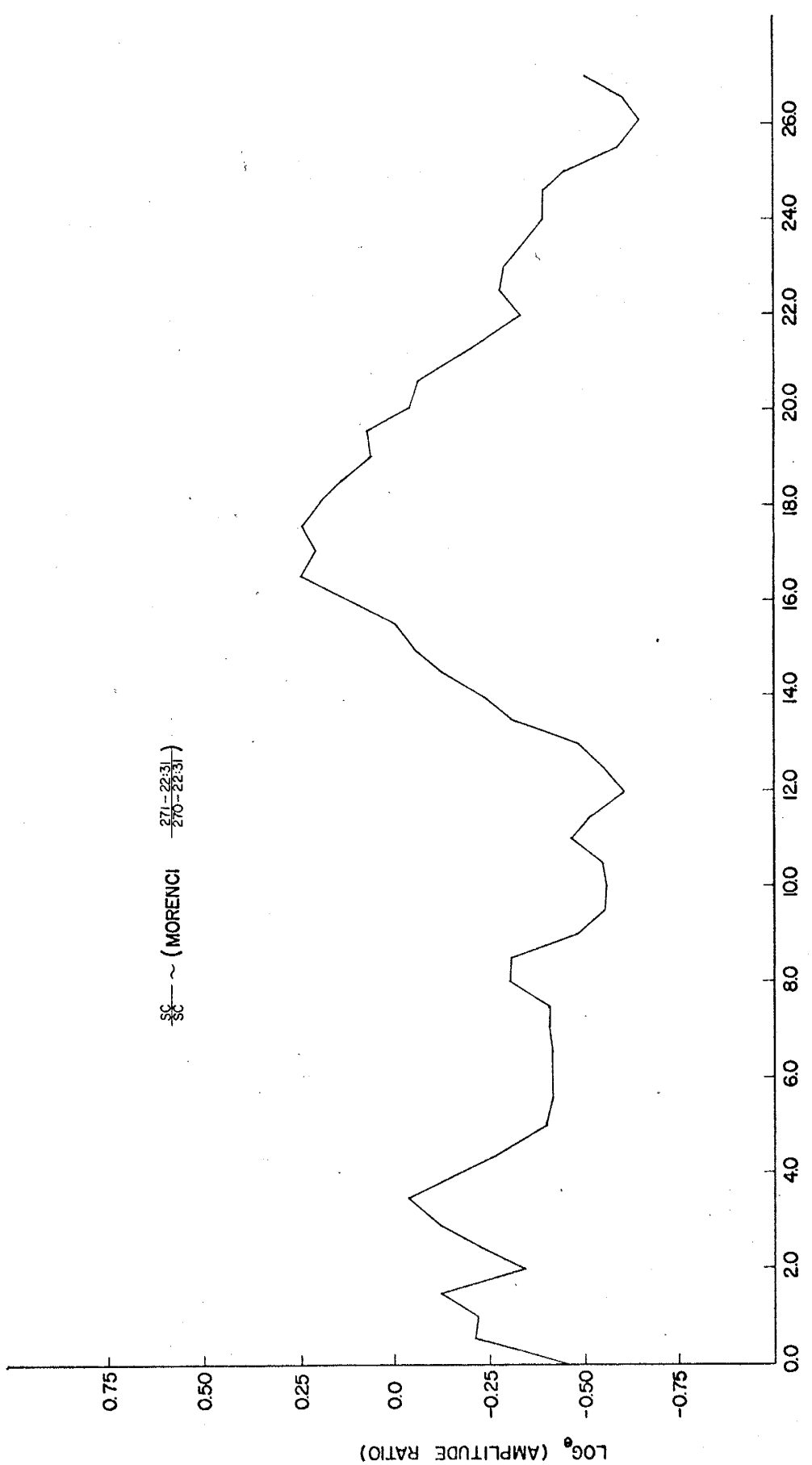

Figure 28. Values of $\log_e$ SC/SC versus frequency for the P_g phase from two different Morenci explosions.

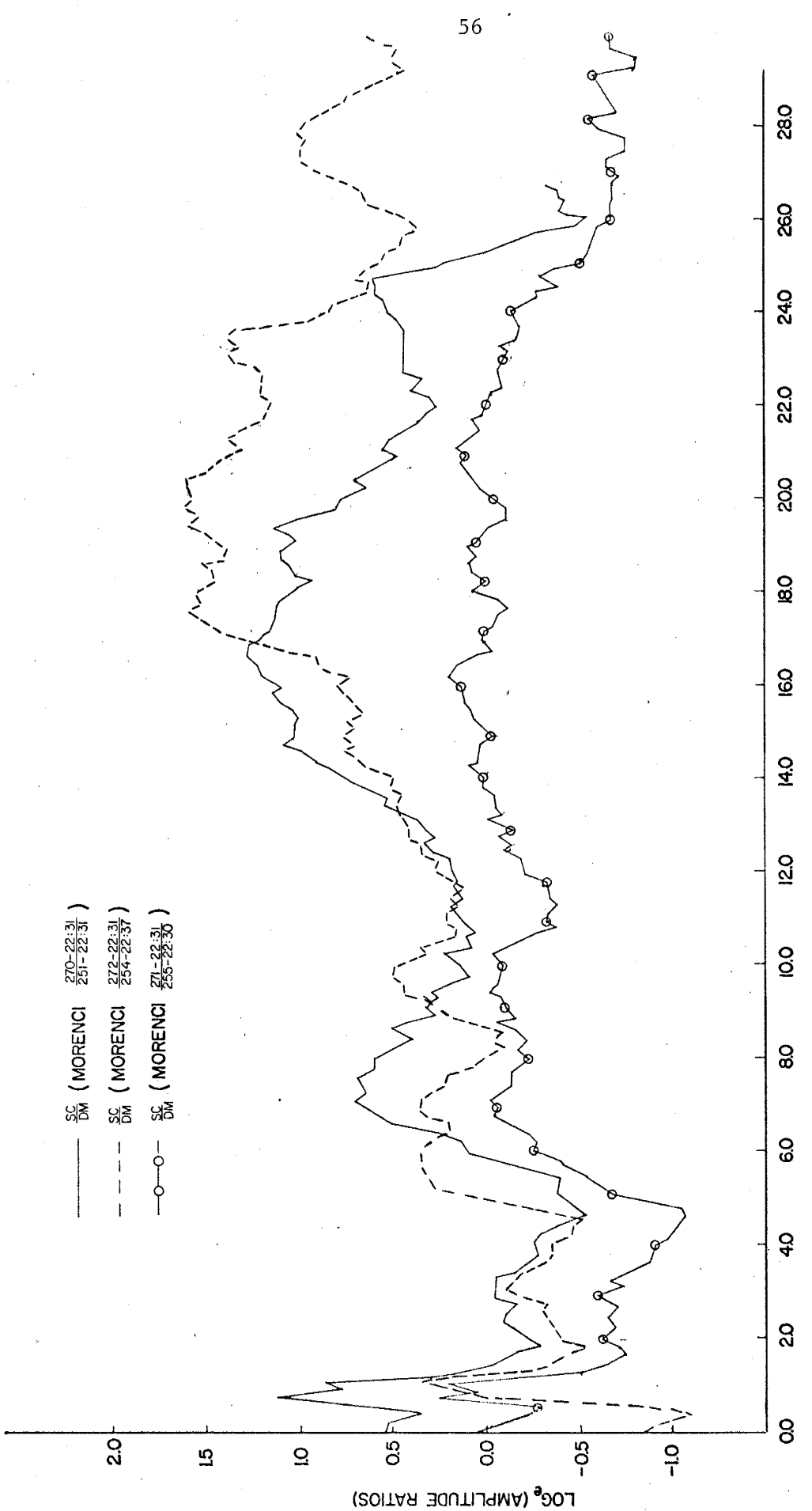

Figure 29. Values of $\log_e$ SC/DM versus frequency for the P_g phase from six different Morenci explosions.

Station WT is located in a tunnel while stations SC and DM lie at the free-surface. Biles (1967) observed the change in recorded amplitude with depth beneath the surface in a tunnel located near the one in which WT is located. Bile's results show that the amplitude at a depth of 45 meters is reduced to 0.5 of its value at the free surface for frequencies as low as 6.0-9.0 Hz. For higher frequencies all amplitudes are reduced by 0.5. This is attributed to the effect of free-surface doubling. Station WT is located at a depth of about 75 meters. Part of the rise in the ratio plots above 4.0 Hz can be attributed to the depth of burial effect. However, the dip in graphs from 10 to 14 Hz cannot be explained in this way.

The probable explanation for undulations in the curve above 4.0 Hz is that free-surface reflections constructively and destructively interfere with the emergent wavetrain at the geophone location. Figure 30 illustrates what may be occurring to an emergent phase. Reflection at the

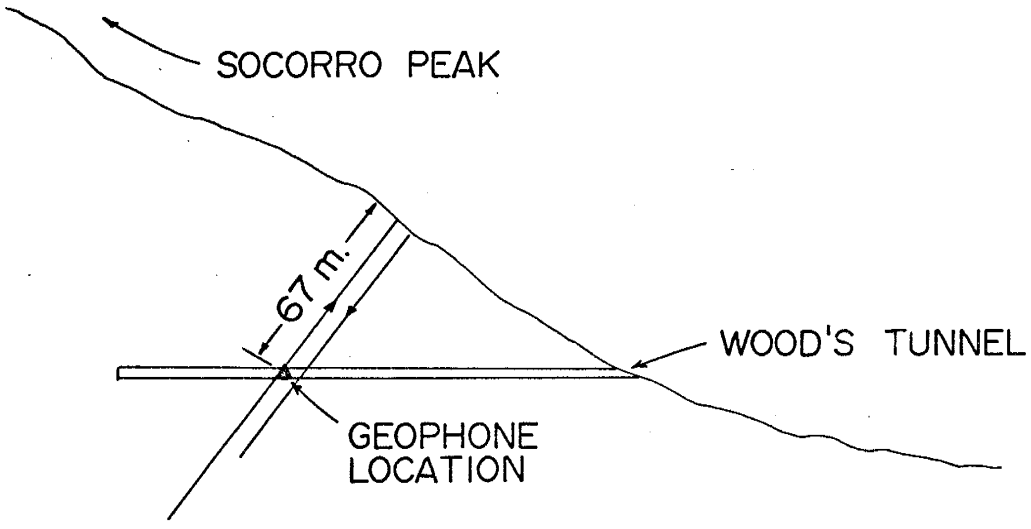

Figure 30. Cross-section showing the mechanism of wave-interference at station WT.

free surface results in a phase change, so that constructive interference occurs at frequencies for which 67 meters equals 1/4 λ, 3/4 λ, etc. and destructive interference occurs at frequencies for which 67 meters equals 1/2 λ and λ etc. The $\log_e$ SC/WT Morenci P_g ratio (Figure 20) shows the first peak for WT at a frequency in the vicinity of 12.0 Hz. The velocity from the geophone to the surface would be given by $f\lambda$ = 12.0 x 4 x 67 meters = 3.2 km/sec. An independent measurement of velocity in Wood's tunnel gave a velocity of 2.5 km/sec. However the rock in the immediate vicinity of the tunnel is probably disturbed which probably accounts for the lower velocity.

A study of the amplitude of the initial P-wave pulse for teleseismic arrivals was undertaken to determine station effects at low-frequencies. Equation 1 shows that an amplitude ratio of a station pair must approach unity as the frequency approaches zero. The dominant frequency for the teleseismic P-arrivals was less than 1.5 Hz, and therefore the effect of attenuation on the teleseismic amplitude ratios is not great. Distance differences to the stations is small because of steep incidence. Also waves at a frequency of less than 1.5 Hz are not reduced at WT because of the location beneath the surface. Table 3 gives a tabulation of the results. Events which showed initial amplitudes of less than 0.5 mm were not considered useful. The data was obtained from smoked-paper seismograms produced by MEQ-800 portable seismographs.

The ratio SC/WT is quite well determined while the ratios DM/WT and DM/SC are poorly determined. A reason for the large standard deviations of the DM/WT and DM/SC ratios is not known.

Because amplitudes of frequencies above 6.0 Hz at WT are reduced to 0.5 of their value at the free surface, then the reference level above

6.0 Hz for SC relative to WT is estimated to be 2.48 (2 x 1.24), the logarithm of which is .91.

Table 3. Amplitudes of the Initial P-wave Oscillation for Teleseismic Arrivals

Teleseism	Amplitudes (mm)			Amplitude Ratios		
	WT	SC	DM	SC/WT	DM/WT	DM/SC
2- 5-76 10:03	1.86	2.26	2.55	1.215	1.37	1.13
2-19-76 18:36	2.98	3.90		1.31		
8-20-76 17:04	1.32	1.48		1.12		
7-29-76 01:52	.57	.67		1.175		
8- 6-75 21:48	1.20	1.56		1.3		
1-27-76 16:11	.73	.92	1.40	1.26	1.92	1.52
3- 9-77 14:37	12.5	14.35	18.3	1.15	1.46	1.27
3-24-76 04:59	3.6				1.11	
4-19-77 22:04		9.1	10.05			1.10
3- 9-77 15:15	1.9				1.04	
6- 7-77 13:42	.77	1.07	.70	1.38	.909	.654
6- 7-77 14:38	1.08	1.34	1.16	1.24	1.07	.865
8-17-77 15:57		.83	.83			1.0
				1.24±.08	1.26±.34	1.07±.28

At this point an estimate of a reference level for DM relative to WT is not considered possible due to the variability of the ratios when DM is involved.

The interference effect, which has been suggested takes place at WT, can only be verified by analysis of data obtained with station WT placed at the tunnel entrance. Unfortunately the effect of interference from the free-surface was not forseen at the start of the project. Digital equipment should not be placed in any tunnel of considerable depth in any future attenuation study.

Calculation of Q for the Upper Crust from Morenci Explosions

If significant station effects occur only at WT, then Q may be

determined from

$$Q = \frac{\pi f r}{v\left[\log_e \frac{A_{SC}/A_{WT}}{A_{DM}/A_{WT}}\right]} \quad . \qquad (17)$$

Because P_g is transmitted in the upper crust, $PS_{SC}(\omega)/PS_{DM}(\omega)$ can be considered negligible such that $A_{SC}(\omega)/A_{DM}(\omega) = 1/P_{SC-DM}(\omega)$ and the Q determined will be that of the direct propagation path between SC and DM.

Shown in Figure 31 is the average $\log_e$ SC/DM ratio when the amplitude of WT is cancelled out. The curve suggests that DM has an abnormally weak amplitude relative to SC at frequencies less than 2.0 Hz, but that the amplitude ratios are about normal beyond 2.0 Hz. The large standard deviations of the teleseismic amplitude ratios when DM is involved may be related to the variability of the amplitudes at DM at frequencies below 2.0 Hz.

The intercept of the segment of the ratio curve in Figure 31 cannot be reliably determined due to fluctuations of the curve. Differences in station effects between SC and DM is considered responsible for the fluctuations, however these effects do not affect the overall rise of the $\log_e$ SC/DM ratio arising from attenuation. Shown in Figure 32 is a smoothed version (13 point moving average) of the $\log_e$ SC/DM versus frequency curve for the Morneci P_g phase which excludes the ratios below 2.0 Hz. A least-squares fit to the smoothed curve has an intercept of 0.14 and a slope of .077. It is assumed that the differences in station effects between SC and DM cancel out over the frequency range 2.0-16.0 Hz. The intercept can be interpreted as the result of geometrical spreading. The Q values

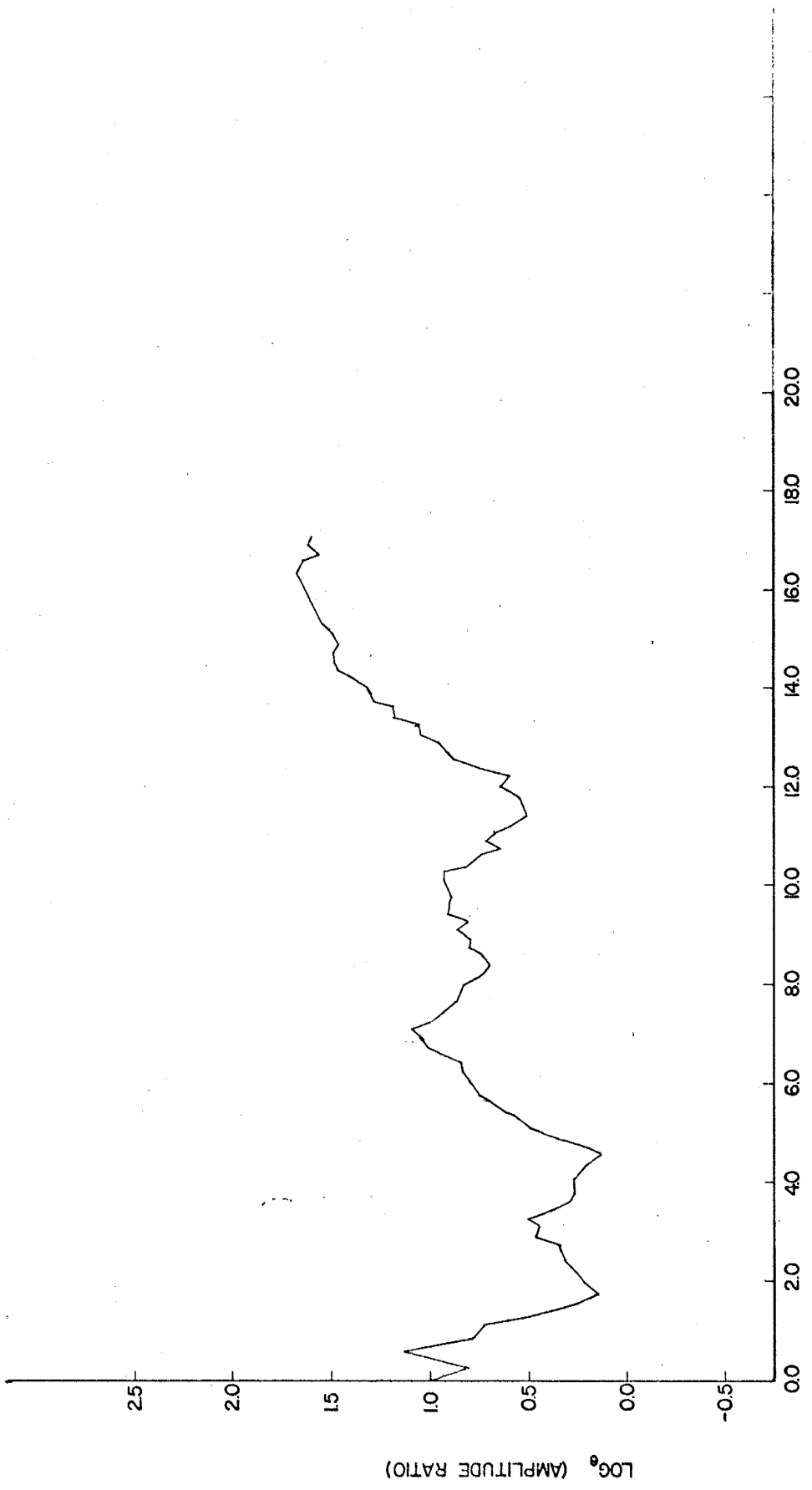

Figure 31. Values of $\log_e$ SC/DM versus frequency for the P_g phase when the amplitude of WT is cancelled out.

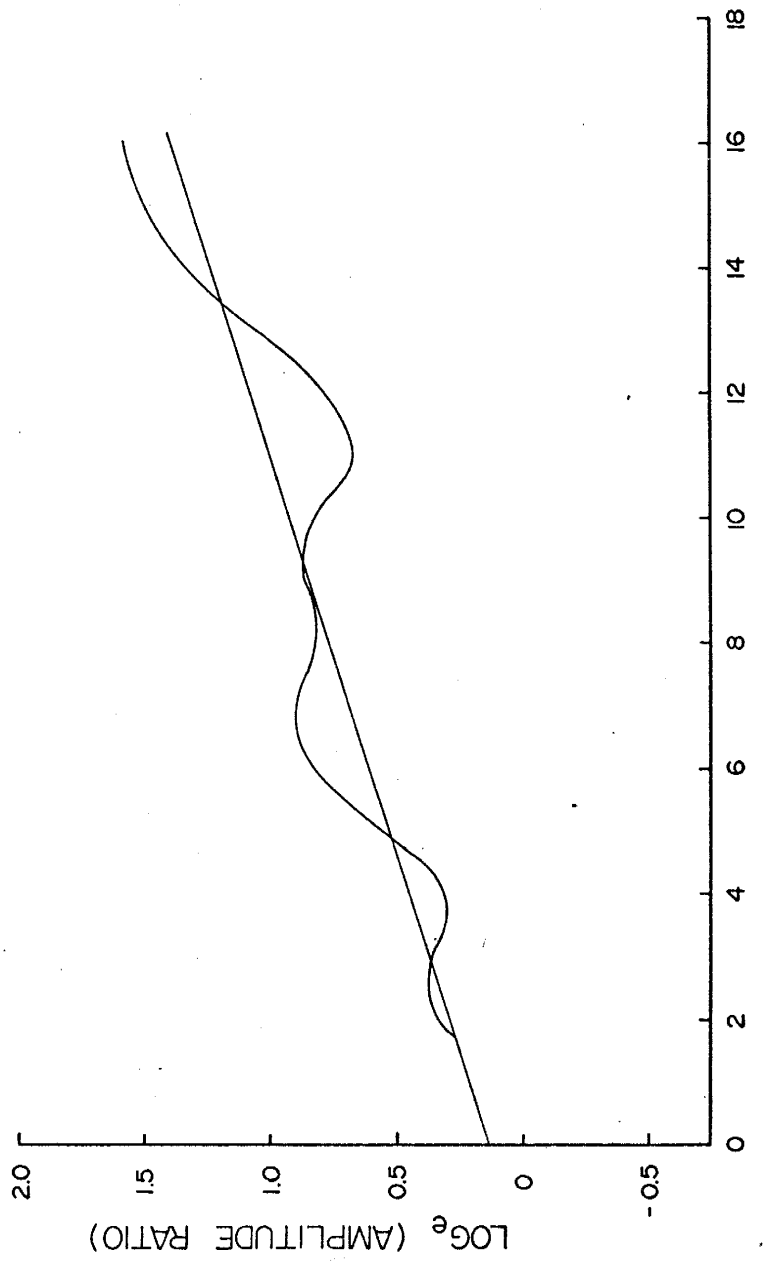

Figure 32. Smoothed values (13 pt. moving average) of $\log_e$ SC/DM versus frequency for the P_g phase when the amplitude of WT is cancelled out.

will be constant with frequency if the correction for geometrical spreading is made, and are given by

$$Q = \frac{\pi f r_{SC-DM}}{v\left[\log_e \frac{A_{SC}}{A_{DM}} - \log_e \frac{G(r_1)}{G(r_2)}\right]} \quad . \tag{18}$$

where $\log_e G(r_1)/G(r_2) = .14$. This gives a Q value for the upper crust of 195. If the geometrical spreading is proportional to 1/r, then the intercept due only to the spreading should be $\log_e$ 261.31/233.24 which is .113. The similarity of the two intercepts indicates that the amplitude effect at stations SC and DM due to the density and velocity of the rock beneath the stations is the same in the frequency range 2.0-16.0 Hz.

Because a reference level for station SC relative to station WT has been estimated to be 0.91 for frequencies above 6.0 Hz, it is assumed that the reference level for station DM relative to station WT is approximately 0.91 also. Shown in Figure 33a are the values of $\log_e$ SC/WT and $\log_e$ DM/WT versus frequency for the Morenci P_g phase in comparison to the reference level of 0.91. Inasmuch as the distances of stations SC and DM from WT is about the same, the positions of the logarithmic ratios relative to the reference line on the graph indicates higher attenuation from SC to WT than from WT to DM.

Microearthquake activity is highest in the area from SC to WT. Results presented in the next section indicate higher attenuation for areas which show higher microearthquake activity, which in turn may be associated with magmatic intrusion. The ratio of $\log_e$ SC/WT versus frequency curve for the P* phase on Morenci recordings, which is discussed later,

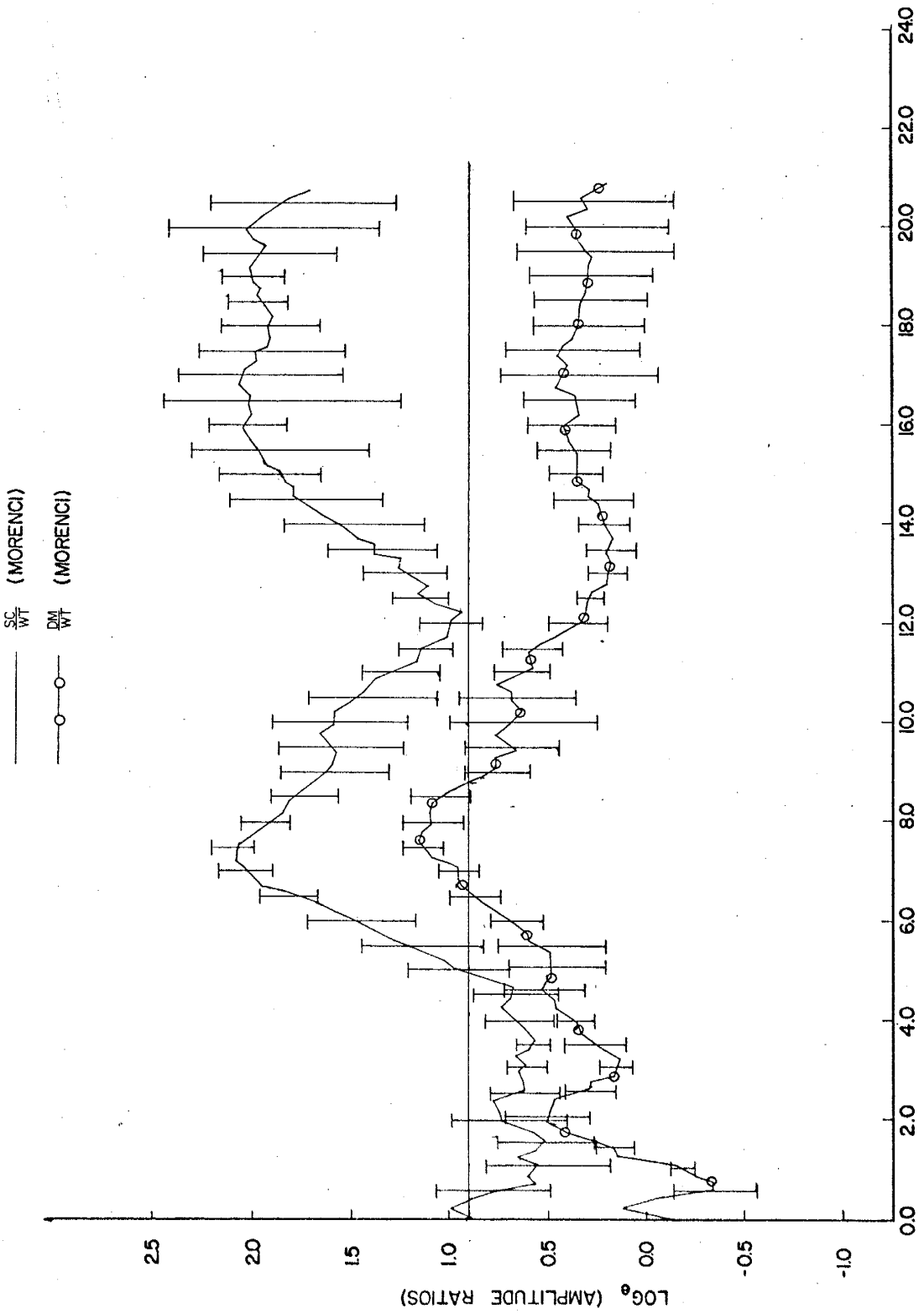

Figure 33a. Values of $\log_e$ SC/WT and $\log_e$ DM/WT versus frequency for the P_g phase from Morenci relative to the reference level of .91.

suggests that a shallow magma body lies west of station WT.

Press (1964) computed Q for the upper crust using underground nuclear explosions from the Nevada test site. The Q he obtained was 260±40. Therefore the Q value obtained in this study may indicate a higher than normal attenuation in the upper crust in the Socorro area of the Rio Grande rift.

Data from Jackpile and St. Anthony Explosions

Variations in the attenuation properties of propagation paths to the north of the station line SC, WT and DM could be detected. If there were no variation, then the ratios $\log_e$ SC/WT and $\log_e$ DM/WT for the various phases from Jackpile and St. Anthony aside from differences arising from station effects should be the same. In addition the ratios should fit below the $\log_e$ SC/WT Morenci P_g curve and above the $\log_e$ DM/WT Morenci P_g curve; approximately along a horizontal line with a value of 0.91. The irregularities in these curves would be primarily the result of station effects at WT because the topography at WT is approximately symmetrical to raypaths from Morenci and to those from the north as is shown in Figure 33b. Figure 34 shows the $\log_e$ SC/WT and $\log_e$ DM/WT Morenci P_g curves and the area between which ratios for Jackpile and St. Anthony explosions should lie if the attenuation along paths to stations SC and DM is the same. Any logarithmic ratio curve for Jackpile data which does not fall within the shaded area in Figure 34 would indicate a variation in the attenuation properties along the two raypaths from the north.

Figure 35 shows the average values of $\log_e$ SC/WT versus frequency for P_g and P*P arrivals from Jackpile explosions. The points along this curve and their standard deviations fit within the shaded area. This indicates that Q for the crust does not vary significantly along paths

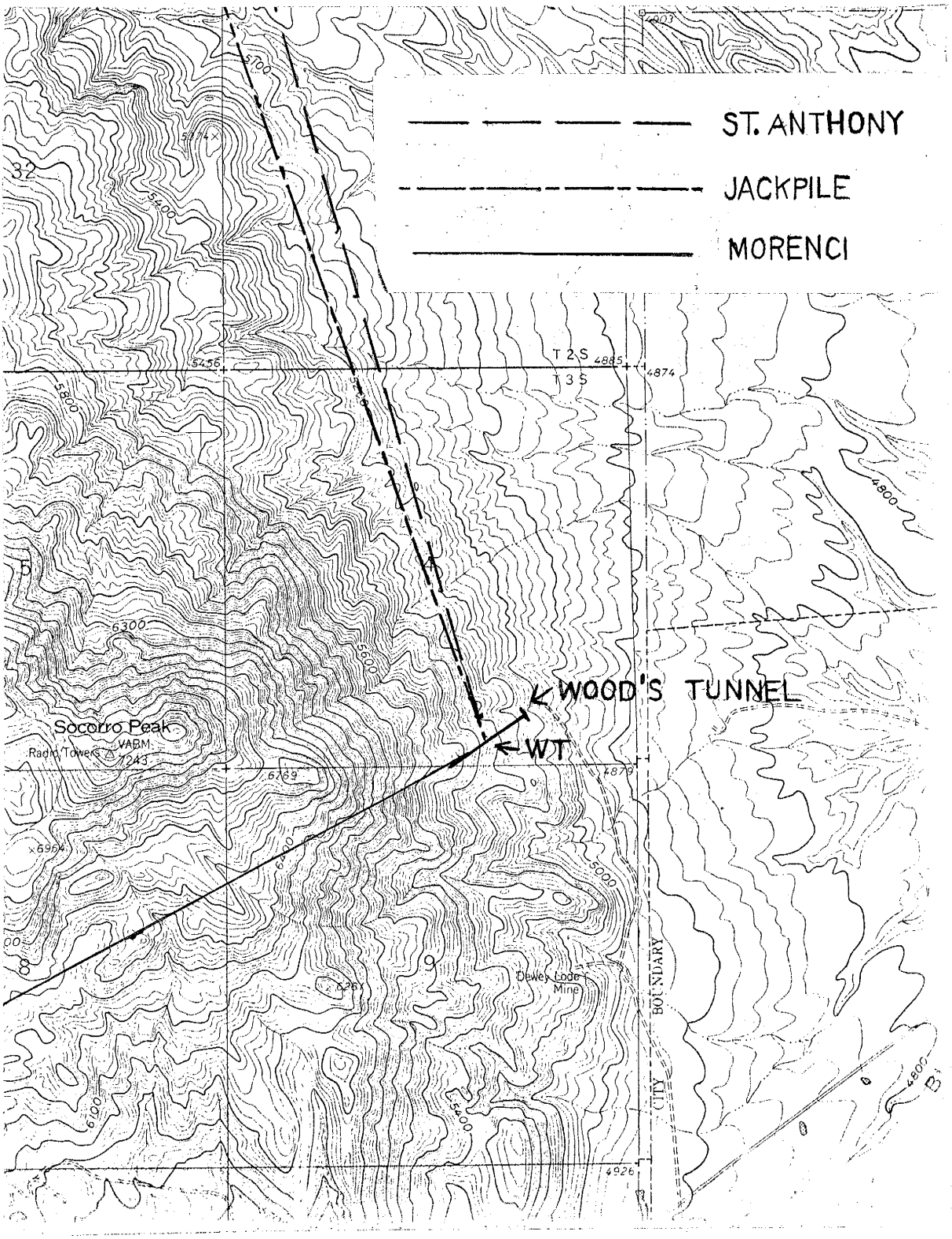

Figure 33b. Topographic map of the Wood's tunnel area showing Wood's tunnel, the location of WT and the raypaths to the explosions.

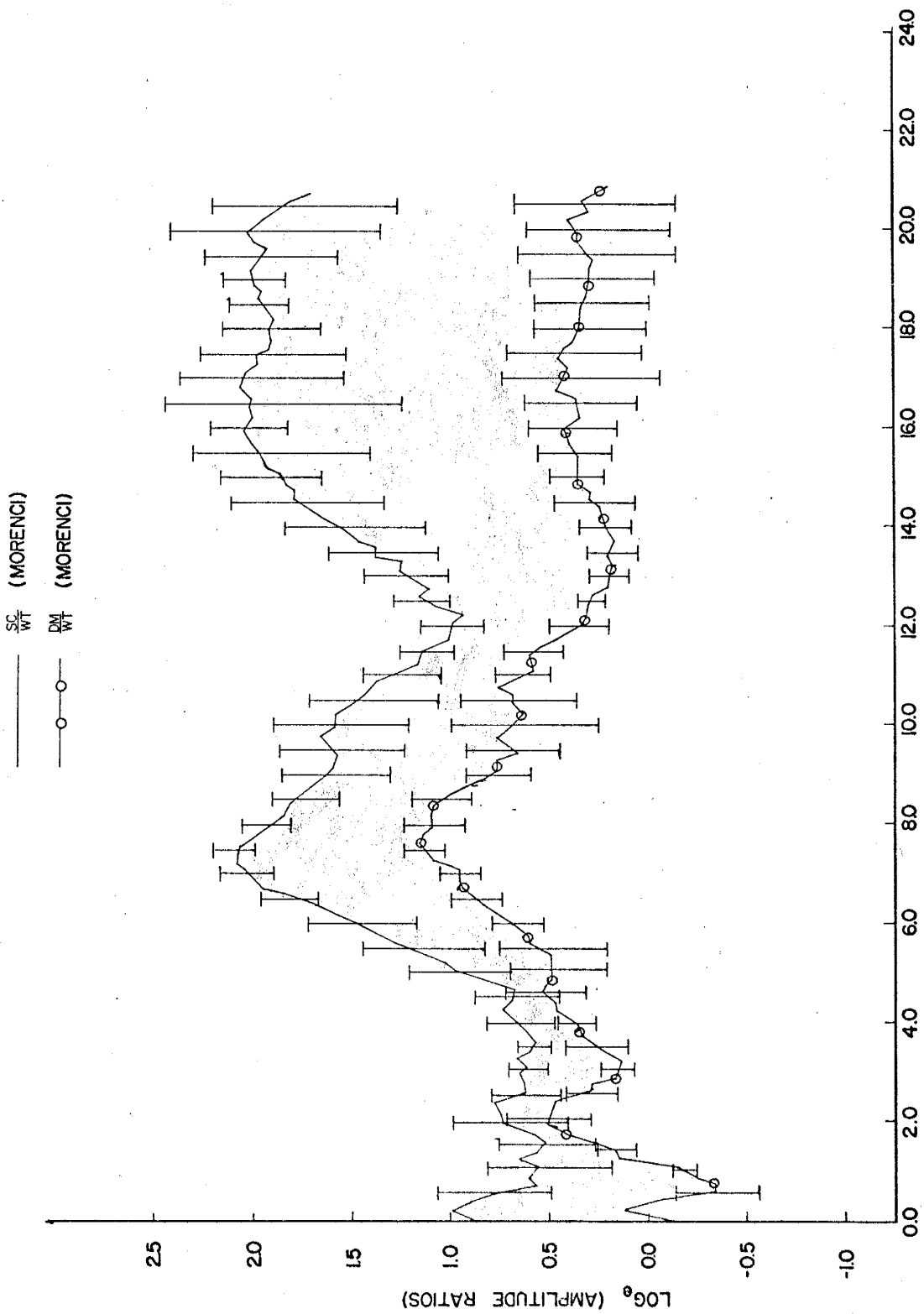

Figure 34. Values of $\log_e$ SC/WT and $\log_e$ DM/WT versus frequency for the Pg phase from Morenci explosions. Ratios for Jackpile and St. Anthony explosions should lie within the shaded area if attenuation to stations SC and DM is the same.

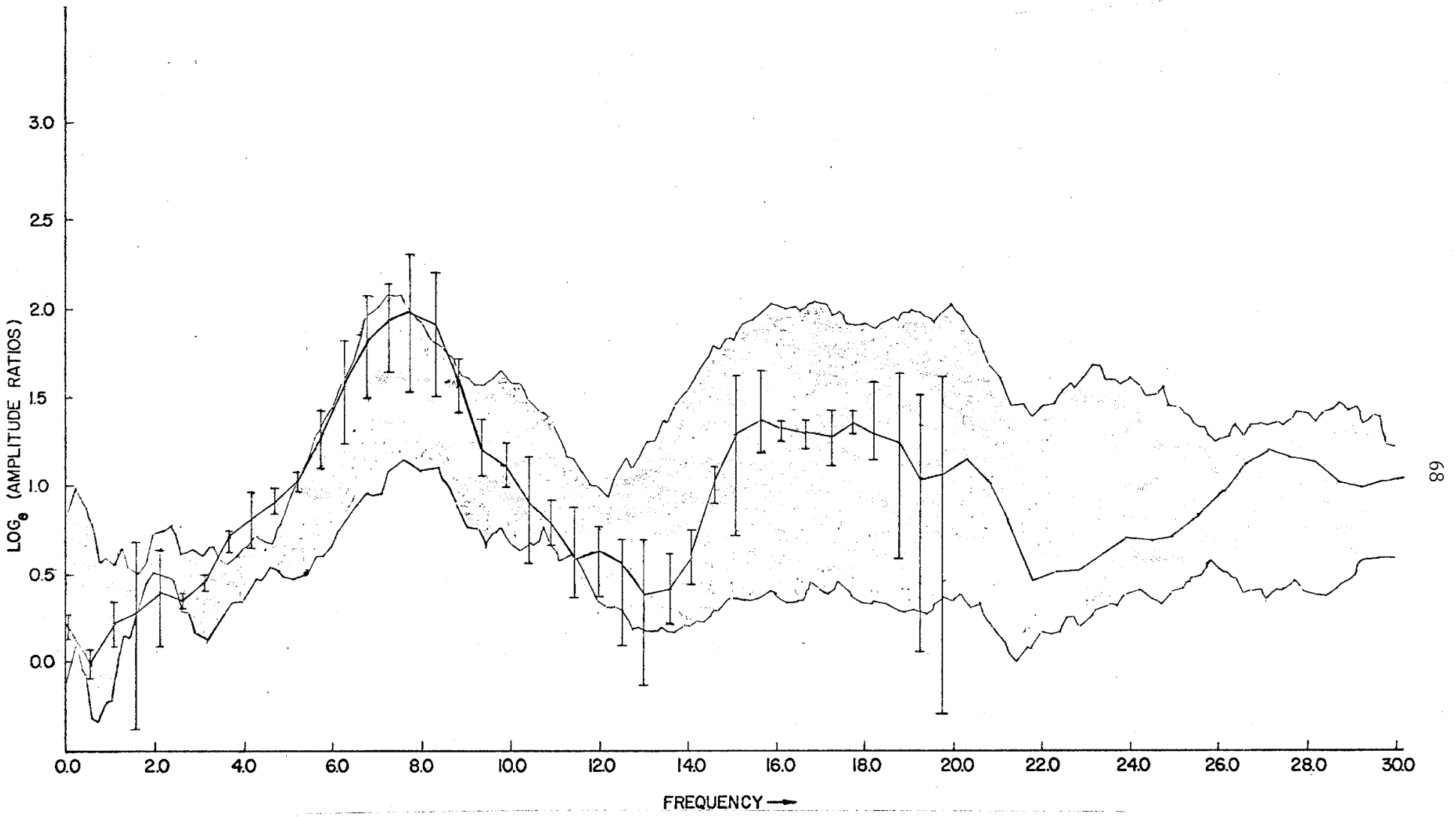

Figure 35. Values of $\log_e$ SC/WT versus frequency for the P_g and P*P arrivals from two Jackpile explosions relative to the constraints imposed by the Morenci P_g data.

from Jackpile to SC and WT.

Figure 36 shows the values of $\log_e$ DM/WT versus frequency for the P_g phase for three Jackpile explosions and one St. Anthony explosion with respect to the constraints discussed earlier. In this case the curves generally lie below the region that would indicate equal attenuation along paths to stations DM and WT, thus an increase in attenuation properties of the upper crust north of DM is indicated. A decrease in Q along this path may result from a change in crustal properties beneath the Rio Grande graben beneath which the energy must pass to reach DM. Because the raypaths to Jackpile converge with distance to the north, it is believed that the anomaly should be located within 30 or 40 km to the north of DM.

Figure 37 is a seismic activity map of the region with the raypaths to DM indicated. The raypath to DM crosses an area in the vicinity of San Acacia which has shown high microearthquake activity in the past. Microearthquake activity in the Rio Grande rift is thought to be associated with magmatic intrusive activity. It is possible that a shallow magma body is present in the San Acacia area which attenuates the P_g to DM. Of special interest in Figure 36 is the St. Anthony event, the log ratios for which lie lower than those for Jackpile. This observation suggests that the position of the attenuating structure in the crust is such that a slight shift in raypaths can cause significant changes in the attenuation.

Figure 38 shows the $\log_e$ SC/WT versus frequency curve for the strong Moho reflection from Jackpile. The ratios lie above the constraints discussed earlier, indicating higher attenuation along the path to WT than to SC. A possible reason for this observation is that the reflected

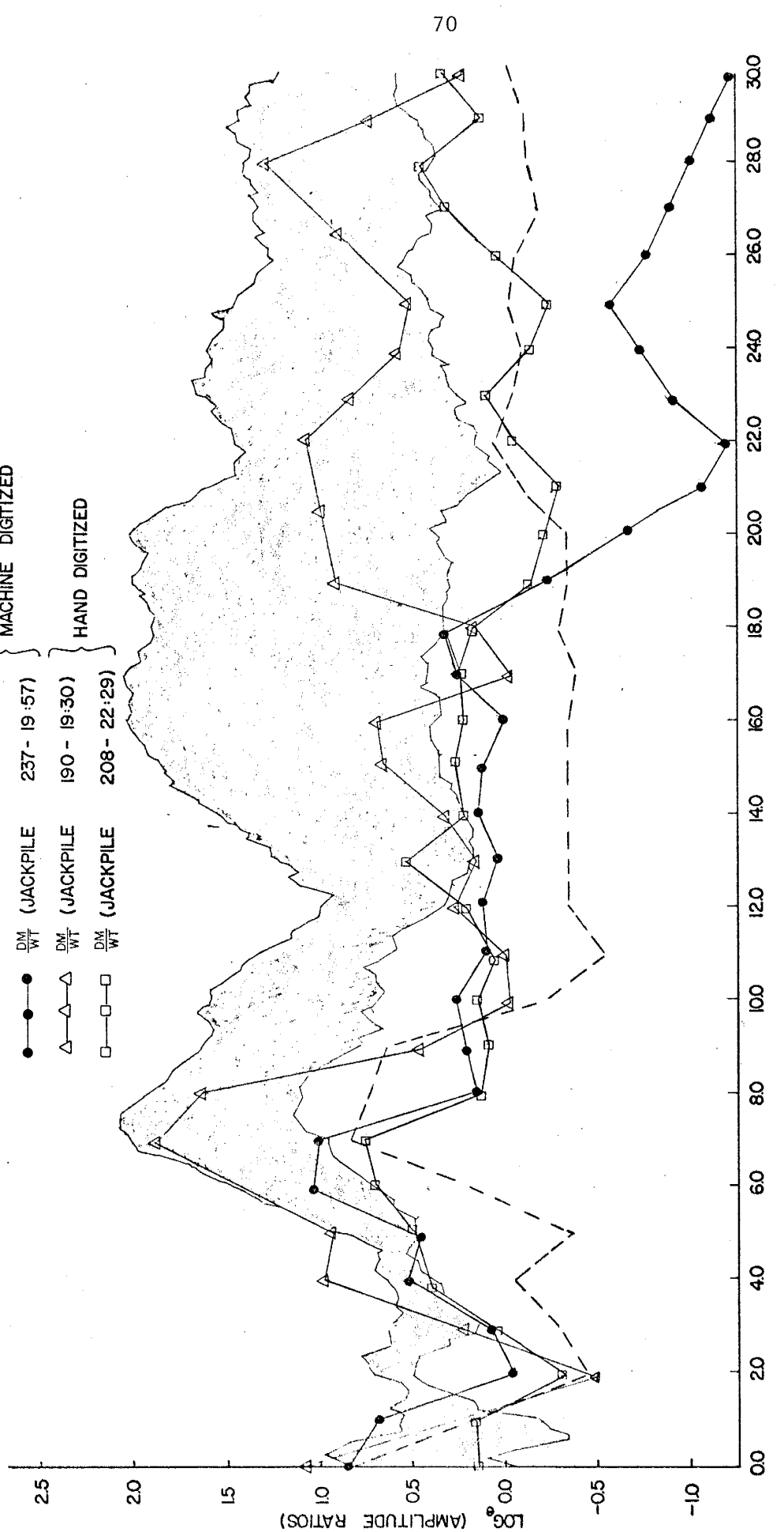

Figure 36. Values of $\log_e$ DM/WT versus frequency for the P_g phase from three Jackpile and one St. Anthony explosion relative to the constraints imposed by the Morenci P_g data.

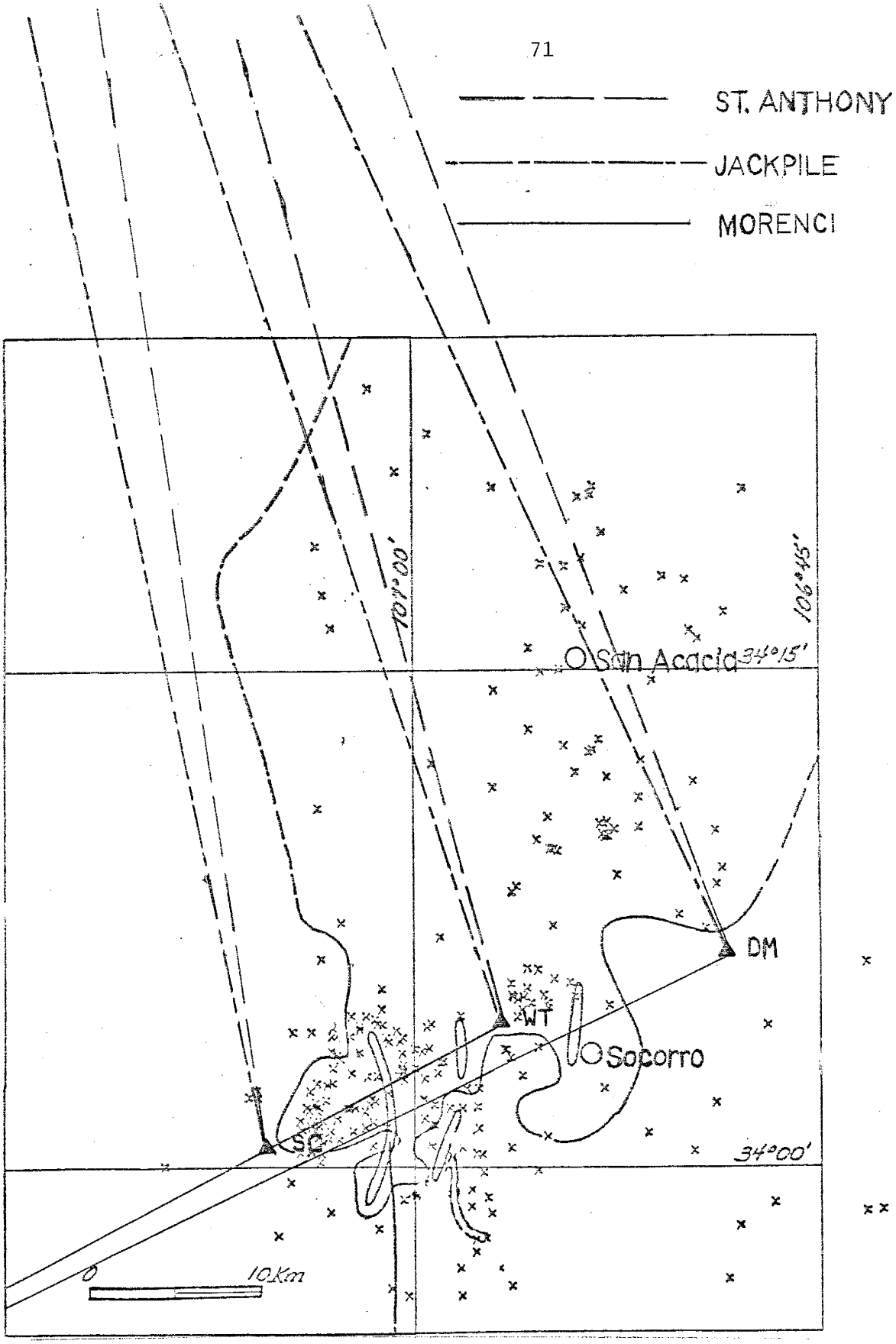

Figure 37. Geographical distribution of microearthquake epicenters in the Socorro area showing raypaths to the explosions, outline of the extensive magma body and positions of proposed shallow magma bodies (from A. R. Sanford, E. J. Rinehart et al., 1977).

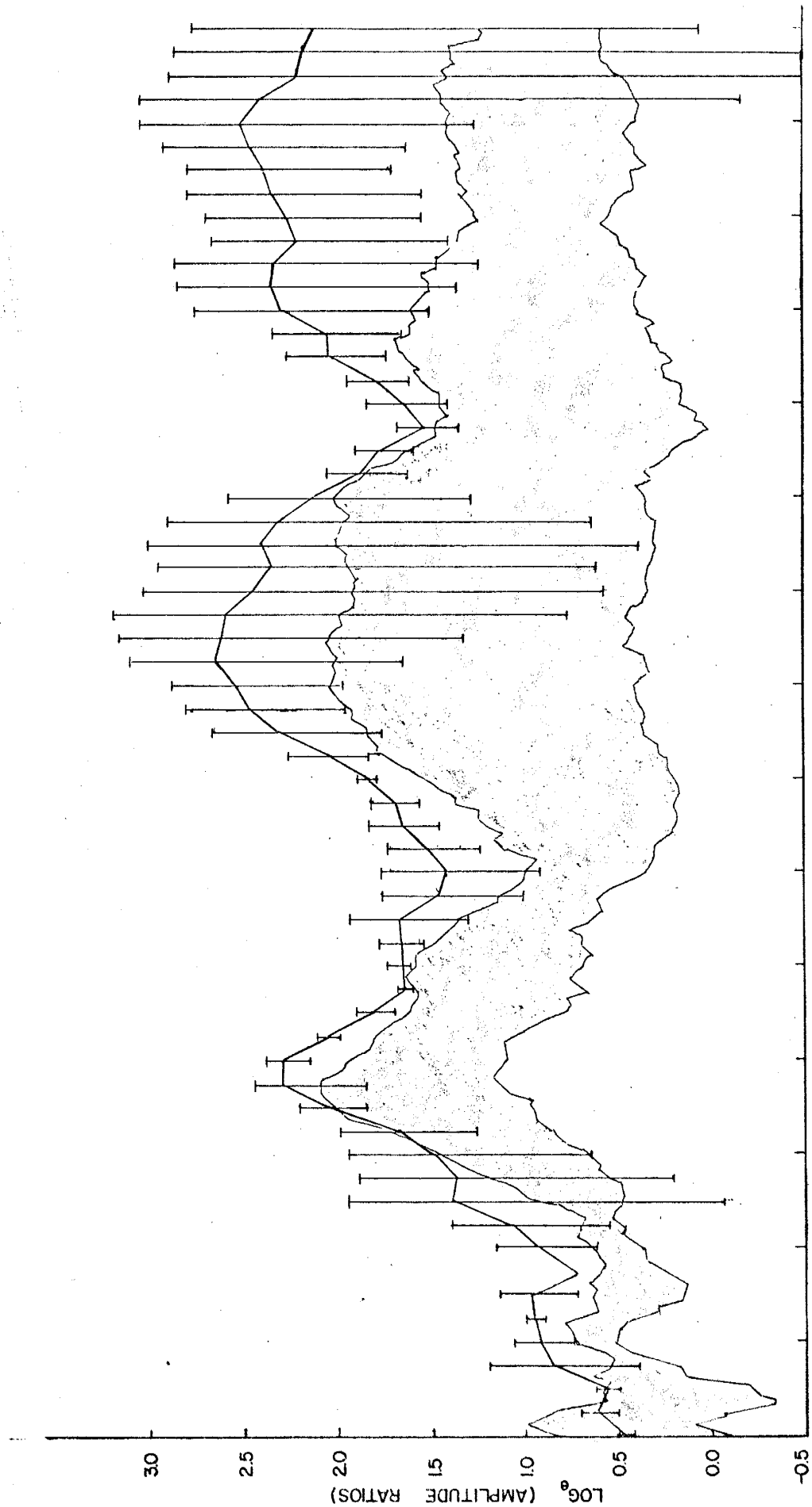

Figure 38. Values of log$_e$ SC/WT versus frequency for the P_mP phase from two Jackpile explosions relative to the constraints imposed by the Morenci P_g data.

energy to station WT passes through the extensive magma body whereas the reflected energy to station SC does not.

Figure 39 compares the $\log_e$ SC/WT versus frequency curve for the P_mP phase with a similar curve for P_g and P*P phases, both curves for the same explosions from Jackpile. The curve for the reflected Moho phase lies above the curve for phases which travel in the upper crust. The values of $\log_e$ SC/WT for the P_g and P*P phases show (Figure 35) that the Q of the upper crust is approximately the same from Jackpile to stations SC and WT. Therefore the variations in the $\log_e$ SC/WT values for Jackpile P_g and P*P phases as a function of frequency primarily represent the station effects $\log_e$ Stat SC(ω)/Stat WT(ω) of station SC relative to station WT, and can be used to filter out the station effects on the $\log_e$ SC/WT versus frequency curve for the P_mP phase.

Note in Figure 39 that there is no striking difference in the two curves until approximately 9.0 Hz. A set of P values (equation (16)) was computed from

$$P = \frac{\pi f \Delta r}{v} \Bigg/ \left[\log_e \left(\frac{SC}{WT} \right)_{P_mP} - \log_e \left(\frac{SC}{WT} \right)_{P_g, P*P} \right] \qquad (18)$$

where r was estimated to be 1.0 km for the length of the passage of the P_mP phase through the magma layer. Figure 40 shows the P values versus frequency. Since P is given by

$$P = \frac{Q_{SC} Q_{WT}}{Q_{SC} - Q_{WT}} \quad ,$$

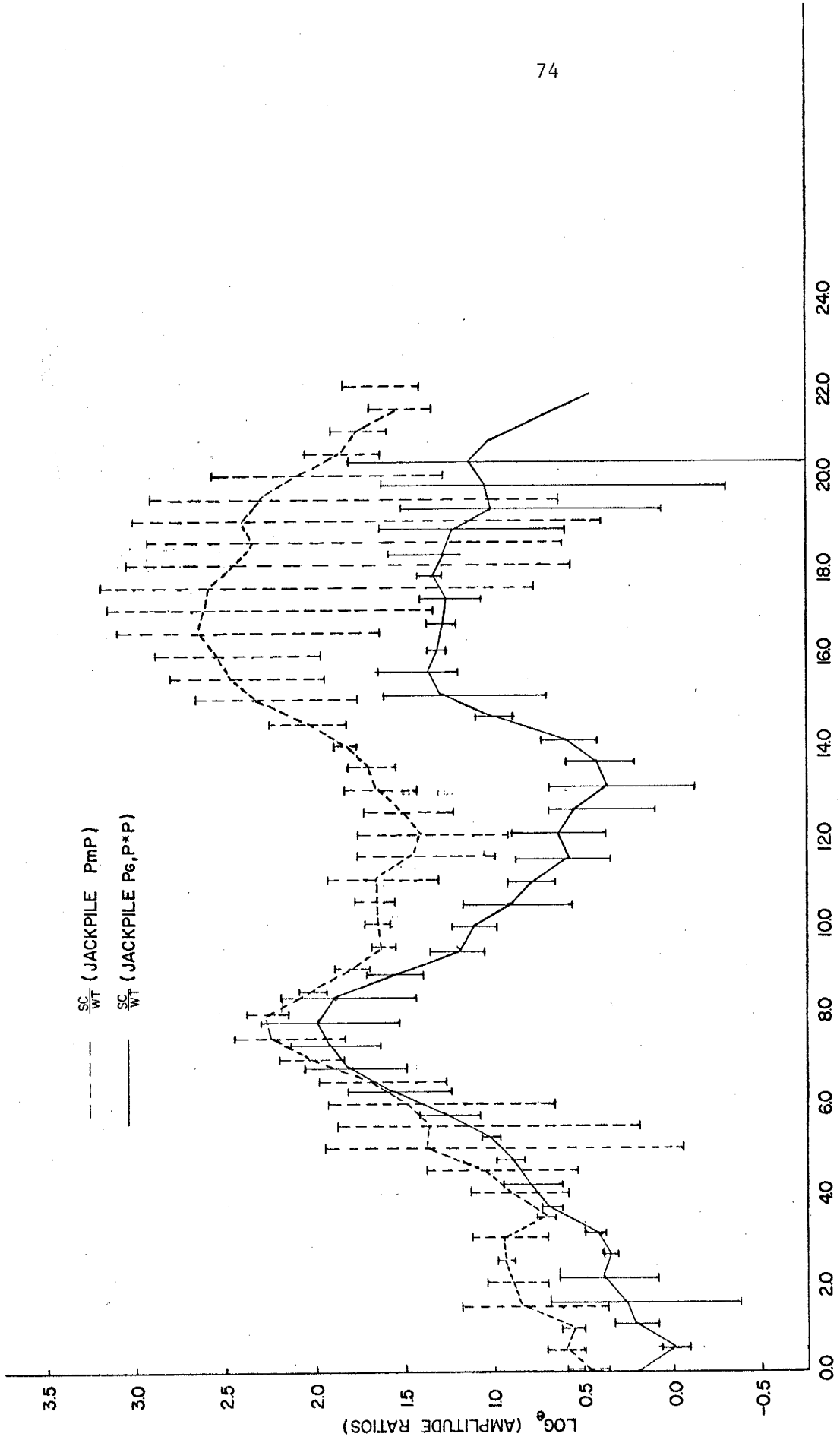

Figure 39. Values of log$_e$ SC/WT versus frequency for the P_mP phase relative to the same curve for the P_g and P*P phases. Data is from two Jackpile explosions.

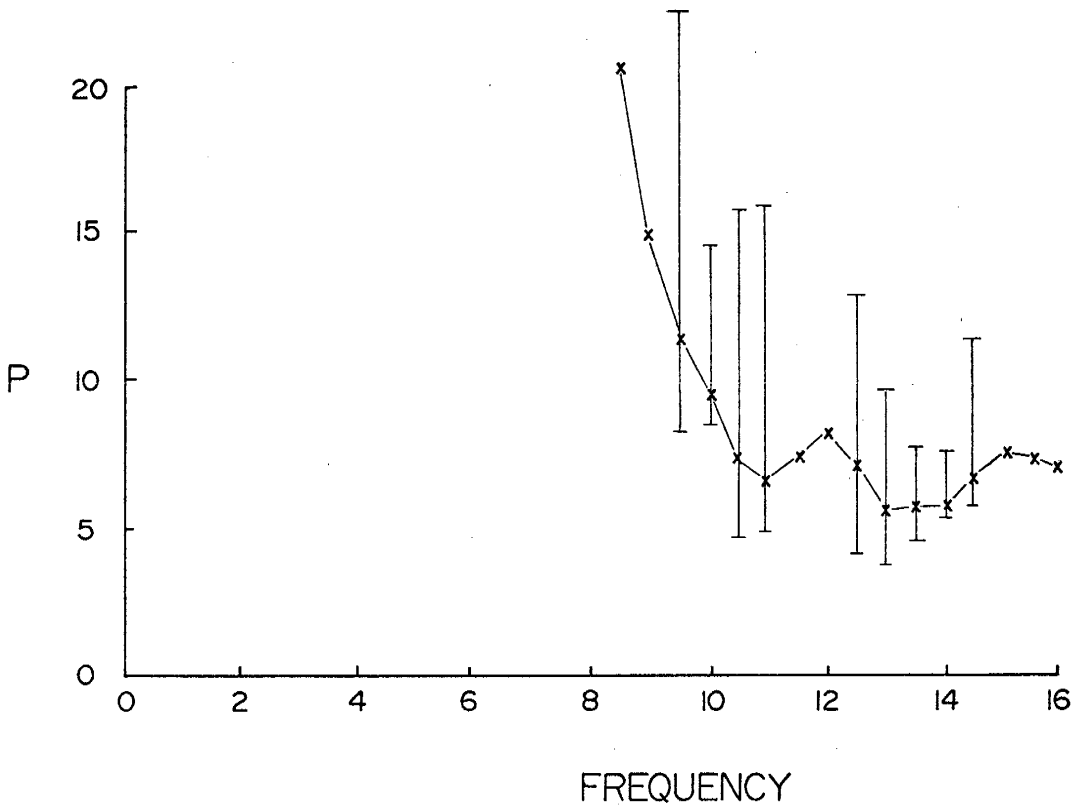

Figure 40. Values of P versus frequency for the P_mP phase from Jackpile explosions to stations SC and WT.

a Q_{WT} which is inversely proportional to frequency would cause P to be inversely proportional to frequency also. Figure 40 suggests this type of behavior for P, and thus the path of P_mP to WT may indeed pass through magma. With the large standard deviations at low frequencies it is possible that a liquid Q type behavior occurs at frequencies lower than 9 Hz.

Shown in Figure 26 are the values of $\log_e$ DM/WT versus frequency for the P_mP phase for one Jackpile event and one St. Anthony event. The

strength of the lower frequency components of the P_mP phase at WT is not understood. However the greater strength of the higher frequency components at DM could be the result of a greater thickness of the extensive magma body along the raypath to WT than is encountered by the raypath to DM. Figure 4 shows that the arrivals to both WT and DM pass through the extensive body. The higher ratios at high frequencies for the St. Anthony event compared to the Jackpile event may indicate relatively large changes in thickness of the magma body over short distances.

Analysis of Morenci P_n Data

The best approach to the interpretation of the Morenci P_n data is a comparison of the values of $\log_e$ SC/WT and $\log_e$ DM/WT versus frequency for the P_n phase. A high Q value for the upper mantle can be expected. Comparison of the Morenci P_n spectra to the Morenci P_g spectra (Figures 9 and 10) show that the dominant frequency of P_n is higher than the dominant frequency of the P_g. Thus the high-frequency content of the explosive pulse is less attenuated in the upper mantle below the Moho than in the upper crust. It is probable that attenuation in the upper mantle is too small to be detectable in the short distance between stations SC and WT and stations WT and DM, and that the $\log_e$ SC/WT and $\log_e$ DM/WT ratios are predominantly shaped by station effects and differences in the emergent raypaths to the stations.

A comparison of the values of $\log_e$ SC/WT and $\log_e$ DM/WT versus frequency for the P_n phase for Morenci explosions is given in Figure 41. The only statistically significant difference between the two curves is centered at 5.0 Hz and indicates a stronger 5.0 Hz signal at DM than SC. Figure 42 shows the plots of $\log_e$ SC/DM for the Morenci P_n phase from different explosions. A strong 5.0 Hz signal at station DM relative to

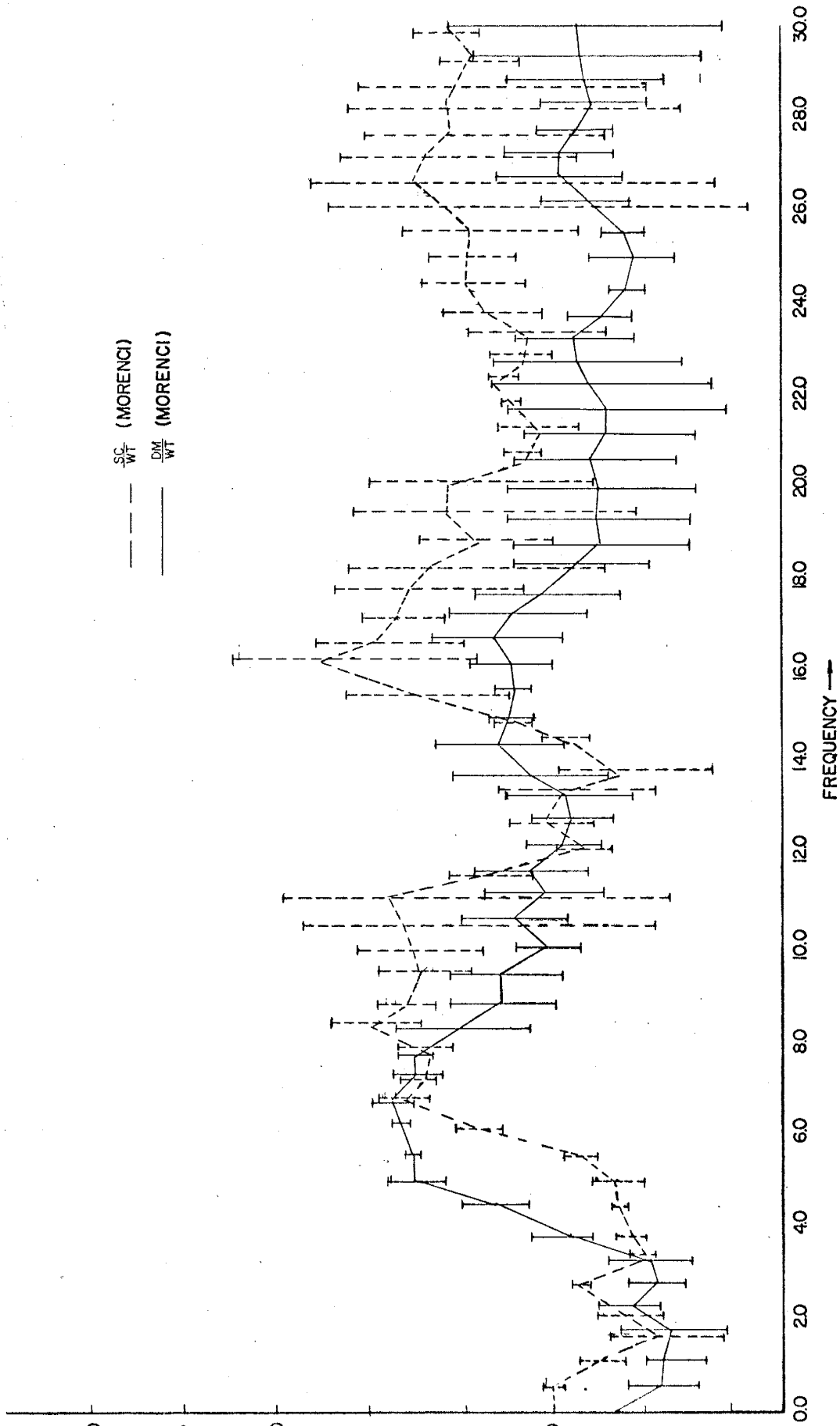

Figure 41. Comparison of values of $\log_e$ SC/WT and $\log_e$ DM/WT for the P_n phase from Morenci explosions.

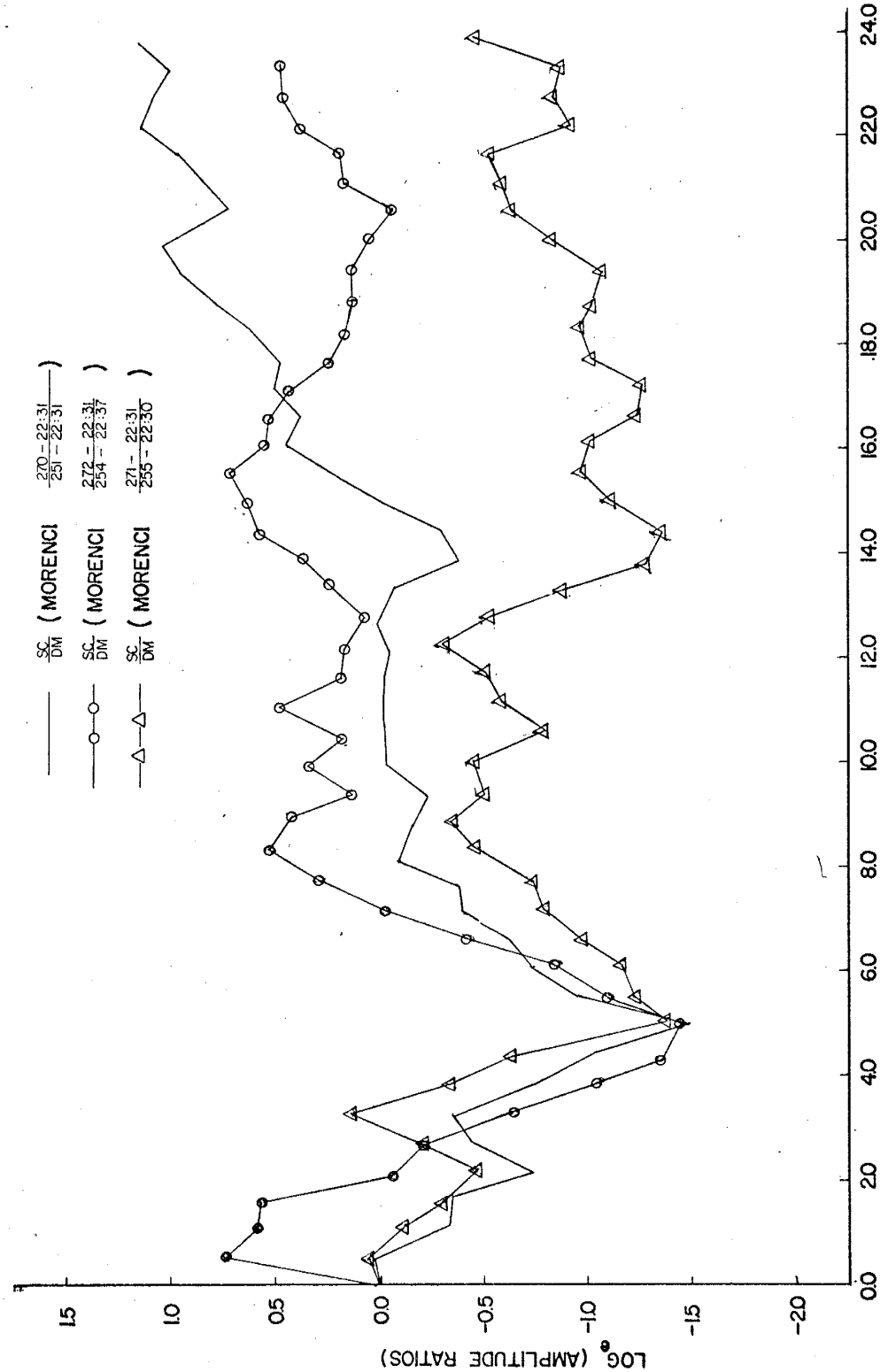

Figure 42. Values of $\log_e$ SC/DM versus frequency for the P_n phase for different explosions recorded at stations SC and DM.

SC is a prominent feature of these plots. The values of $\log_e$ SC/DM versus frequency for the Morenci P_g phase (Figure 31) suggest a similar signal strength at 5 Hz but much less prominent. Curves of $\log_e$ DM/WT versus frequency for the Morenci P_g (Figure 21), the Jackpile P_g (Figure 25) and Jackpile P_mP (Figure 26) phases do not show a strong 5.0 Hz signal at station DM. Therefore a strong 5.0 Hz signal at station DM is only a feature of the Morenci P_n phase.

The strength of the 5.0 Hz signal in the Morenci P_n phase at station DM is not readily explained as a station effect at DM. The enrichment of signals in a narrow band centered at 5 Hz cannot be explained by wave interference caused by rock layering beneath station DM, since a similar enrichment should also appear at higher frequencies.

A possible explanation for the 5.0 Hz enrichment is an interference pattern caused by the extensive magma body. As is shown in Figure 4 the Morenci P_n raypath to DM must pass through the southwestern margin of the extensive magma body. The upper surface of the body is known to produce strong S-wave reflections from microearthquakes. It is probable that the lower surface is a good reflector also. Figure 43 is an illustration of

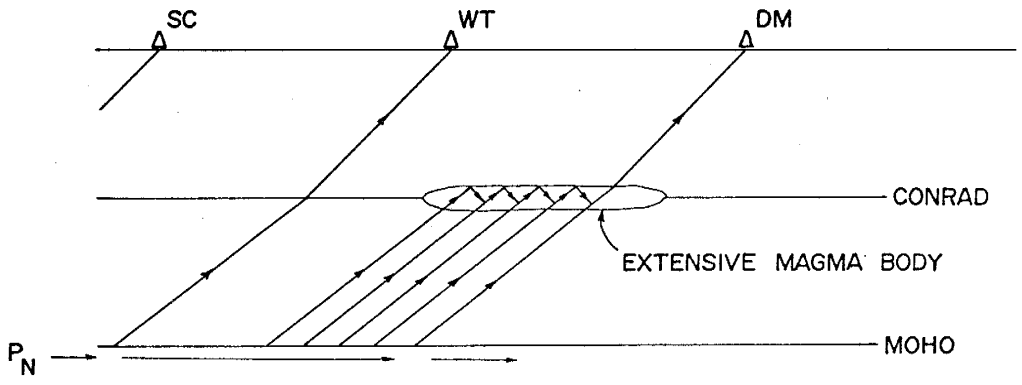

Figure 43. Constructive and destructive wave interference in the extensive magma body.

the mechanism. The interference would be subject to attenuation characteristic of a liquid, such that a rapid damping of the constructive interference pattern with frequency would be expected. This would explain why the 5.0 Hz peak at station DM for the Morenci P_n phase is not repeated at 10.0, 15.0 Hz etc. If this speculation is correct, then accurate determination of the thickness of the magma layer could be made if the compressional velocity of the magma and of the upper and lower surroundings were known. Analysis of Morenci explosion data simultaneously recorded at stations SC and DM or at stations WT and DM (with WT placed at the tunnel entrance) could resolve the problem.

Analysis of Morenci P* Data

Shown in Figure 22 are the values of $\log_e$ SC/WT versus frequency for the section of the seismograms from Morenci explosions at stations SC and WT which contain the P* arrival which was identified in Figure 7. The arrival was outstanding at station SC for the Morenci event shown in Figure 7, but less noteworthy on the other Morenci events. The standard deviations of the $\log_e$ SC/WT ratios in Figure 22 show that the shape of the curve is reasonably determined. Comparison with the $\log_e$ SC/WT versus frequency curve for the Morenci P_n (Figure 18) suggests that the P* phase is attenuated more than the P_n phase to station WT at the higher frequencies (12.0-16.0 Hz).

The shape of the $\log_e$ SC/WT versus frequency curve for the Morenci P* phase is similar to the shape of the $\log_e$ SC/WT versus frequency curve for the P_mP phase from Jackpile explosions. It is possible that the shape of the $\log_e$ SC/WT ratio curve for the Morenci P* phase is a result of passage of the P* raypath through a shallow magma body to station WT. Shuleski (1976) proposed a shallow magma body to the west of station WT

on the basis of screening of SV waves from microearthquakes. The values of $\log_e$ SC/WT for the Morenci P_n (Figure 18) show that the high frequency content of the Morenci P_n phase is the same at stations SC and WT. If a shallow magma body causes greater attenuation of the Morenci P* phase to station WT, then it should lie to the west of the Morenci P_n raypath to WT as is shown in Figure 44.

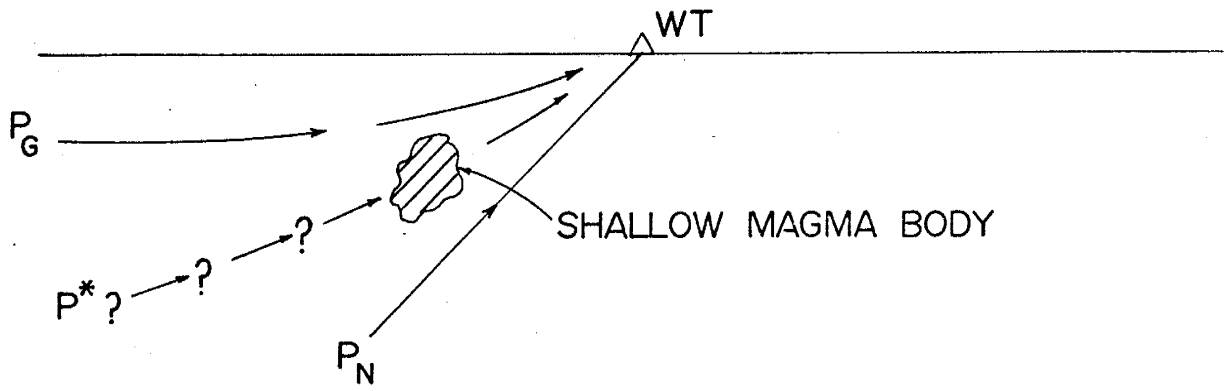

Figure 44. Raypaths of P-phases from Morenci explosions to station WT, and a possible position of a shallow magma body.

The apparent higher attenuation of the Morenci P_g phase between stations SC and WT than between stations WT and DM may be the result of one or more shallow magma bodies along the Morenci P_g raypath to station WT.

Summary

In this study a total of 125 seconds of digitized P-phases from mining explosions recorded at three sites in the Socorro area was Fourier transformed in an effort to resolve differences in seismic wave attenuation of segments of the crust under the Rio Grande rift, and to detect, if possible, any attenuation anomaly caused by an extensive magma body which lies approximately at the 18 km level in the crust. The P_g data from Morenci explosions suggests that attenuation is greater in the upper crust to the west of station WT than to the east of station WT. The P_g and P*P data from Jackpile explosions shows that the Q value of the upper crust along three raypaths to the north of the three station sites is similar along two raypaths to stations SC and WT but is less along the third raypath to station DM. These results indicate that attenuation is greater along raypaths which cross areas that have high microearthquake activity, which in turn may be associated with magmatic activity. A calculation of Q from the P_g phase of Morenci explosions across a 28 km segment of the upper crust in the rift produced a value, 195, which is lower than published values determined from P_g phases from the Nevada test site (Press, 1964).

Attenuation effects of the extensive magma body were found, namely a higher attenuation for the P_mP phase from Jackpile explosions at stations where the P_mP raypath passes through the magma layer. Q calculated from this data appears to be frequency dependent as would be expected for passage through a magma layer.

Greater attenuation was observed for the Morenci P_n phase at station DM, the raypath for which passes through the southern margin of the magma body. However, the attenuation was of a smaller magnitude than the

attenuation for the Jackpile P_mP phase passing through the central portions of the magma layer.

P_n energy passing through the southern margin of the extensive magma body on its way to station DM was found to have strong signals in a narrow frequency range centered at 5 Hz. A suggested explanation for this observation is constructive interference within the magma layer.

ACKNOWLEDGMENTS

I express my sincere thanks to Dr. Allan R. Sanford for the critical review of this paper and especially Dr. Sanford's patience and help during all phases of this research. I also sincerely express my thanks to Charles B. Moore to whose ability and generosity I owe the quality of the digitizing.

References Cited

Biles, N. E. (1967). A study of vertical ground motion showing the free surface effect, M. S. Thesis, Geoscience Dept., New Mexico Inst. Mining and Tech.

Gutenberg, B. (1956). Effects of ground on shaking in earthquakes, Trans. Amer. Geophys. Union 37, 757-760.

Knopoff, L. (1964). Q, Rev. Geophysics 2, 625-660.

Press, F. (1964). Seismic wave attenuation in the crust, Journ. Geophys. Res. 69, 4417-7718.

Rinehart, E. J. (1976). The use of microearthquakes to map an extensive magma body in the Socorro, New Mexico area, M. S. Independent Study, Geoscience Dept., New Mexico Inst. Mining and Tech.

Sanford, A. R., O. Alptekin, and T. R. Toppozada (1973). Use of reflection phases on microearthquake seismograms to map an unusual discontinuity beneath the Rio Grande rift, Bull. Seismol. Soc. Amer. 63, 2021-2034.

Sanford, A. R., R. P. Mott, Jr., P. J. Shuleski, E. J. Rinehart, F. J. Caravella, R. M. Ward, and T. C. Wallace (1977). Geophysical evidence for a magma body in the crust in the vicinity of Socorro, New Mexico, Amer. Geop. Union Geop. Mon. 20, 385-403.

Sanford, A. R., E. J. Rinehart, P. J. Shuleski, J. A. Johnston (1977). Evidence from microearthquake studies for small magma bodies in the upper crust of the Rio Grande rift near Socorro, New Mexico, Paper presented at the A.G.U. 1977 Fall meeting. San Francisco, Dec. 5-9.

Shuleski, P. J. (1976). Seismic fault motion and Sv wave screening by shallow magma bodies in the vicinity of Socorro, New Mexico, M. S. Independent Study, Geoscience Dept., New Mexico Inst. Mining and Tech.

Toppozada, T. R. and A. R. Sanford (1976). Crustal structure in central New Mexico interpreted from the Gasbuggy explosion, Bull. Seismol. Soc. Amer. 66, 877-886.